| Title	SOLID STATE HIGH RESOLUTION NMR OF ^<19>F IN SOME FLUORINE-CONTAINING COMPOUNDS
Author(s)	Yoshioka, Yoshichika
Citation	大阪大学, 1983, 博士論文
Version Type	VoR
URL	https://hdl.handle.net/11094/24338
rights	
Note	

SOLID STATE HIGH RESOLUTION NMR OF ^{19}F

IN SOME FLUORINE-CONTAINING

COMPOUNDS

BY

YOSHICHIKA YOSHIOKA

Thesis

Submitted to

The Graduate School of Faculty of Science

Osaka University

in Partial Fulfilment of the Requirements

for the Degree of Doctor of Science

1983

Doctoral Committee:

  Professor Hideaki Chihara, Chairman

  Professor Keiji Kuwata

  Professor Yoshimasa Kyogoku

  Associate Professor Nobuo Nakamura
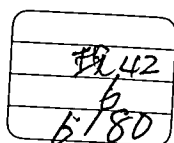
Dedicated to

Father and Mother,

and

Brothers and Sisters.

narrow is beautiful and loquacious

Acknowledgments

First of all, it should be mentioned that the work of this thesis has been carried out under the guidance of Professor Hideaki Chihara.

I wish to express my sincere thanks to Professor Hideaki Chihara for his kind guidance and encouragements, and stimulative discussions filled with his deep insight into science.

I would like to thank Associate Professor Nobuo Nakamura, who guided me to NMR method, for his many valuable suggestions, criticisms, and encouragements.

I wish to thank all the members of the Chihara Laboratory for their useful discussions and encouragements. Especially the author is indebted to Mr. K. Ichimura, Dr. K. Negita, and Dr. S. Takeda in constructing the spectrometer, and Mr. H. Nakayama in processing the data, and Dr. T. Atake, Dr. Y. Yamamoto, Mr. Y. Akagi, Mr. Y. Yoshimoto, Dr. S. Miyajima, Mr. T. Tsukamoto, and Mr. H. Gyoten for their stimulative discussions and heartfelt encouragements.

I would also like to thank Dr. M. Hashimoto, Dr. T. Hasebe, Dr. B. K. Chaudhuri, Dr. A. Fuyuhiro, Dr. K. Tanaka, Mr. K. Sakano, Mr. T. Fukumoto, Mr. N. Morokoshi, Mr. T. Kohda, and all my friends for their considerate encouragements.

Contents

Abstract

The chemical shift data of variety of nuclei can provide important information about molecular structure, electronic structure, chemical exchange, and so on. However, traditional high-resolution NMR experiments on liquids or solutions give only the time-averaged chemical shifts due to rapid molecular motions. In order to study the structures and properties of molecules and ions in more detail, it is highly desirable to obtain the complete data of the chemical shielding tensors which are essentially anisotropic, reflecting the anisotropy of chemical bonds. Such data became available by performing variety of tricky high resolution NMR experiments on solid state which have been developed since late 1960's.

The main aim of the present work is to obtain complete chemical shielding tensor of ^{19}F in some fluorine-containing materials and to relate these data to the molecular and/or ionic structure as well as to the chemical bonding in these compounds.

To perform such a kind of experiment, a spectrometer based on the multiple pulse technique was designed and constructed. The spectrometer works at 40 MHz and the optimum line width of ^{19}F in CaF_2 single crystal is 8.5 ppm (340 Hz) which corresponds to sufficient resolution to observe the anisotropy of the ^{19}F chemical shift, because the ^{19}F chemical shift anisotropy extends over 150 ppm in normal substances.

The ^{19}F chemical shift anisotropies were measured in an aromatic conjugated system, 1,3,5-trichloro-2,4,6-trifluorobenzene, and a series of inorganic complex compounds, K_2MF_6; M = Si, Ge, Sn.

The values of the maximum and the minimum principal components of the ^{19}F shielding tensor in 1,3,5-trichloro-2,4,6-trifluorobenzene were determined to be + 85 ppm and - 43 ppm respectively. The most shielded direction is perpendicular to the molecular plane and the least shielded direction is perpendicular to the C-F bond but lying in the molecular plane. The value of the most shielded and the least shielded components vary gradually from sym-$C_6H_3F_3$, sym-$C_6Cl_3F_3$, to C_6F_6, whereas the C-F bond direction components remain nearly constant in the series of the above compounds. The semi-quantitative analysis of the shielding tensors in these compounds leads to a conclusion that the substitution of the ring protons of C_6H_6 by fluorine or chlorine brings about some measurable change in the σ-electron density but give rise to little change in the π-electron distribution. The high-resolution NMR of single crystal of sym-$C_6Cl_3F_3$ together with a pulsed ^{35}Cl NQR measurement revealed that the molecules undergo the three-fold reorientation about its molecular C_3 axis at a rate of 2 kHz at 300 K.

In a series of inorganic compounds, K_2MF_6; M = Si, Ge, Sn, the shielding tensors are all axially symmetric and the most shielded direction is parallel to the M-F (M = Si, Ge, Sn) bond. A gradual change of the shielding tensor elements (bond direction and perpendicular to the bond) were observed on going from K_2SiF_6, K_2GeF_6, to K_2SnF_6 except for the component perpendicular to the bond in K_2SiF_6. From the analysis of shielding tensor components, it is indicated that the π-backbonding effect on the electronic structure in the MF_6^{2-} ions is the

strongest in the Si-F system, being consistent with the fact that the Si has the extraordinarily low electronegativity compared with C, Ge, and Sn.

1 Introduction

The nuclear magnetic resonance frequency of a nuclear spin S is essentially determined by an applied static magnetic field Ho. The Zeeman Hamiltonian for an isolated spin with the gyromagnetic ratio γ is given by

$$Hz = -\gamma \hbar Ho S \qquad (1-1)$$

and the nuclear resonance frequency (the angular Larmor frequency) is given by

$$\omega = -\gamma Ho. \qquad (1-2)$$

But there are many interactions of S with other nuclear spins and/or with electrons surrounding it which may contribute to shifting the resonance frequency.

In a nuclear magnetic resonance experiment the resonance frquency of a nuclear spin S with the gyromagnetic ratio γ is determined not only by the external magnetic field but also by the interaction of the nuclear spin with the surrounding electrons. In diamagnetic materials with neither net electron spin n nor orbital angular momentum and when no other interactions such as quadrupolar interactions, spin rotation interaction etc. do not exist, the chemical shift is a second-order effect, its magnitude being proportional to the external magnetic field Ho, and can be represented by the Hamiltonian:

$$\underline{Hcs} = \gamma \underline{Ho} \cdot \underline{\sigma} \cdot \underline{S} \qquad (1-3)$$

where $\underline{\sigma}$ is a dimensionless, second-rank tensor, representing the anisotropic shift of the resonance frequency in bulk matter with respect to that of a bare nucleus. In Eq.(1-3) $Hz >> Hcs$ is assumed. The nature of the $\underline{\sigma}$ tensor is determined by the electron

distribution around the resonant nucleus and therefore its measurement provides information about the structure and properties of chemical bond. However, in gaseous, liquid, and plastic phases[1] the rapid, three dimensional molecular motion averages out the anisotropic part of this chemical shift tensor, leaving only the isotropic part:

$$\sigma_i = (1/3)\text{Tr}(\underline{\sigma}) = (1/3)(\sigma_{11} + \sigma_{22} + \sigma_{33}), \quad (1-4)$$

where σ_{11}, σ_{22}, and σ_{33} are the principal components of the chemical shift tensor. Although useful information about the nature of the chemical bond or bonds can be derived from the measurement of chemical shift in these materials very important knowledge about anisotropy around the nucleus of interest may be completely lost.

In a usual solid in which no rapid molecular rotation is excited the chemical shift tensor may not be averaged out. Therefore the resonance frequency of a nuclear spin in a solid depends on the orientation of the external field with respect to the axes of chemical shift tensor in the sample. When one measures the angular dependence of the chemical shift, the anisotropic components of $\underline{\sigma}$ can be determined. Since the complete determination of the chemical shift tensor provides information about the local symmetry of the electron cloud around the nucleus and allows one to draw a more detailed picture of the chemical bonding of a certain atom than the isotropic chemical shift measured in solution does. It also gives information about the nature of solid such as molecular motion, intermolecular or inter ionic interactions, conductivity, ferroelectricity, etc.

From the symmetry of the chemical shift tensor, we can obtain

the data about the symmetry of molecule and crystal. If there is
a molecular motion, the chemical shift tensor is partially averaged,
and so the analysis of the chemical shift data gives the knowledge
of the type and the correlation time of molecular motion.

Although the chemical shift in solids gives us the important
informations as described above, the chemical shift may usually
be obscured by strong dipolar interaction in solid state and so
only limited number of investigations in this field have been made
so far.

High resolution NMR spectrum in solid state was firstly
obtained by Magic Angle Spinning technique (MAS). Andrew et al.[2]
and Lowe[3] independently reported MAS method and the subject has
considerably developed both theoretically[4] and experimentally.[5]
In this technique a solid specimen is spun at an angular frequency
ω_r in a high static magnetic field about an axis inclined by an
angle β with respect to the field direction. When β is equal
to $54°44'$ and the ω_r is larger than the dipolar line width, the
motional narrowing of the dipolar width is realised and the trace
of chemical shift tensor is obtained. This special angle is
called the 'Magic Angle'.

Waugh et al.[6] obtained the high resolution spectrum of ^{19}F
in CaF_2 single crystal by the pulse technique in 1968. By this
technique dipolar Hamiltonian is averaged out in spin space and
brought to be nearly zero, and then chemical shift can be observed.
This technique is applicable to abundant spins (^1H, ^{19}F, etc.) and
gives full chemical shift tensor values. To improve the resolution,
several pulse sequences have been developed.[7]

The third technique was proposed by Pines et al.[8] By this
technique chemical shift tensors for rare spins (^{13}C, ^{15}N, etc.)
can be obtained. Since the line width for the rare spins is usually
very small the resonance of rare spins gives us high resolution
spectrum without any special techniqe, but it is necessary to
accumulate FID to obtain the signal with good S/N ratio. The
problem was how to accumulate quickly where the spin-lattice
relaxation times of rare spins are very long. They solved this
problem by the use of abundant spins as thermal reservor.

The multiple pulse technique was adopted in this work to
obtain chemical shift tensors of abundant spins such as ^{1}H and
^{19}F, and a 40 MHz spectrometer for WAHUHA-4 and MREV-8 pulse
sequences was constructed.

Measurements were made for ^{19}F in an aromatic conjugated
system (1,3,5-trichloro-2,4,6-trifluorobenzene) and a series of
inorganic compounds (K_2MF_6; M = Si, Ge, Sn).

References to Chapter 1

1) T. Hasebe, N. Nakamura, and H. Chihara, Bull. Chem. Soc. Japn., 53, 896 (1980).

2) E. R. Andrew, A. Bradbury, and R. G. Eades, Nature, London, 182, 1659 (1958).

3) I. J. Lowe, Phys. Rev. Lett., 2, 285 (1959).

4) E. R. Andrew and A. Jasinski, J. Phys. C4, 391 (1971).

5) E. R. Andrew, L. F. Farnell, M. Firth, T. D. Gledhill, and I. Roberts, J. Mag. Reson., 1, 27 (1969).

6) J. S. Waugh, L. M. Huber, and U. Haeberlen, Phys. Rev. Lett., 20, 180 (1968).

7) a) P. Mansfield, J. Phys. C4, 1444 (1971).

   b) W. K. Rhim, D. D. Elleman, and R. W. Vaughan, J. Chem. Phys., 58, 1772 (1973).

   c) D. P. Burum and W. K. Rhim, J. Chem. Phys., 71, 944 (1979).

   d) D. P. Burum, M. Linder, and R. R. Ernst, J. Magn. Reson, 44, 173 (1981).

8) A. Pines, M. G. Gibby, and J. S. Waugh, Chem. Phys. Lett., 15, 373 (1972).

2 The Methods to Obtain the High Resolution NMR Spectrum in Solid

2-1 Introduction

There are three principal methods and their combinations to obtain the high resolution NMR spectrum in solid. A brief review will be given about the line width in solids and the methods to eliminate the dipolar line width in order to uncover the small chemical shift interactions. The secular part of homonuclear Hamiltonian, which gives rise to line broadning in solid state, can be described as follows,

$$H_d = (1/2)\gamma_I^2 \hbar^2 \sum_{i<j} r_{ij}^{-3}(1 - 3\cos^2\theta_{ij})(\underline{I}_i \cdot \underline{I}_j - 3I_{iz}I_{jz})$$
$$= \alpha \sum_{i<j} A \cdot B \cdot C$$

where

$$\alpha = (1/2)\hbar^2 \gamma_I^2$$
$$A = r_{ij}^{-3}$$
$$B = 1 - 3\cos^2\theta_{ij}$$
$$C = \underline{I}_i \cdot \underline{I}_j - 3I_{iz}I_{jz}.$$

H_d can be made substantially zero if one can bring the term A, B, or C to zero.

In the case of rare spin resonance the separation between the resonating spins is very large and therefore the term A becomes very small and so chemical shift can easily be observed. If the NMR signal is very weak and there are other abundant spins in the system the signal enhancement by the use of cross polarization between the rare and the abundant spins can realized. This special technique is called Proton Enhanced NMR.

The term B can be brought to nearly zero by the magic angle

spinning method and this technique can apply to any system.

The term C is expected to become zero only when an averaging of this term is performed by the use of special pulse sequence. The method is called Multiple Pulse NMR.

In the next section the Multiple Pulse NMR method will be reviewed, which is the method that has been adopted in this Dissertation, and in the latter sections other methods will be described.

2-2 Line Narrowing by Multiple Pulse NMR

In this method, Hamiltonian is perturbed in spin space by the radio-frequency (RF) pulses. The repetition times of RF pulses are short compared with the spin-spin relaxation time, and so spins feel average Hamiltonian in their relaxation process. Therefore high resolution spectrum can be obtained, if dipolar Hamiltonian becomes zero by averaging Hamiltonian through the perturbation of RF pulses.

In this section, averaging Hamiltonian theory will be described first, and later the reason why high resolution spectrum can be obtained by special pulse sequences such as WAHUHA-4 and MREV-8 is described. The pulse sequences for WAHUHA-4 and MREV-8 are $(\tau\text{-}P_{-x}\text{-}\tau\text{-}P_y\text{-}2\tau\text{-}P_{-y}\text{-}\tau\text{-}P_x\text{-}\tau\text{-})_n$ and $(\tau\text{-}P_x\text{-}\tau\text{-}P_y\text{-}2\tau\text{-}P_{-y}\text{-}\tau\text{-}P_{-x}\text{-}2\tau\text{-}P_{-x}\text{-}\tau\text{-}P_y\text{-}2\tau\text{-}P_{-y}\text{-}\tau\text{-}P_x\text{-})_n$ respectively as shown in Fig. 2-1, where P_i represents the 90° pulse along i axis.
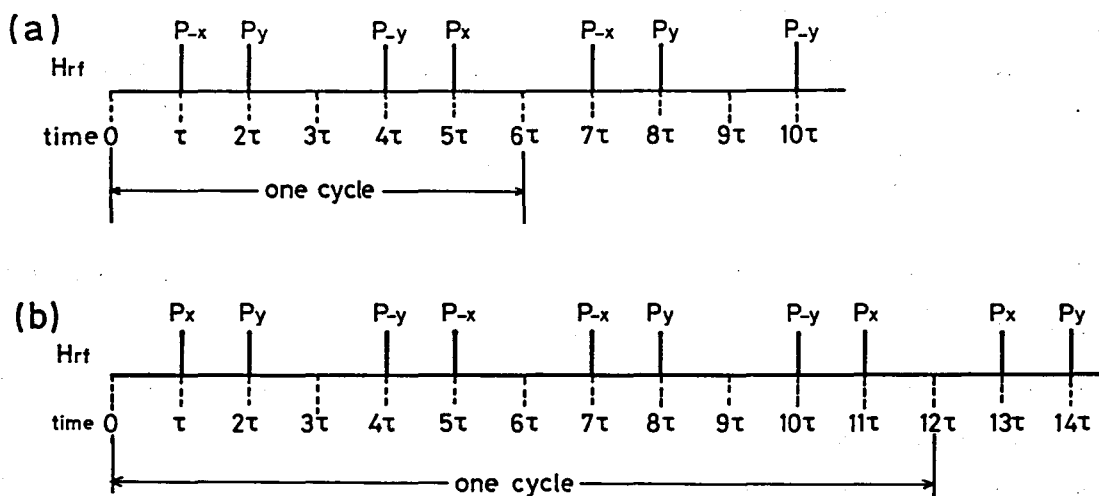

Fig. 2-1. Pulse sequences for (a) WAHUHA-4 and (b) MREV-8.

The usual detection of an NMR signal rests upon the fact that an ensemble of nuclear spins, initially polarized along the z axis as determined by the static magnetic field H_o, will produce a non-vanishing component of the magnetization in the x-y plane when disturbed from equilibrium by an RF field. This component rotates about the z axis at the Larmor frequency, $|\omega_o| = |\gamma H_o|$ (40 MHz for ^{19}F at a field of 1 T), and induces a voltage in an inductor oriented with its axis perpendicular to H_o, which is part of a resonant circuit tuned at ω_o. The observable, then, is a quantity proportional to $<I_y(t)>$, the expectation value of the transverse component (here phase sensitive detection is assumed to set to detect the y-component of the magnetization in the rotating frame) of the spin angular momentum. In terms of the density matrix representation of the time-dependent Schrödinger equation

$$<I_y(t)> = \text{tr } \rho(t)I_y \qquad (2-1)$$

where the density matrix operator, $\rho(t) = \Psi(t)\Psi^*(t)$, is given as the solution of the time dependent Schrödinger equation (with $\hbar = 1$),

$$i\frac{\partial\rho(t)}{\partial t} = [H,\rho]. \qquad (2-2)$$

A specification of $\rho(t)$, i.e. the r.h.s. of eq. 2-2, will therefore specify the time evolution of transverse magnetization observed in a pulsed NMR experiment. It has been recognized that this time domain signal can be converted to the frequency domain absorption signal via Fourier transformation

$$I(\omega) \propto \text{Re}\int_0^\infty e^{-i\omega t}I_y(t)\,dt. \qquad (2-3)$$

The Hamiltonian contains in general time-dependent and time-independent terms. The Hamiltonian may be separated into externally controllable terms (the static and the radio-frequency fields), and uncontrollable terms inherent in the system under study (dipolar fields, quadrupolar interactions, shielding, etc.). It is very convenient to convert the coordinate to the rotating frame in order to discuss the interactions within the system as well as between the system and the external RF field. The rotating frame is chosen so that the Zeeman interaction vanishes effectively, therefore the Hamiltonian accessible to the experimenter as $H_{rf}(t)$, the time-dependent (e.g. pulsed) radio-frequency interactions can easily be treated in this coordinate system. For an ideal delta function pulse along the x axis in the rotating frame, for example,

$$H_{rf} = -\gamma H_{1x} I_x = - \omega_{1x} I_x, \qquad\qquad (2\text{-}4)$$

and the condition that the magnetic moment be rotated by 90° is

$$-\int_0^t H_{rf}(t')dt' = \int_0^t \omega_{1x}dt' = \int_0^{\pi/2} d\theta = \pi/2. \qquad (2\text{-}5)$$

In terms of rotation operators corresponding to a "θ pulse" along an axis ν, for example, the component of angular momentum along an axis η will be transformed to

$$e^{iI\nu\theta} I_\eta e^{-iI\nu\theta} = I_\eta \cos(\theta \cdot \varepsilon_{\nu\eta\lambda}) - I_\lambda \sin(\theta \cdot \varepsilon_{\nu\eta\lambda}),$$
$$\qquad\qquad (2\text{-}6)$$

where ν, η, and λ are some permutation of x,y,z. $\varepsilon_{\nu\eta\lambda}$ is the Levi-Cevita symbol which is unity for ν, η, and λ in cyclic order (e.g. z, x, y), -1 for antisymmetric order (e.g. z, y, x),

and zero if $\nu = \eta$. So, for example,

$$e^{(\pi/2)iI_y} I_z e^{-(\pi/2)iI_y} = - I_x \qquad (2-7)$$

is a new spin angular momentum operator after having been converted from the z-component of the original spin angular momentum by applying the 90° pulse along the y axis of the rotating frame.

The Hamiltonian not accessible to the experimenter (except by manipulation with H_{rf}) is represented by H_{int}. Among number of components in H_{int}, we concentrate our attention to two internal Hamiltonians. One is the secular part of the homonuclear dipolar Hamiltonian within a spin pair i and j. It is given by

$$H_d = \alpha_d (3\cos^2\theta_{ij} - 1)(\underline{I}_i \cdot \underline{I}_j - 3I_{iz}I_{jz}) \qquad (2-8)$$

where

$$\alpha_d = (1/2)\hbar\gamma^2/r_{ij}^3 \cdot s^{-1} \qquad (2-9)$$

and θ_{ij} specifies the angle between the inter nuclear vector $\underline{r}_{ij}$ and external magnetic field $\underline{H}_o$. The second is the anisotropic chemical shift interaction

$$H_c = \alpha_c (3\cos^2\theta - 1)I_z \qquad (2-10)$$

where

$$\alpha_c = \omega_o (1/3) \left[\sigma_{33} + (1/2)(\sigma_{11} + \sigma_{22}) \right] \cdot s^{-1}. \qquad (2-11)$$

Here θ is the angle between the principal z axis of the shielding tensor $\underline{\sigma}$ and $\underline{H}_o$. σ_{33} is the z component of the shielding tensor.

In terms of H_{rf} and H_{int}, eq. 2-2 becomes

$$i\frac{\partial\rho}{\partial t} = \left[(H_{rf} + H_{int}),\rho\right]. \tag{2-12}$$

A transformation to the frame of the RF is made formally as specified by the relation

$$\rho(t) = U_{rf}^{-1}\widetilde{\rho(t)}U_{rf}. \tag{2-13}$$

U_{rf} is determined by H_{rf} via the differential equation (with h = 1)

$$i\frac{\partial U_{rf}}{\partial t} = H_{rf}U_{rf}. \tag{2-14}$$

In the frame of the RF the equation of motion of the density operator is

$$i\frac{\partial\widetilde{\rho}}{\partial t} = \left[\widetilde{H_{int}},\widetilde{\rho}\right]. \tag{2-15}$$

In this frame, H_{int} is controlled by H_{rf} via the relation

$$\widetilde{H_{int}}(t) = U_{rf}^{-1}H_{int}U_{rf}. \tag{2-16}$$

Note the effect of transforming to the frame of the RF, i.e (2-13), is to remove H_{rf} from the description of $\widetilde{\rho}$ (2-15). In addition, U_{rf} is a well known solution [1] to eq. 2-14; the operator that transforms from time 0 to time t is

$$U_{rf}(t,0) = T \exp\{-i\int_0^t H_{rf}(t')dt'\} \qquad (2-17)$$

where T is the Dyson time ordering operator. It suffices here to say that if

$$\int_0^t H_{rf}(t')dt' = 0, \qquad (2-18)$$

then U_{rf} will be unity. Two obvious examples of causes where eq. 2-17 become unity are:

(i) H_{rf} is a 180° pulse at a given phase, followed by a 180° pulse with the same phase. This sequence give rise to a rotation by 360°, being equivalent to no rotation at all.

(ii) Two ideal 90° pulse sequence with opposite phases to each other. Again the net transformation by the two successive pulses corresponds to leaving the spin system unchanged.

It is important to note that (i) and (ii) hold only when any interactions in the spin system does not "strongly" affect ρ in the time over which $H_{rf}(t')$ is integrated. This imposes that

$$|H_{rf}(t')| \gg |H_{int}|. \qquad (2-19)$$

In other words, if the dipolar field is of the order of 5×10^{-4} T, then the magnitude of the RF field should be greater than 5×10^{-3} T. Furthermore the time over which H_{rf} is applied must be short compared with T_2, i.e. short compared with the dipolar line width α_d. For protons with $\gamma = 4.25$ kHz/10^{-4} T, a value of a dipolar field of 5×10^{-4} T corresponds to a dipolar line width of roughly 20 kHz, so $T_2^* \sim 16$ μs

If a suitable coordinate system can be chosen it is possible to eliminate any special interaction from the description of ρ as follows. Suppose a transformation

$$\tilde{\rho} = U_{int}^{-1} \tilde{\tilde{\rho}} U_{int},\qquad (2\text{-}20)$$

where U_{int} varies according to the Liouville equation

$$i\frac{\partial U_{int}}{\partial t} = \widetilde{H_{int}} U_{int}.\qquad (2\text{-}21)$$

The condition that

$$U_{int}^{-1} \widetilde{H_{int}} U_{int} = 0$$

lead to the result

$$i\frac{\partial \rho}{\partial t} = \left[0,\tilde{\tilde{\rho}}\right] = 0.\qquad (2\text{-}22)$$

This implies that $\tilde{\tilde{\rho}}$ appears static in this frame. At time $t = t_c$ the solution of eq. 2-21 is given either by the Dyson expression, e.g. eq. 2-17, or by the Magnus expansion [1],

$$U_{int} = \exp\{-it_c\left[\overline{H}_{int}^{(0)} + \overline{H}_{int}^{(1)} + \cdots\right]\},\qquad (2\text{-}23)$$

where the zeroth-order term is given

$$\overline{H}_{int}^{(0)} = (1/t_c)\int_0^{t_c} \widetilde{H_{int}}(t)\,dt\qquad (2\text{-}24)$$

the first order term by

$$\overline{H}_{int}^{(1)} = -(i/2t_c) \int_0^{t_c} dt \int_0^t dt' \left[\widetilde{H_{int}}(t), \widetilde{H_{int}}(t')\right].$$

(2-25)

The higher term may be obtained by using higher commutators. The density operator in the frame of detection at time t_c is given by

$$\rho(t_c) = U_{int}^{-1} U_{rf} \widetilde{\widetilde{\rho}} \, U_{rf} \, U_{int}.$$

(2-26)

If ρ is formally identified to $\rho(0)$, then eq. 2-26 formally expresses a clue to calculate the time evolution of ρ. If both U_{int} and U_{rf} become unity at time t_c, then

$$\rho(t_c) = \rho(0),$$

(2-27)

and a measurement of an observable, as given by eq. 2-1, at a spcified time t_c, will yield the same result as at time $t = 0$; i.e. it means that in the above-specified coordinate system one can measure any physical quantity under the condition that the time-dependent interaction in the system is effectively zero. In particular, if H_{int} is the homonuclear dipolar interaction (2-8), then measurement of the transverse magnetization at time t_c gives a signal which is unaffected by the homonuclear dipolar interactions and therefore not damped. If H_{rf} is both cyclic,

$$T \exp\left[-i\int_0^t H_{rf}(t)dt\right] = 1$$

(2-28)

and periodic,

$$H_{rf}(t + t_c) = H_{rf}(t)$$

(2-29)

then, via eq. 2-16, $\widetilde{H_{int}}$ will be periodic, such that, for example, for the zeroth-order term at time $2t_c$,

$$
\begin{aligned}
U_{int}(2t_c,0) &= U_{int}(2t_c,t_c)\ U_{int}(t_c,0) \\
&= \exp\{-i\bar{H}_{int}^{(0)}\cdot t_c\}\ \exp\{-i\bar{H}_{int}^{(0)}\cdot t_c\} \\
&= \exp\{-2it_c\bar{H}_{int}^{(0)}\} \qquad\qquad (2\text{-}30)
\end{aligned}
$$

and at a time nt_c where n is an integer,

$$
U_{int}(nt_c,0) = U_{int}^{\,n}(t_c,0). \qquad\qquad (2\text{-}31)
$$

The system therefore looks as if behaved under the influence of some 'average' Hamiltonian, $\bar{H}_{int}^{(0)}$, over the cycle time in question.

If $U_{int}(t_c,0)$ is unity, so do $U_{int}(nt_c,0)$, and if U_{rf} is also unity at these times, both ρ and the expectation value of $I_y(t)$ will be unaffected by H_{int} at the 'window' at nt_c, here the window means the sampling interval between the RF pulses. A familiar example of this situation is the refocussing of a static field inhomogeneity, where the refocussing means the returning to the initial state of the static field after the perturbation of the RF pulses, with operator $-\delta\omega I_z$, by a sequence of two 180^o_x pulses, at echo (cycle) time 4τ, as indicated in Fig. 2-2. Where H_{rf} and $\widetilde{H_{int}}$ become zero as eqs. 2-32 and 2-33.

$$
\int_0^{4\tau} H_{rf}(t)dt = \pi\left[I_z - I_z\right] = 0 \qquad\qquad (2\text{-}32)
$$

$$
(1/4\tau)\int_0^{4\tau}\widetilde{H_{int}}(t)dt = (1/4\tau)\left[\tau I_z - 2\tau I_z + \tau I_z\right] = 0
$$
$$
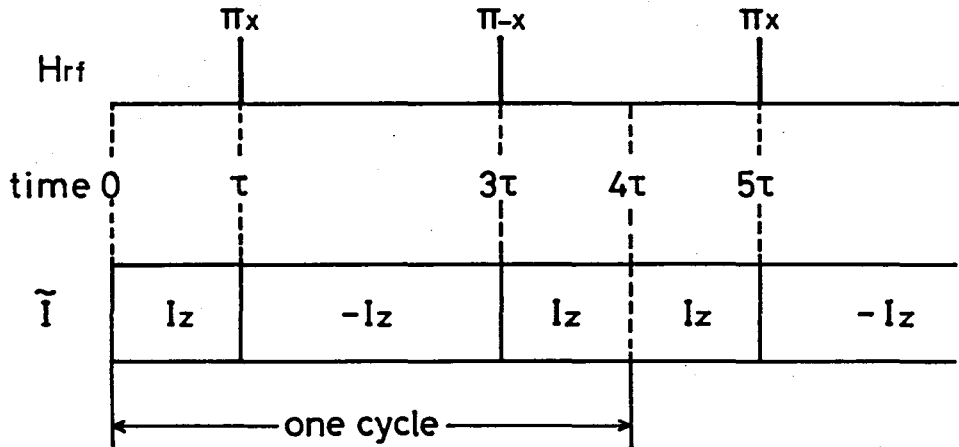\qquad\qquad\qquad\qquad\qquad (2\text{-}33)
$$

Fig. 2-2. The refocussing scheme of a static field inhomogeneity with operator $-\delta\omega I_z$, by a sequence of two π_x pulses, at echo (cycle) time 4τ.

In the case of WAHUHA-4 multiple pulse experiment (see Fig. 2-1), the behavior of I_z, and therefore the two spin Hamiltonian $I_{z1}I_{z2} \equiv Z$ is indicated in Fig. 2-3. Under the assumption of ideal delta function pulses, $\widetilde{H_{int}}$ is need not considered during the pulses as in eq. 2-34.

$$\int_0^{6\tau} H_{rf}(t)\,dt = (\pi/2)\left[-I_x + I_y - I_y + I_z\right] = 0 \qquad (2-34)$$

The integration of the spin portion of $\widetilde{H_{dip}}$ over the time $0 \le t \le 6\tau$ gives rise to
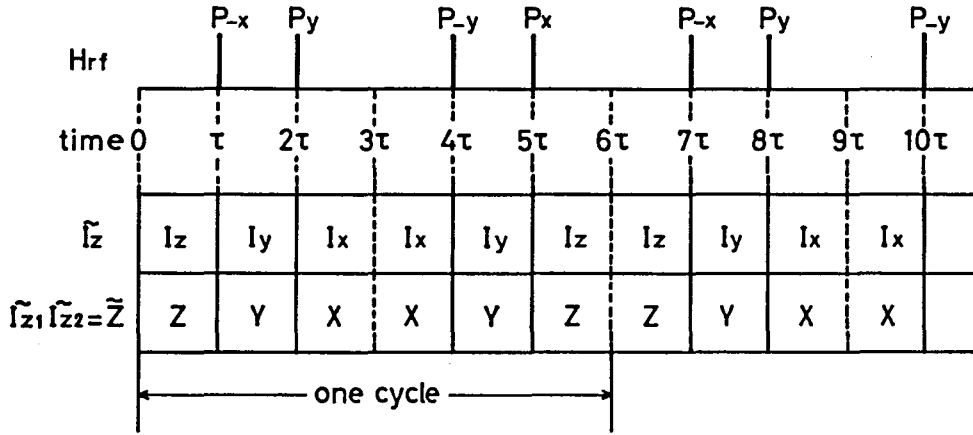
H_{rf}	P-x	Py		P-y	Px		P-x	Py		P-y
time 0	τ	2τ	3τ	4τ	5τ	6τ	7τ	8τ	9τ	10τ
$\tilde{I}_z$	Iz	Iy	Ix	Ix	Iy	Iz	Iz	Iy	Ix	Ix
$\tilde{I}_{z1}\tilde{I}_{z2}=\tilde{Z}$	Z	Y	X	X	Y	Z	Z	Y	X	X

|←————— one cycle —————→|

Fig. 2-3. The refocussing scheme and the behavior of I_z in WAHUHA-4 pulse sequence.

$$\int_0^{6\tau} \widetilde{H_{dip}}(t)dt = \alpha_d \int_0^{6\tau} (\widetilde{\underline{I}_1 \cdot \underline{I}_2} - \widetilde{3I_{z1}I_{z2}})dt$$

$$= \alpha_d \{6\tau \underline{I}_1 \cdot \underline{I}_2 - 3\tau(Z + Y + 2X + Y + Z)\}$$

$$= 6\tau\alpha_d(\underline{I}_1 \cdot \underline{I}_2 - \underline{I}_1 \cdot \underline{I}_2)$$

$$= 0 \qquad\qquad (2-35)$$

This indicates that the homonuclear dipolar Hamiltonian vanishes under the $(\tau,\ 90^o_{-x},\ \tau,\ 90^o_y,\ 2\tau,\ 90^o_{-y},\ \tau,\ 90^o_x,\ \tau)$ pulse sequence. Therefore, the free-induction decay (FID) signal sampled every 6τ time in WAHUHA-4 pulse sequence is not influenced by the homonuclear dipolar interaction, and then gives a high resolution NMR spectrum.

- 21 -

The chemical shift interaction is reduced a little as can be seen in eq. 2-36,

$$(1/6\tau)\int_0^{6\tau} H_c(t)dt = (1/6\tau)\alpha_c(3\cos^2\theta - 1)(\tau I_z + \tau I_y + 2\tau I_x$$

$$+ \tau I_y + \tau I_z)$$

$$= (1/3)\alpha_c(3\cos^2\theta - 1)(I_x + I_y + I_z)$$

$$= (1/\sqrt{3})\alpha_c(3\cos^2\theta - 1)\,\overline{I}_z \qquad (2\text{-}36)$$

where

$$\overline{I}_z = (1/\sqrt{3})(I_x + I_y + I_z).$$

The standard and multiple pulse chemical shift Hamiltonians are essentially the same. They differ in two minor points only: the multiple pulse chemical shift Hamiltonian contains an extra factor (scaling factor) of $1/\sqrt{3}$ and the spin operator is not along the z direction of the rotating frame, but along the [111] direction of the rotating frame.

The analogous scheme for MREV-8 pulse sequence is given in Fig. 2-4.

The integral of the H_{rf} and $\widetilde{H_{dip}}$ over the time $0 \leq t \leq 12\tau$ (one cycle) becomes zero. The treatment in this case is almost the same as that encountered in eqs. 2-34 and 2-35. The chemical shift interaction is
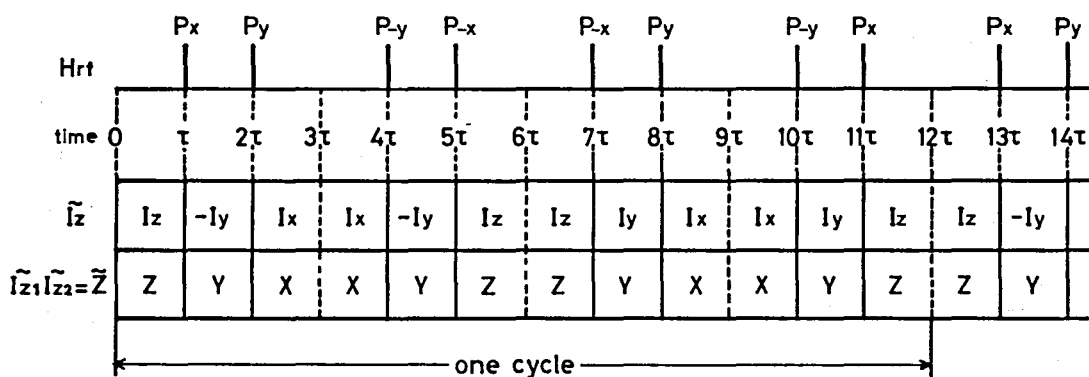
Fig. 2-4. The refocussing scheme and the behavior of I_z in MREV-8 pulse sequence.

$$(1/12\tau)\int_0^{12\tau} H_c(t)\,dt = (1/3)\alpha_c(3\cos^2\theta - 1)(I_x + I_z)$$

$$= (\sqrt{2}/3)\alpha_c(3\cos^2\theta - 1)\,\overline{I}_z ,$$

$$(2\text{-}37)$$

where

$$\overline{I}_z = (1/\sqrt{2})(I_x + I_z).$$

The multiple pulse spectrum is thus free from dipolar broadning. Scaling factor is $\sqrt{2}/3$ and the spin operator is not along the z axis of the rotating frame, but again along a cube face diagonal.

- 23 -

2-3   Magic Angle Specimen Rotation

Magic angle spinning technique (MAS) is the simplest approach
to the problem of removing dipolar interaction in solids proposed
by Andrew et al.[2] and Lowe.[3]   This subject has been developed
considerably both theoretically[4] and experimentally.[5]

In this technique, the solid specimen is rotated at high speed
about an axis tilted by 54.74° from the direction of the static
external magnetic field; This special angle is called the magic
angle.   Of course, the motion of the molecule in the solid is
correlated, unlike that of a liquid, and the dipolar interaction
is reduced in this instance by virtue of the rotational
transformation dependence of the strength of dipolar interaction on
the angle between the rotation axis and the static field vector.

Rotation at the magic angle also removes chemical shift
anisotropy.   In this sense the absorption line shape is more akin
to that of liquid.   Unfortunately, the applicability of the MAS
technique is limited to rather narrow lines because the rate of the
sample rotation should be greater than the dipolar line width in
order to attain effective line narrowing.   The static dipolar line
width can vary from a few kiloherz in usual phosphorus compounds
to a few tens of kiloherz for fluorinated compounds to at most
one hundred kiloherz for the broadest proton line in number of
inorganic and organic materials.   Practical problem is that the
rate of sample rotation can not exceed 10 kHz because of the
difficulty of mechanical device construction.   Nevertheless,
valuable results have been obtained by the MAS method.

Briefly theoretical examination of the MAS technique is as
follows.   The truncated dipolar interaction Hamiltonian, for all

nuclear pairs i, j in the solid, both like and unlike, is

$$H_d = \sum_{i<j}(1/2)\gamma_i\gamma_j\hbar^2 r_{ij}^{-3}(\underline{I}_i\cdot\underline{I}_j - 3I_{iz}I_{jz})(3\cos^2\theta_{ij} - 1),$$

$$(2-38)$$

where γ_i, γ_j are the nuclear gyromagnetic ratios, $\underline{r}_{ij}$ is the internuclear displacement, and θ_{ij} is the angle between $\underline{r}_{ij}$ and the Zeeman field $\underline{Ho}$, which is directed along the z axis in the laboratory frame (see Fig. 2-4).
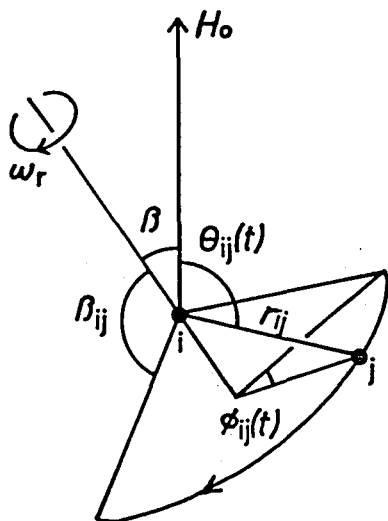

Fig. 2-4. Diagram illustrating the motion of typical internuclear vector $\underline{r}_{ij}$ when a solid is rotated with angular velocity ω_r about an axis inclined to angle β to $\underline{Ho}$.

Since the dipolar field is usually very small compared with Ho, the NMR spectrum can be calculated by treating H_d as a perturbation on the Zeeman term H_z,

$$H_z = - \sum_i \gamma_i\hbar\underline{I}_i\cdot\underline{Ho}. \qquad (2-39)$$

Since the isotropic average $\overline{\cos^2\theta_{ij}} = 1/3$, it follows from eq.(2-38) that isotropic average of the dipolar Hamiltonian, $\overline{H_d} = 0$, and rapid isotropic motion in liquid state therefore averaged out the dipolar interaction in the NMR spectrum.

In a solid specimen, irrespective monocrystalline, polycrystalline or amorphous, being rotated uniformly with angular velocity ω_r along the axis by an angle β from the static magnetic field $\underline{Ho}$, every internuclear vector $\underline{r}_{ij}$ in the solid undergoes a motion illustrated in Fig. 2-4. Then the angle θ_{ij} becomes time dependent, and the factor $(3\cos^2\theta_{ij} - 1)$ in eq. (2-38) too.

According to the theorem for the spherical harmonics

$$\cos\theta_{ij} = \cos\beta\cdot\cos\beta_{ij}' + \sin\beta\cdot\sin\beta_{ij}'\cdot\cos(\omega_r t + \phi_{oij}),$$

$$(2\text{-}40)$$

where β_{ij}, ϕ_{ij}, etc. are illustrated in Fig. 2-3 and ϕ_{oij} is the initial value of ϕ_{ij}. Substitution of Eq.(2-40) into Eq.(2-38) gives

$$H_d = (1/2)\sum_{i<j}(1/2)\gamma_i\gamma_j\hbar^2 r_{ij}^{-3}(\underline{I}_i\cdot\underline{I}_j - 3I_{iz}I_{jz})$$
$$\times\{(1/2)(3\cos^2\beta - 1)(3\cos^2\beta_{ij} - 1)$$
$$+(3/2)\sin2\beta\cdot\sin2\beta_{ij}\cdot\cos(\omega_r t + \phi_{oij})$$
$$+(3/2)\sin^2\beta\cdot\sin^2\beta_{ij}\cdot\cos2(\omega_r t + \phi_{oij})\}. \qquad (2\text{-}41)$$

The first term in the curly bracket is constant, while the second and the third terms are periodic with zero mean value. It is convenient to divide H_d into two terms, its mean value $\overline{H_d}$ and the remainder, which is periodic with mean value:

$$H_d = \overline{H_d} + (H_d - \overline{H_d}). \qquad (2\text{-}42)$$

The first term on the right hand side is constant and gives a reduced dipolar interaction and the narrowed spectrum, while the second term, which is periodic in ω_r and $2\omega_r$, gives rise to rotational side bands at multiples of ω_r. The explicit form of $\overline{H_d}$ is

$$H_d = (1/2)(3\cos^2\beta - 1)\sum_{i<j}(1/2)\gamma_i\gamma_j\hbar^2 r_{ij}^{-3}$$
$$x(\underline{I}_i\cdot\underline{I}_j - 3I_{iz}I_{jz})(3\cos^2\beta_{ij}' - 1). \qquad (2\text{-}43)$$

Comparing Eq.(2-38) and Eq.(2-43), it can be seen that the spectrum for polycrystalline or amorphous material retaines the identical shape, but is reduced in width by a scale factor

$$F(\beta) = \left[(1/2)(3\cos^2\beta - 1)\right]. \qquad (2\text{-}44)$$

Some particular values for $F(\beta)$ are calculated below

For $\quad \beta = 0, \qquad\qquad\qquad F(\beta) = 1;$

$\qquad \beta = (\pi/2), \qquad\qquad\qquad F(\beta) = 1/2;$

$\qquad \beta = \arccos(1/\sqrt{3}) = 54^\circ 44'08'', \; F(\beta) = 0.$

Rotation about $\underline{H}_0$ has no effect, rotation about an axis normal to $\underline{H}_0$ halves the spectral width, while rotation about an axis making the magic angle, $54^\circ 44'08''$, to $\underline{H}_0$ reduces the dipolar broadning to zero.

Although line narrowing can be performed in this way, there is an inevitable disadvantage in the MAS technique that removes chemical shift anisotropy at the same time. It turns to advantage when one studies a spectrum of powdered samples in which there are many magnetically inequivalent nuclear spins that will make the spectrum too complicated and/or in which there is a large anisotropy in the chemical shift.

2-4 Proton Enhanced NMR

Another approach to the high resolution solid state NMR is called Proton Enhanced Nuclear Induction Spectroscopy (Proton Enhanced NMR)[6] or Cross Polarization NMR. This technique is applicable only to rare spins such as ^2D, ^{13}C, ^{15}N, ^{29}Si, etc. The reason can easily be understood by coming back to the dipolar Hamiltonian. Secular part of dipolar Hamiltonian between homonuclear spins is

$$H_{II} = (1/2)\gamma_I^2 \hbar^2 \sum_{i,j} r_{ij}^{-3}(1 - 3\cos^2\theta_{ij})(\underline{I}_i \cdot \underline{I}_j - 3I_{iz}I_{jz})$$

and between heteronuclear spins is
$$\text{(2-45)}$$

$$H_{IS} = \gamma_I\gamma_S \hbar^2 \sum_{i,j} r_{ij}^{-3}(1 - 3\cos^2\theta_{ij})I_{iz}S_{jz}. \qquad \text{(2-46)}$$

H_{IS} depends on r_{ij}^{-3}; therefore, it is negligible between rare spins. When the system contains a large number of abundant spins such as ^1H, or ^{19}F, so that H_{IS} is appreciably large, high resolution NMR spectrum of rare spins in solid state is expected to be observed by the decoupling technique to eliminate H_{IS}. However, in the case of rare spins a signal with good S/N ratio can hardly be obtained due to low natural abundance. Since spin-lattice relaxation time is usually very long for rare spins, the signal accumulation and averaging technique is inefficient.

A. Pines et al.[6] could solve this problem by combining the ideas of double resonance[7] with the decoupling scheme. In this technique abundant spin I is used to polarise the rare spins S and receive the excess energy from the rare spin as a resorvoir. Since the T_1 of S is determined by that of I, the recovery of magnetization is fast enough to permit rapid accumulation of the signal.

The general procedure is shown schematically in Fig. 2-5 and described below.
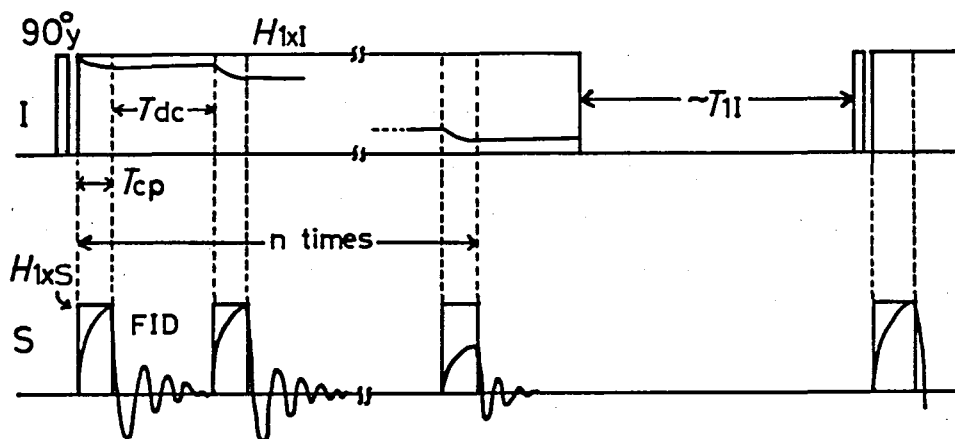
Tcp   cross polarization
Tdc   I decoupling
T_{1I} spin lattice relaxation time of
       abundant spin I

Fig. 2-5. The pulse sequence for cross-polarization NMR.
During the contact pulse, the Hartmann-Hahn condition,
$\gamma_I H_{1xI} = \gamma_S H_{1xS}$, must be met.

(1) Polarize I in high external field. (2) Cool I to a low spin temperature in the rotating frame (spin lock). (3) Establish I-S contact for a time T_{cp} (under the Hartmann-Hahn cross relaxation condition, $\gamma_I H_{1I} = \gamma_S H_{1S}$). (4) Recorde the S free induction decay while I is decoupled. Steps (3) and (4) are repeated N_I/N_S times while the I polarization is depleted and meanwhile the S signal is accumulated, here N_I and N_S are the number of I and S spins respectively in the system. Then the

accumulated signal of S is Fourier transformed to obtain the spectrum.

The Hartmann-Hahn condition states that the Zeeman levels of I and S have the same value in the rotating frame, and so the energy exchange can occur between I and S via dipolar interaction H_{IS}. As a result, the S spin polarization occurs efficiently in the direction of H_{1S} and the enhanced signal of S can be obtained.

This technique is applicable only to rare spins, but yields informations on the components of the shielding tensors.

References to Chapter 2

1) R. M. Wilcox, J. Math. Phys., $\underline{8}$, 962 (1967).

2) a) E. R. Andrew, A. Bradbury, and R. G. Eades, Nature, London, $\underline{182}$, 1659 (1958).

   b) E. R. Andrew, A. Bradbury, and R. G. Eades, Archs Sci., Geneve, $\underline{11}$, 223 (1958).

3) I. J. Lowe, Phys. Rev. Lett., $\underline{2}$, 285 (1959).

4) E. D. Ostroff and J. S. Waugh, Phys. Rev. Lett., $\underline{16}$, 1097 (1966).

5) P. Mansfield and D. Ware, Phys. Rev. Lett., $\underline{22}$, 133 (1966).

6) A. Pines, M. G. Gibby, and J. S. Waugh, Chem. Phys. Lett., $\underline{15}$, 373 (1972).

7) S. R. Hartmann and E. L. Hahn, Phys. Rev., $\underline{128}$, 2042 (1962).

3 Determination of Chemical Shift Tensors

3-1 Single Crystal Study

Since chemical shift is usually very small compared with the Larmor frequency $(10^{-4} \sim 10^{-6})$, we may apply first-order perturbation theory to calculation of the chemical shift Hamiltonian. In the presence of the chemical shift perturbation the energy eigenvalue for the spin I can be formally written as

$$<m|\gamma \underline{Ho} \cdot \underline{\sigma} \cdot \underline{I}|m> = m\gamma\sigma_L \underline{Ho}, \tag{3-1}$$

where σ_L represents the component of $\underline{\sigma}$ parallel to $\underline{Ho}$. When the chemical shift tensor in some coordinate system (x,y,z) is represented by

$$\underline{\sigma} = \begin{pmatrix} \sigma_{xx} & \sigma_{xy} & \sigma_{xz} \\ \sigma_{yx} & \sigma_{yy} & \sigma_{yz} \\ \sigma_{zx} & \sigma_{zy} & \sigma_{zz} \end{pmatrix} \tag{3-2}$$

σ_L can be written as[1]

$$\sigma_L = \underline{n} \cdot \underline{\sigma} \cdot \underline{n}^{-1} = \sigma_{xx}\sin^2\theta \cdot \cos^2\phi + \sigma_{yy}\sin^2\theta \cdot \sin^2\phi + \sigma_{zz} \cdot \cos^2\theta$$
$$+ \sigma_{yx}\sin^2\theta \cdot \sin 2\phi + \sigma_{zx}\sin 2\theta \cdot \cos\phi$$
$$+ \sigma_{xy}\sin 2\theta \cdot \sin\phi. \tag{3-3}$$

where $\underline{n}$ is the unit vector along $\underline{Ho}$, defined by the polar angle θ and the azimuthal angle ϕ in the coordinate system (x,y,z).

A common procedure to find the six independent components of the chemical shielding tensor is to rotate the crystal around the three orthogonal axes and measure the shifts as a function of the rotation angle ρ. Such a rotation pattern for K_2GeF_6 single crystal is shown in Fig.5-13. From the analysis of the rotational patterns, full tensor components can be determined.

3-2 Powder Pattern Study

For a polycrystalline or amorphous solid, the orientation of the chemical shift tensor with respect to the static magnetic field is randomly distributed and thus a characteristic 'powder pattern' is obtained.

The powder pattern is calculated as follows,[2]

$$f(\sigma) = \pi^{-1}(\sigma - \sigma_{11})^{-\frac{1}{2}}(\sigma_{33} - \sigma_{22})^{-\frac{1}{2}}K(m) \qquad (3-4)$$

with

$$m = (\sigma_{22} - \sigma_{11})(\sigma_{33} - \sigma)/(\sigma_{33} - \sigma_{22})(\sigma - \sigma_{11}) \qquad (3-5)$$

when

$$\sigma_{33} \geq \sigma \geq \sigma_{22}$$

and

$$f(\sigma) = \pi^{-1}(\sigma_{33} - \sigma)^{-\frac{1}{2}}(\sigma_{22} - \sigma_{11})^{-\frac{1}{2}}K(m) \qquad (3-6)$$

with

$$m = (\sigma - \sigma_{11})(\sigma_{33} - \sigma_{22})/(\sigma_{33} - \sigma)(\sigma_{22} - \sigma_{11}) \qquad (3-7)$$

when

$$\sigma_{22} > \sigma \geq \sigma_{11}$$

and also

$$f(\sigma) = 0 \qquad (3-8)$$

when

$$\sigma > \sigma_{33} \text{ and } \sigma < \sigma_{11}.$$

Here $K(m)$ is the complete elliptic integral of the form,

$$K(m) = \int_{0}^{\pi/2} (1 - m\sin^2 r)^{-\frac{1}{2}}dr. \qquad (3-9)$$

In equations (3-4) $\sim$ (3-8), σ_{11}, σ_{22}, and σ_{33} are the principal values and the definition $\sigma_{33} \geq \sigma_{22} \geq \sigma_{11}$ has been adopted as a matter of convention.

In the case that $\underline{\sigma}$ has the axial symmetry, e.g., $\sigma_{11} = \sigma_{22}$, the powder pattern takes the form

$$f_{ax}(\sigma) = (1/2)(\sigma_{33} - \sigma_{11})^{-\frac{1}{2}}(\sigma - \sigma_{11})^{-\frac{1}{2}} \qquad (3\text{-}10)$$

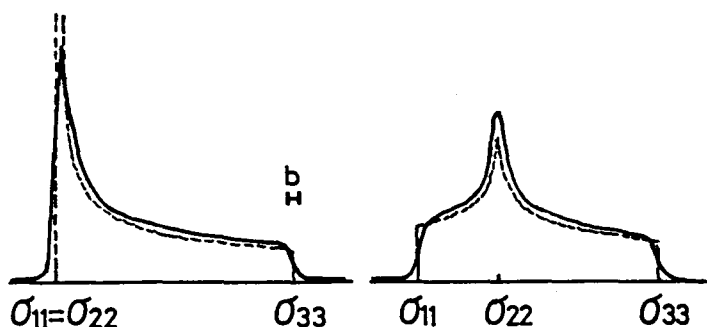The line shapes with and without the axial symmetry are shown in Fig. 3-1.

Fig. 3-1. Schematic representation of theoretical powder line shapes. Broken line: zero line width case. Solid line: the theoretical curves convoluted with Lorentzian broadning functions, where width b is indicated. (a) axially symmetric tensor, (b) $\sigma_{11} < \sigma_{22} < \sigma_{33}$.

It is evident from Fig. 3-1 how the magnitudes of the principal shielding components (σ_{11}, σ_{22}, σ_{33}) can be determined directly from the powder pattern. However, the orientation of the σ tensor can not be obtained. Therefore it is not possible to relate the shielding tensor to the molecular bond frame from the powder pattern. Only in special case where there is a high crystal symmetry and simple molecular or ionic structure, analysis of the

chemical shift data can be used to elucidate the bond structure as will be described in § 5-2. Mehring et al.[3] could determine the shielding tensor direction in the molecular frame with the aid of knowledge of the type of molecular motion. Only from the powder pattern analysis, very interested information about molecular motion has been obtained, such as jump motion in P_4,[4] $C_6(CH_3)_6$,[5] and so on.

References to Chapter 3

1) J. A. Weil, T. Buck, and J. E. Clapp, Adv. Magn. Reson., <u>6</u> 183 (1973).

2) N. Bloembergen and T. J. Rowland, Acta Metall., <u>1</u>, 731 (1953).

3) M. Mehring, R. G. Griffin, and J. S. Waugh, J. Am. Chem. Soc., <u>92</u>, 7222 (1970).

4) H. W. Spiess, Chem. Phys., <u>6</u>, 217 (1974).

5) D. E. Wemmer, D. J. Ruben, and A. Pines, J. Am. Chem. Soc., <u>103</u>, 28 (1981).

4 Construction of Spectrometer for High Resolution NMR in Solid

4-1 Introduction

In the present work the spectrometer was designed to work at 40 MHz (suitable to ^{19}F resonance at 1 T), whose organization is shown in Fig. 4-1.
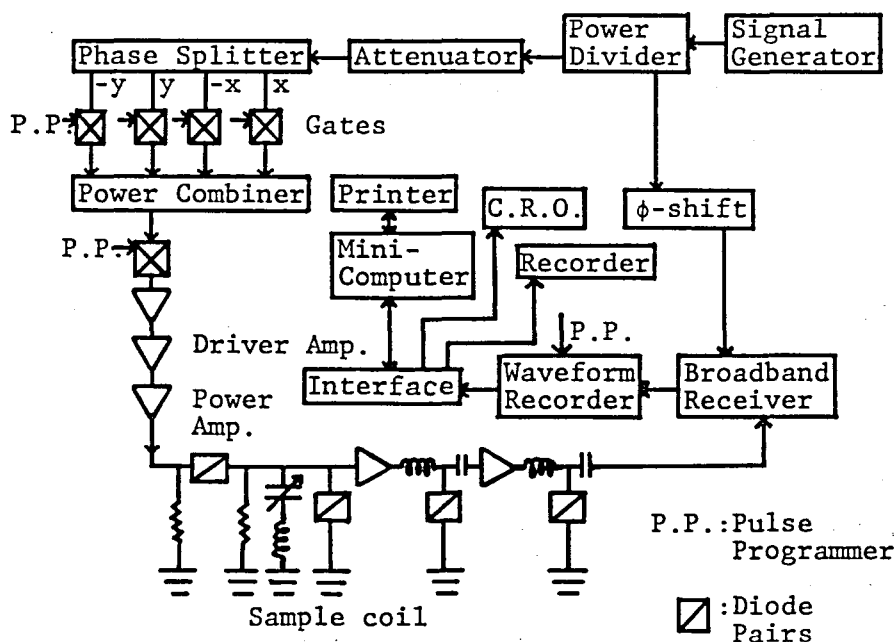
Fig. 4-1. Organization of spectrometer. This spectrometer operates at 40 MHz.

A carrier signal from a signal generator is divided into two channels by a power divider. One carrier is fed into a broadband receiver for phase sensitive detection and another one through an

attenuator to a phase splitter [1] in which carriers with four
different phases are produced. These four independent carriers are
fed into the RF gates which are controlled by DC pulses generated in
the pulse programmer and connected into the RF pulses with four
different phases. The four RF-outputs of the RF gates are combined
by a power combiner and used to drive an RF power amplifier. This
amplifier can produce the RF pulses with the power greater than
1 kW which are then fed into the sample coil via matching unit.
The FID signal induced at the sample coil is led into a broadband
receiver, amplified, and connected into a video signal through the
phase sensitive detection. Passive dampers [2] are inserted between
the sample coil and the receiver to protect the receiver from the
high power RF pulses and to make the dead time of the receiver
system short. The FID signal after phase sensitive detection is
digitally recorded by a waveform recorder. The digital data are
then transfered into a minicomputer through a home-built interface,
accumulated when necessary, and Fourier-transformed to give an
NMR absorption spectrum. The data can be displayed on a CRO or
recorded on an X-Y recorder through an interface system. The
pulse intervals, the repetition period of the sequence, and the
data aquisition timing are controlled by a pulse programmer.

For the readers convenience to follow the each section in this
Chapter, a simplified block diagram of the spectrometer is presented
in Fig. 4-2. The labels (A - J) in this block diagram indicate
the subsection number where the interpretation of the individual
components is given. The following particular cases were taken on
designing the spectrometer: In multiple pulse high resolution NMR
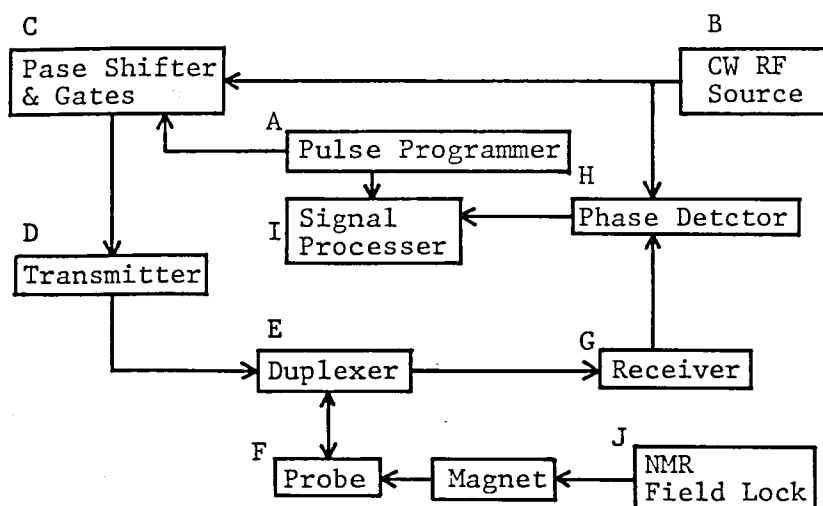experiments, it is necessary to reduce the dipolar interaction

C
```
Pase Shifter
& Gates
```
B
```
CW RF
Source
```

A
```
Pulse Programmer
```
H

D
I
```
Signal
Processer
```
```
Phase Detctor
```

```
Transmitter
```

E
```
Duplexer
```
G
```
Receiver
```

F
J
```
Probe
```
```
Magnet
```
```
NMR
Field Lock
```

Fig. 4-2. Block diagram of the spectrometer. Each block is labeled by a character (A - J) to which each subsection in section 4-2 corresponds.

Hamiltonian, H_{int}, between the nuclear spins to zero or approximately zero by some means. This can be realized in the case of abundant spin system by applying a set of the RF pulses with specified phases to the system to average out the H_{int}. In order to average out the H_{int} effectively by the use of the RF pulses the following condition should be satisfied:

$$\gamma H_{rf} \gg |H_{int}|/\hbar$$

where γ is the gyromagnetic ratio of the nuclear spin, and H_{rf} the strength of the RF magnetic field. Since the local dipolar field of

protons (and fluorines) in solids may amount an order of 20 G, H_{rf} must in general be greater than 100 G, corresponding to an RF pulse power of about 1 kW. An RF power transmitter stage was designed to meet the above condition (see 4-2-D).

The interval of pulses should be shorter than the spin-spin relaxation time, since the multiple pulse technique can be effective only when H_{int} can be regarded as the average Hamiltonian. This requires that the interval of pulses is shorter than 10 μs, a typical spin-spin relaxation time in proton or fluorine systems. Moreover, to observe the FID between these pulse sequences the dead time of the receiver should be less than a few microseconds. A preamplifier (gain 40 dB) with a recovery time of about 3 μs together with dampers to prevent the large amplitude RF pulses to pass into the receiver system were designed (4-2-E).

In multiple pulse technique, a sequence of four (WAHUHA-4) or eight (MREV-8) independent pulses with a certain intervals are used. The sequences consist of the combination of four pulses, whose phases differ by 90°, 180°, or 270° with each other. Therefore, the four phase-shifters or splitters and the four independent RF gates are needed. The phase error should be less than 3°. Hence the controlable phase splitters [1] were employed to achieve this condition (4-2-C).

The intervals of pulses also should be precisely adjusted (less than ten nano seconds). The clock synchronous TTLs were adopted to produce WAHUHA-4 and MREV-8 pulse sequences and monostable multivibrators were employed to adjust the pulse widths of the four pulses independently.

It is desirable to maintain good stabilities of the RF source

and the Zeeman field to within 1 ppm for ^{19}F and 0.1 ppm for ^{1}H in order to make the signal accumulation technique effective. The Zeeman field source is a JEOL JM-310 electromagnet which is designed for wide line NMR. Its stability is not sufficiently high for high resolution NMR. Therefore, NMR static field locking system was developed (4-2-J).

4-2 Spectrometer Design and Construction

A. Pulse Programmer

The pulse programmer consists of a single 10 MHz clock pulse
oscillator, the time multiplier, and the pulse sequence generator.
The pulse sequence generator is constructed from TTL logic circuits
situated on plug-in cards. The plug-in pulse programmer was
designed to provide the timing for WAHUHA-4 and MREV-8 multiple
pulse experiments.

The pulse programmer must provide a) the trigger pulse to
initialize the whole system including the transient recorder, b) a
sequence of four (WAHUHA-4) or eight (MREV-8) independent pulses,
P_x, P_{-x}, and so on, to excite the RF gates, the intervals and
widths of which are precisely controlable, c) the sampling pulses
for the transient recorder at the interval 6τ to collect the FID
signal, d) a long pulse to hold the field-lock system during the
pulse sequence, and must generate a waiting period during which
the magnetization can return to the original value with the time
constant T_1, the spin-lattice relaxation time. Therefore this
waiting period has to be determined in relation to T_1 of the spin
system.

Timing chart for WAHUHA-4 method, e.g., is shown in Fig. 4-3.
The MREV-8 pulse sequence is analogous to this scheme.

A pulse programmer which performs the above-mentioned functions
was designed and constructed: The cicuit diagram is given in
Figs. 4-4 and 4-5.

A combination of 10 MHz quartz oscillator and frequency
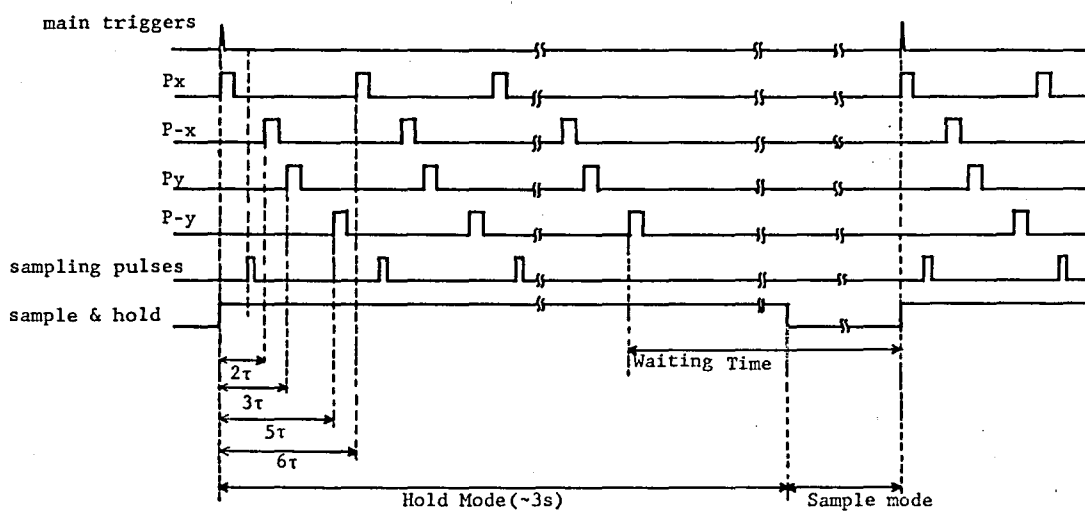divider provide the clock pulse. The cyclic triggering pulses for

main triggers

Px

P-x

Py

P-y

sampling pulses

sample & hold

2τ

3τ

5τ

6τ

Waiting Time

Hold Mode(~3s)

Sample mode
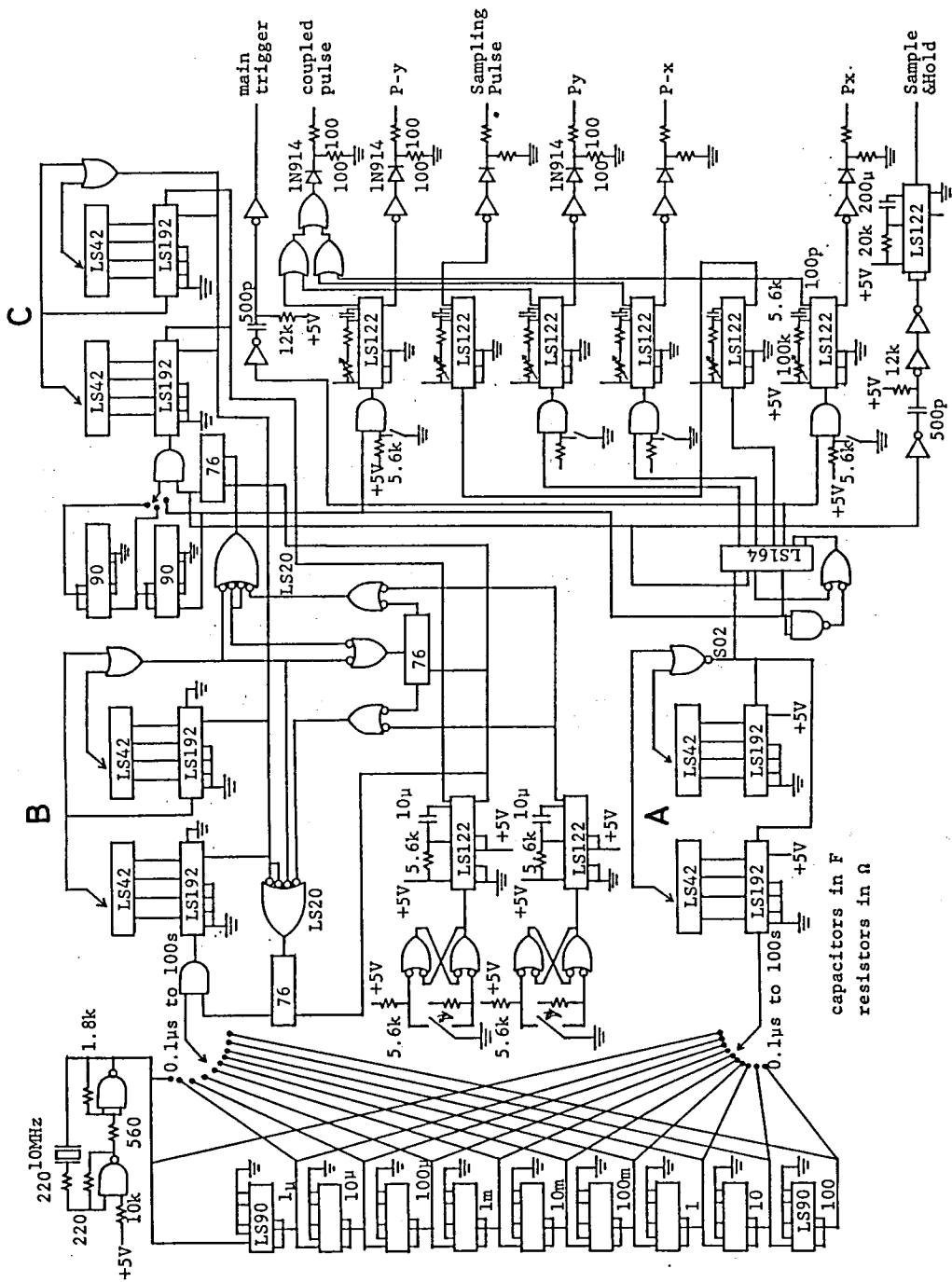
Fig. 4-3. Timing chart for WAHUHA-4.

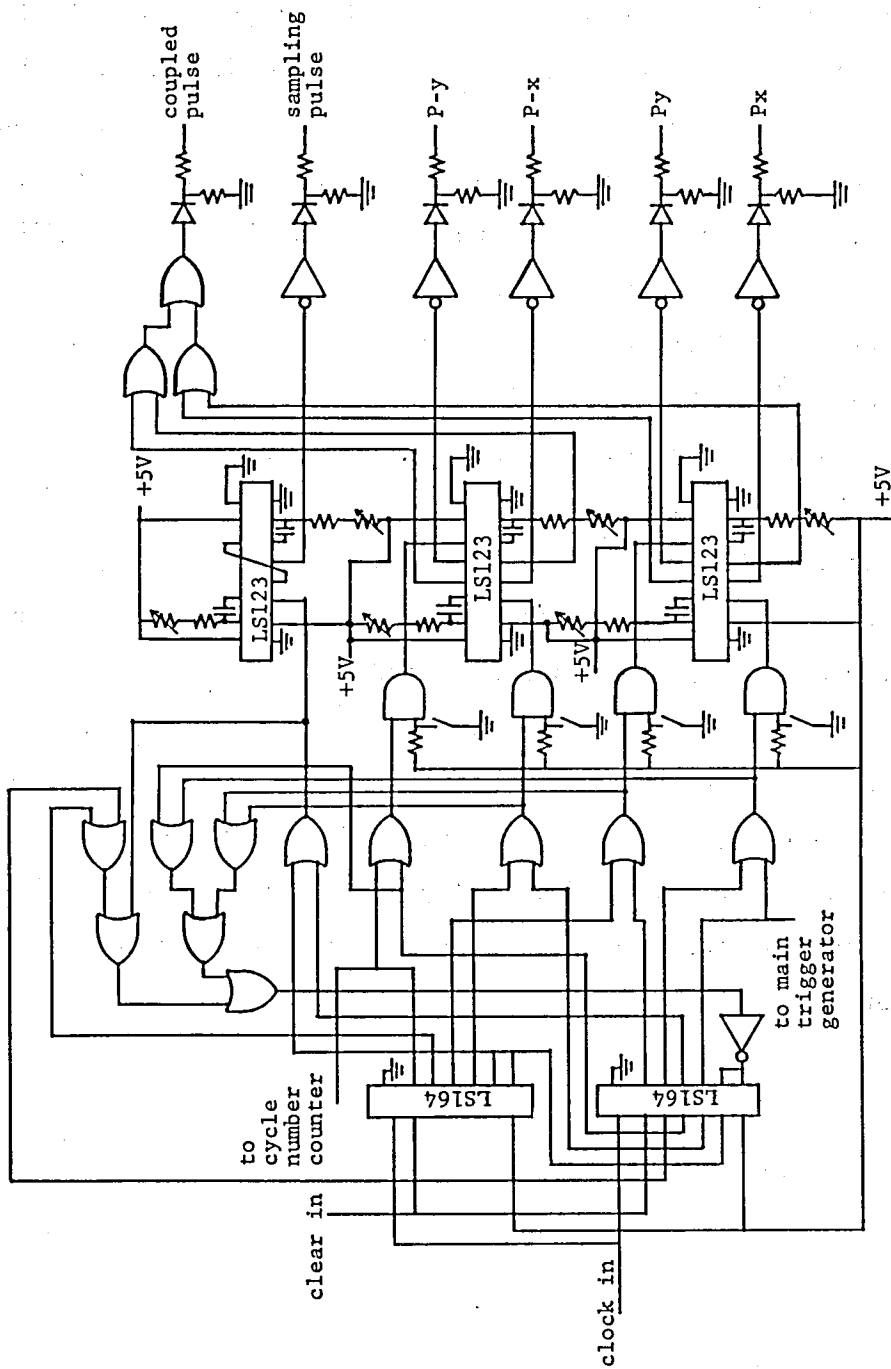Fig. 4-4. Organization of pulse programmer for WAHUHA-4.

- 44 -

Fig. 4-5. Organization of plug-in unit for MREV-8.

$P_x \sim P_{-y}$ in WAHUHA-4 sequence with the cycle time 6τ is generated by employing an 8 bit parallel-out serial shift registor SN74LS164 as the 6-bit ring counter which is driven by the clock pulse. The pulse interval, τ, corresponds to the cycle time of clock introduced in SN74LS164 and is set by the counter A, the waiting time by the counter B, and cycle number by the counter C. Cycle time for MREV-8 is 12τ, therefore two SN74LS164s are used.

The output of SN74LS164, used as triggering pulse, are fed into monostable multivibrators (SN74LS122, SN74LS123) which generate the pulse with finely adjustable width to drive the RF gate. A long holding pulse for the field-lock device and the sampling pulse for FID are also obtained using SN74LS122.

All adjustment operation can be done with nobs, dials, etc. on the front panel except when program card is replaced (MREV-8 or WAHUHA-4). The front view of the pulse programmer is shown in Fig. 4-6. The pulse interval and the waiting time can be changed from 0.1 µs to 9900 s, and the cycle number from 1 to 9900 times. The pulse width can be varied from 0.4 µs to 7.0 µs continuously by changing the resistance of helipot connected to monostable multivibrator.
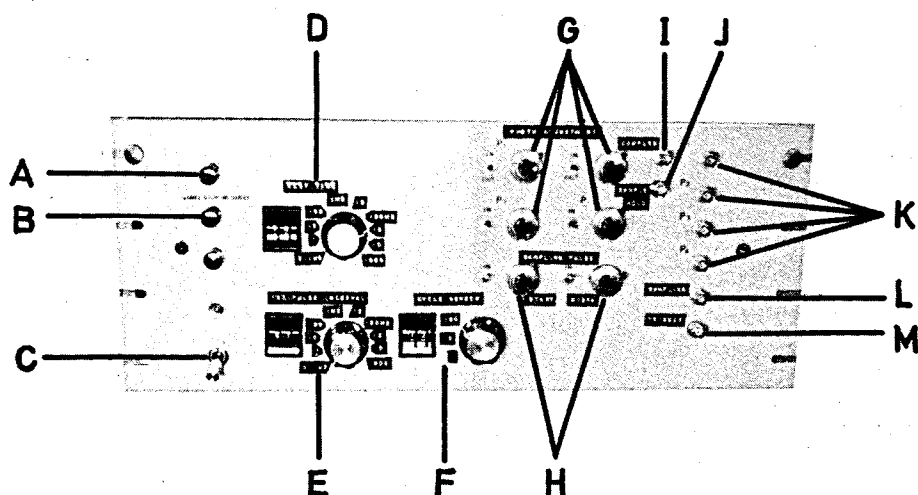
Fig. 4-6. Front panel of the pulse programmer. Functions
are follows. A: reset, B: start, C: power switch, D: waiting
time, E: pulse interval setting, F: cycle number setting,
G: pulse width adjustment, H: sampling time setting, I: output
to second gate, J: output to sample & hold circuit, K: outputs
to first gates, L: output to waveform recorder for sampling,
M: output to waveform recorder for trigger.

B CW RF Source

The spectrometer is designed to work at 40 MHz to study ^{19}F
resonances. The frequency synthesizer (model 3325A Hewlett-
Packard) was employed as 40 MHz RF source. The frequency of this
synthesizer is stabilized to within 0.1 ppm when the room
temperature is constant but varies about 0.4 ppm by the change
of 1 $^{\circ}$C of room temperature.

C. Phase Splitter and Gate

Multiple pulse experiment requires 90° pulses along the x,
-x, y, and -y directions in the rotating frame, corresponding to
four different carriers with relative phases 0°, 90°, 180°,
and 270°. To generate four 90° pulses with a specified exact
phase relation with each other, three phase splitters (one 0°-90°
and two 0°-180°) were constructed and shown in Figs. 4-7 and 4-8.
These are minor modifications of a circuit originally designed by
Jeffrey.[1] The fine adjustment of the phase is done by variable
capacitor and the pulse-height is controled by variable resistors
equipped at the bases of transistors.

Each of four CW outputs of the phase splitter is fed into a
solid state gate (model SW-1, R&K) which is driven by the pulse
from the pulse programmer, and the RF pulses from the four gates
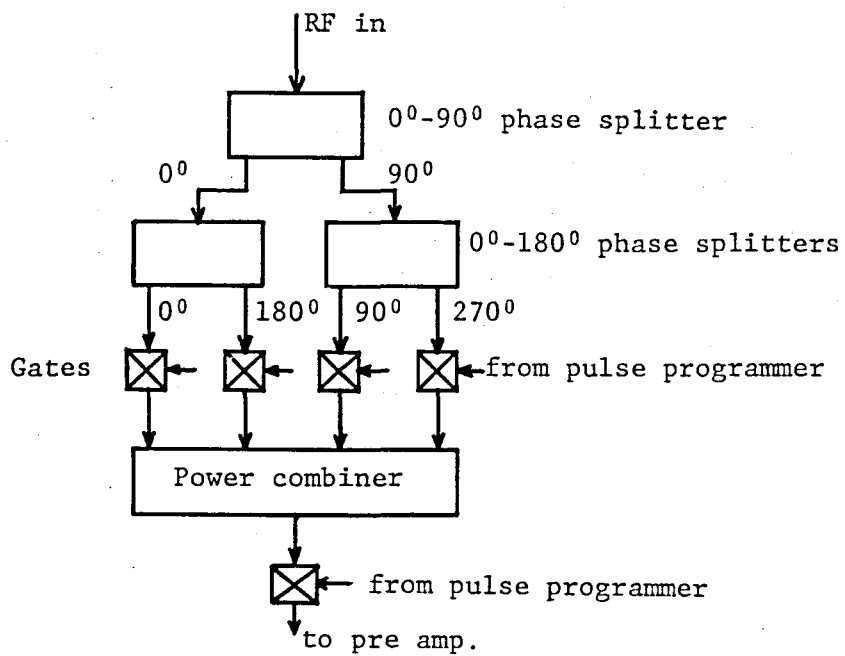are combined with a power combiner (model PD-3, R&K).

RF in

0⁰-90⁰ phase splitter

0⁰   90⁰

0⁰-180⁰ phase splitters

0⁰   180⁰   90⁰   270⁰

Gates ← from pulse programmer

Power combiner

← from pulse programmer

to pre amp.

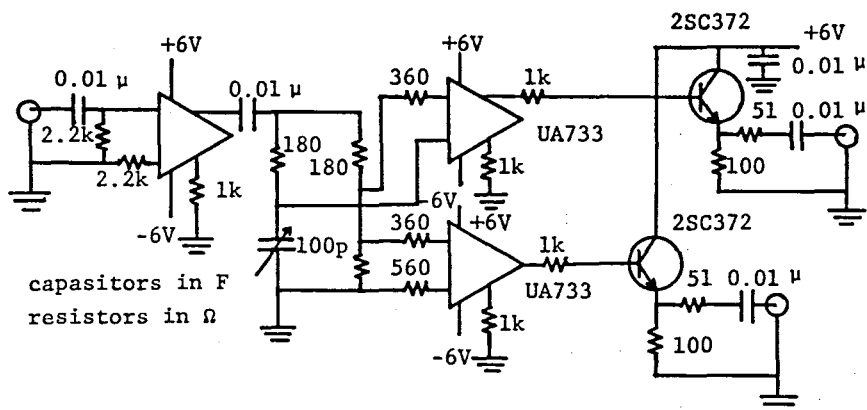Fig. 4-7.   RF pulse modulator with four different carriers.
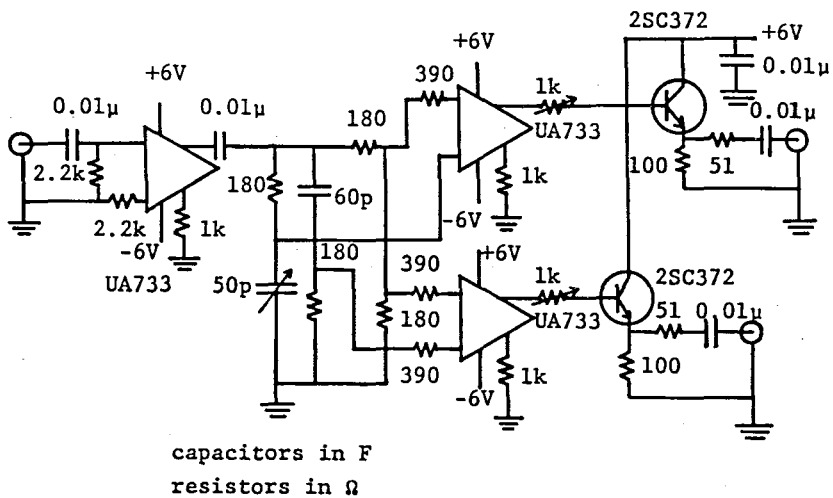
Fig. 4-8a. 0° - 90° phase splitter.

Fig. 4-8b. 0° - 180° phase splitter.

- 50 -

D. Transmitter

Multiple pulse line narrowing experiments require that

$$\gamma H_1 \gg |H_{int}|/\hbar \tag{4-1}$$

where H_{int} is the "magnitude" of the interaction Hamiltonian between the nuclei, γ the gyromagnetic ratio, and H_1 is the RF magnetic field strength in the rotating frame (see § 2-2). Since the local dipolar field of protons in solids is of order of 20 G, H_1 fields of greater than 100 G should be applied to the sample. The H_1 field in a sample coil is given by[3]

$$H_1 = 3(PQ/\nu_o V)^{\frac{1}{2}} = 3(P/\Delta \nu V)^{\frac{1}{2}} \tag{4-2}$$

where H_1 is the rotating field in Oe, P the RF power in watts, $Q = \nu_o/\Delta\nu$ the quality factor of the coil, ν_o the resonance frequency of the circuit in MHz, and V is the volume of the coil in cm^3. The band width $\Delta\nu$ of an RLC circuits is related to the rise time T_r of the pulsed H_1 field as follows

$$T_r = 2/(\pi\Delta\nu) = 2Q/(\pi\nu_o). \tag{4-3}$$

In order to reduce possible error in the phase adjustment at the transient time during the rise and fall period of the pulsed H_1 field, T_r has to be very short. If T_r is $\leq$ 200 ns, i.e., $\Delta\nu \sim 3.3$ MHz, and so Eq.(4-3) indicates that under these conditions, even with such small volumes of the sample coil as 0.25 cm^3, an RF power of at least 1 kW is needed to produce field greater than 100 G.

The transmitter consists of three stages as follows (Fig. 4-2).
1) Tuned preamplifier 2) Wideband driver stage 3) Tuned power amplifier

Tuned preamplifier is composed of two stages of 20 dB amplifier each using 3SK40 as shown in Fig. 4-9.[4]

3SK40
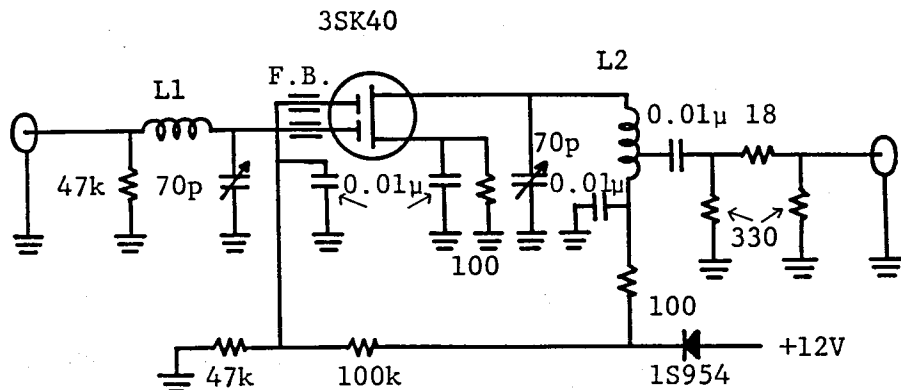
resistors in Ω
capasitors in F

Fig. 4-9. Tuned preamplifier.

2) The driver stage amplifier is a commercial, solid-state, broadband amplifier (model 4020L, Electronic Navigation Industries) which generate 20 W RF pulses.

3) Tuned power amplifier is a home-built tuned class C amplifier using 2B46P and 2B29P shown in Fig. 4-10. The 2B46P is first driven by the broadband amplifier described in 2). And then RF pulses are amplified by a 2B29P. In multiple pulse experiments, the complete pulse burst length might range from 10 ms to seconds. The RF power supplied to the probe was kept constant over the whole burst by using a capacitor with large capacity in the power suuply. Although this final amplifier can produce pulses of more than 1 kW, it was operated at less than the maximum power to avoid the droop of pulse heights.
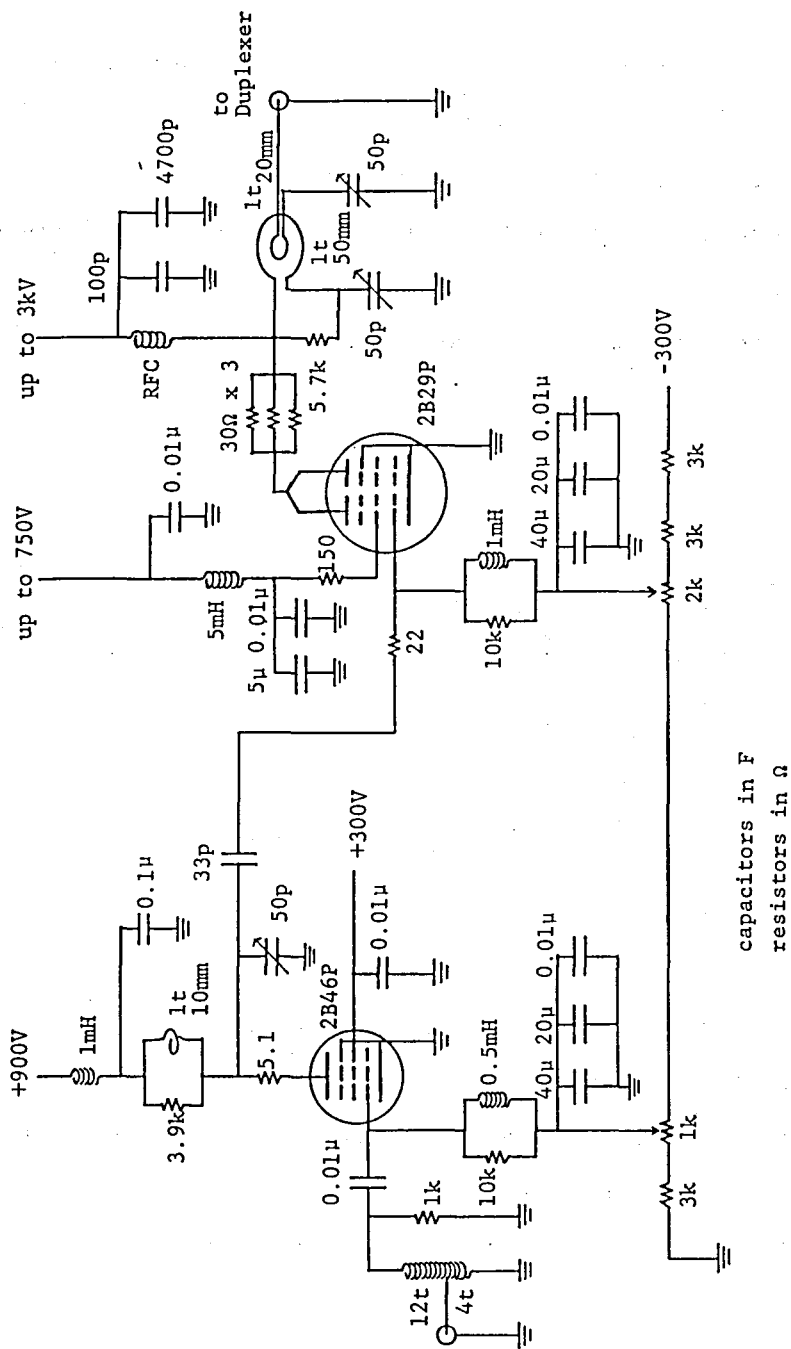
Fig. 4-10. 40 MHz tuned amplifier providing more than 1 kW of RF pulse power.

capacitors in F
resistors in Ω

E.   Duplexer

The ideal duplexer is a fast single-pole, double-throw switch which connects the probe to the transmitter and disconnects the receiver in the transmitter mode, whereas during signal reception the probe is connected to the receiver and completely disconnected from the transmitter.

Duplexer and preamplifier are shown in Fig. 4-11.
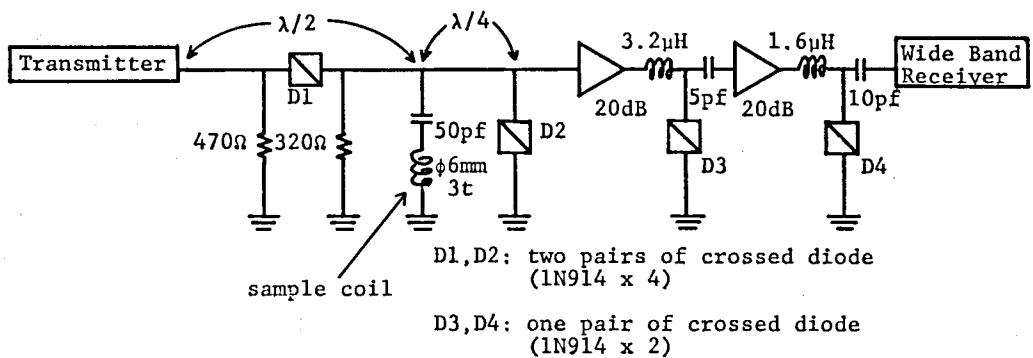

Fig. 4-11.   Duplexer and preamplifier.

In order to minimize the power loss in the transmitter stage the $\lambda/2$ cable was emplyed to connect the transmitter with the probe.[5]   The $\lambda/4$ cable with diode short[5] and passive dampers[6] were adopted between receiver amplifiers to make the dead time of the receiver system short.   The dead time of this spectrometer is about 5 µs.

F. Probe

The probe consists of a single coil in a series tuned circuit which can be tuned easily and can provide RF power to the sample efficiently. The position and the form of the probe are shown in Fig. 4-11.

G. Receiver

The chief requirements for the receiver are to have a low noise figure of a few dB, sufficient band width of several tens kilohertz to pass the nuclear signals without distortion, and the short recovery time of a few microseconds from the 1 V overload that may appear at the output of the duplexer.

Two homebuilt tuned preamplifiers and a commercial wideband receiver (model 625 , Matec) were employed in this stage. Passive dampers are placed between them. Preamplifiers are the same as that shown in Fig. 4-9. Noise figure of the preamplifier is 2.0 dB and its gain is 20 dB. A white noise is suppressed by this tuned amplifier. Although there is a little loss due to passive dampers, the total gain is more than 100 dB, and so NMR signal can be easily detected.

H. Phase Detection

A commercial double balanced mixer (model MC-13, R&K) was employed for the phase detection circuit.

I. Signal Processing

Multiple pulse NMR experiments require sampling of FID in a certain time interval. A typical output from the spectrometer's phase detector and the timing of sampling are shown in Fig. 4-12.

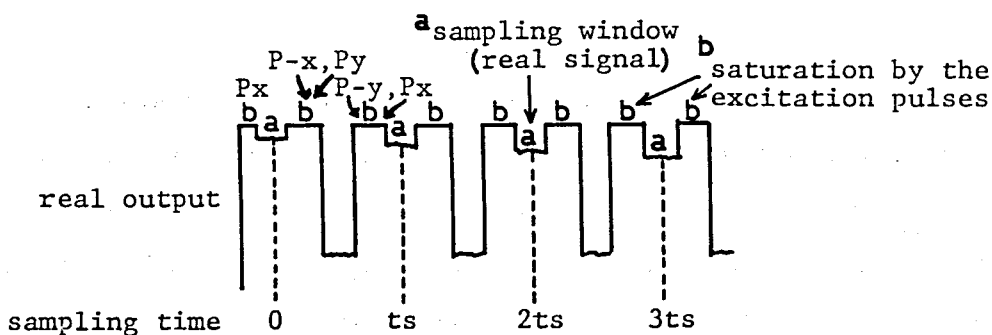Fig. 4-12. Actual receiver output during a multiple pulse experiment.

Real signal appears at time intervals labeled by a. b represents the saturated parts due to RF pulses. Signals must be sampled in multiple pulse sequence, that is, real signal parts are recorded digitally with an interval of t_s. Therefore short recovery time is also required for digital memory since sampling window (part a

in Fig. 4-12) lasts only a few microseconds after pulses.
Commercial waveform recorder (model 805, Biomation) was employed,
which is gated by the series of the sampling pulses at τ, 7τ, $\cdots$
in Fig. 4-3, where 6τ is equal to t_s in Fig. 4-12, and collects
the nuclear signal there. This waveform recorder can collect the
data up to 2048 points, and converts analog data to 8-bit digital
ones. Digital data memorized in the waveform recorder are then
transformed into a minicomputer (NOVA-01) through a home-built
interface and accumulated when necessary, and Fourier-transformed
to give an NMR absorption spectrum.

The data accquisition process is controled using ASSENBLY
program of NOVA-01 and processing afterwards, such as Fourier
transform, is performed with BASIC program.[6] Data can be displayed
on CRO and recorded on an X-Y recorder through an interface.

When the sampling interval is 40.2 μs and there are 1024 data
points, the spectrum resolution is 24.29 Hz and covers the
frequency range of 24.88 kHz. In multiple pulse experiments,
above values are to be multiplied by about $\sqrt{3}$ due to scaling
factor (see § 2-2). The BASIC program for data processing is
listed in the appendix.

J. NMR Field Lock

When signal averaging is necessary, of major importance is
the stability of the DC field for a long time. The DC field
source is a JEOL JM-310 electromagnet which is designed for wide

line NMR: Its stability is not sufficiently high for the high

resolution spectra and therefore a unique NMR static field lock

system is employed to keep the H_o constant. The principle is as

follows. ^{1}H signal in H_2O doped with $CuSO_4$ is detected in a CW

mode as the reference signal, fed into a lock-in amplifier. Its

output is the derivative of the resonance line as shown in

Fig. 4-13 and so between the points a and b it is propotional

roughly to the deviations of the H_o from the central position O.
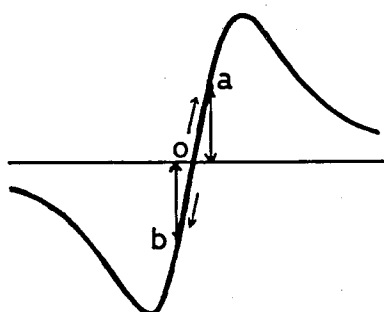

Fig. 4-13.

The lock point in NMR signal.

This output voltage (i.e. the error voltage) is amplified and

used through a power amplifier to drive the modulation coils wound

around the pole-pieses of the magnet in a negative-feedback manner,

so that *Ho* is pulled back to the exact resonance point O.

Fig. 4-14 is the block diagram of the field stabilizer. Usual NMR

field lock systems adopt the Zeeman modulation technique to detect

the reference signal but it is unsuitable for the high

resolution multiple pulse experiment because even a small

modulation of the *Ho* affect the nuclear signal collected over a

long time. Therefore the method of frequency modulation was

F.M.

Signal Generator

Power Divider

Auto Lock-in Amp.

φ shift

Hybrid Junction

50 Ω

Double Balanced Mixer
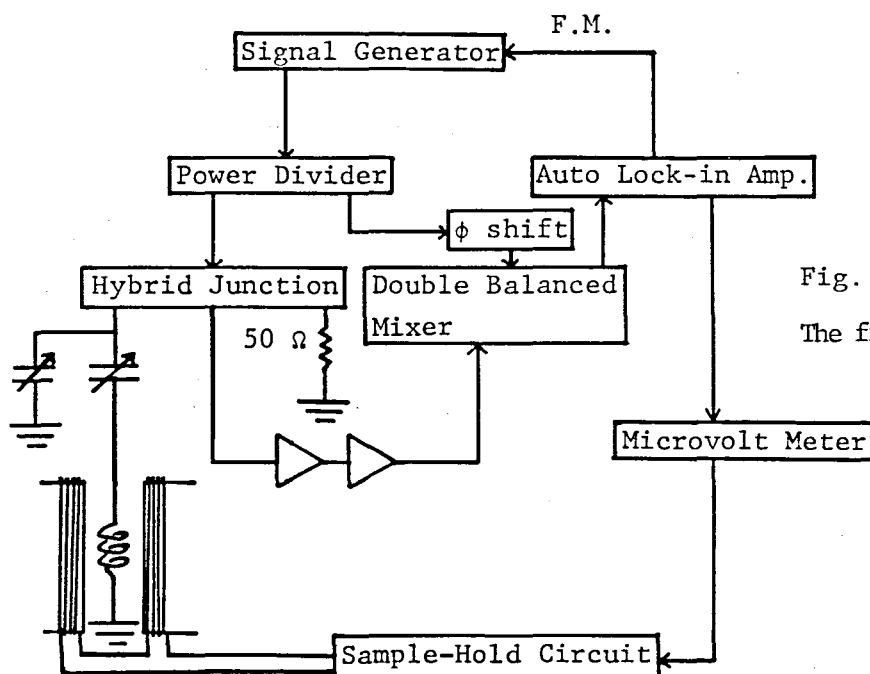
Microvolt Meter

Sample-Hold Circuit

Fig. 4-14.

The field stabilizer

adopted. In order to make the system to be able to respond to the temperature change of the sample and to avoid possible interference between the field lock system and the pulse spectrometer assembly, the external lock technique is employed.

Signal generator (model 3000, Wavetek) frequency-modulated by auto lock-in amp. provides the carrier frequency at 42.538 MHz (suitable for ^{1}H resonance at 1 T) with the stability of ± 0.1 ppm over a day. The carrier signal is divided into two channels by a power divider (model PD-1, R&K). One carrier is fed into a double balanced mixer (model M-13, R&K) and another one through a hybrid junction (model HYB-1, R&K) to the probe coil (with water) which is

shielded in a copper can. The output of the hybrid junction is
amplified by two stage tuned amplifiers (gain 40 dB, the same as
in Fig. 4-9) and conducted to double balanced mixer in which the
phase sensitive detection is performed. The output voltage of
lock-in amp. supplies current to the modulation coil through a
D.C. amplifier and a sample-hold circuit. The sample-hold circuit is
needed to avoid the effects of high power RF pulses, the details
of which are shown in Fig. 4-15. IH5040 and IH5042 (Intersil) are
analog switches.
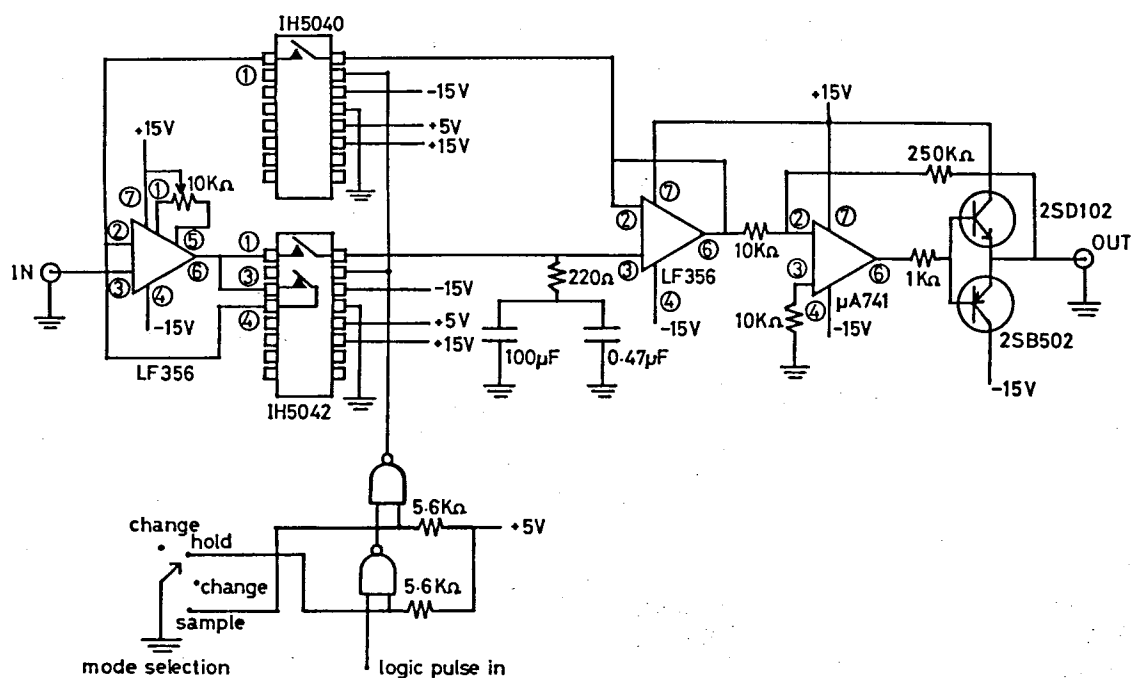

Fig. 4-15. Sample—hold circuit.

Another simpler sample-hold circuit was later designed as shown in Fig. 4-16 by using an analog memory (model EUW-AlC, National).
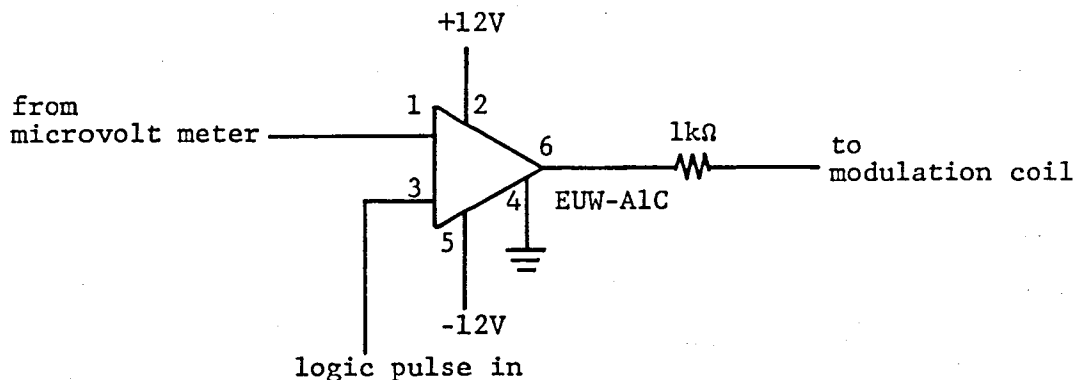

Fig. 4-16. Sample-hold circuit.

Both apparatus can be used successfully to control the static high field Ho. The overall stability of the Ho with the present field-lock system is better than $\pm$ 1 ppm ($\pm$ 40 Hz).

4-3 Operation

This section presents a brief example of the operation of the spectrometer.

The multiple-pulse line-narrowing experiments involve application of a series of 90° pulses with exactly defined phases between which the sampling points of the magnetization lie. As the number of sampling points is usually 512 or 1024, even small error in the pulse width or the phase, or the phase error at rise and fall transients of pulses will accumulate quickly to produce a fatal error for the experiment. Hence, in order to obtain high resolution NMR spectra careful adjustment of those quantities is necessary. A description of the adjustment procedure to obtain the optimum condition of the spectrometer will be given here. The test sample is protons in $CuSO_4$ doped water.

(1) pulse width adjustment

A string of simple kind of pulses $(90^{O}_{x}-t-90^{O}_{x}-t-90^{O}_{x}-t-)_{n}$ is applied, where t is about 100 μs. The signal at the sampling window appears at the points "+, 0, -, 0, +, 0, -, ⋯" as shown in Fig. 4-17, but due to imperfect nature of the pulse shape and/or due to the deviation from the exact 90°, the signal usually decays as t increases.
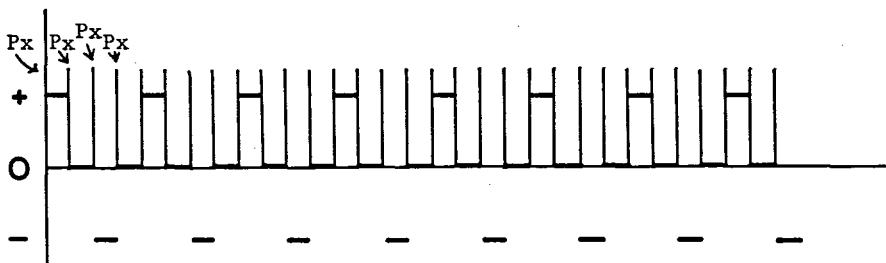

Fig. 4-17. Receiver output in $(90^{O}_{x}-t-90^{O}_{x}-t-)_{n}$ pulse train.

Optimum condition for this P_x pulse can be found by changing the pulse width and looking for the point for which the decay rate of the signal becomes minimum. The same procedure is repeated for each of the pulses with different phases.

(2) phase adjustment of x against -x

A flip flop sequence $(90^o_x-t-90^o_{-x}-t-90^o_x-t-90^o_{-x}-t-)_n$ is employed as shown in Fig. 4-18, where t is about 100 μs. The signals labelled by "+, 0, +, 0, +, 0,···" decay with time and the optimum point will be obtained by adjusting the relative phases of P_x and P_{-x} so that the decay time constant becomes maximum.
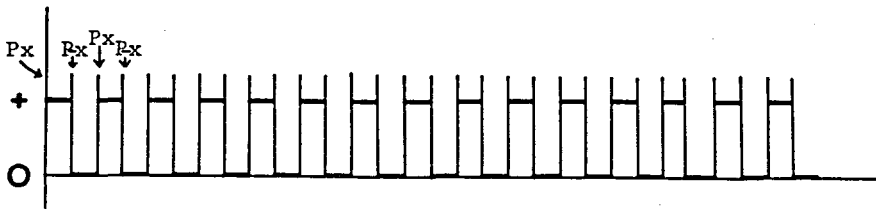
Fig. 4-18. Receiver output in $(90^o_x-t-90^o_{-x}-t-)_n$ pulse train.

(3) phase adjustment of x against y

A pulse sequence $(90^o_x-t-90^o_y-t-90^o_y-t-90^o_x-t-)_n$ is employed.[7] The signal appears as "+, +, +, 0, 0, 0, -, -, -, 0, 0, 0, +, +, +, ···". The optimum point will be obtained by adjusting the relative phases of P_x and P_y so that the decay time constant becomes maxmum.

(4) final pulse width adjustment

Finally fine pulse width adjustment is done by applying multiple pulse sequence (WAHUHA-4 or MREV-8) on CaF_2 single crystal.

Adjustment of the pulse width of each of four pulses from P_x to P_{-y} is carried out by a trial and error iterative procedure so that the decay rate of the FID becomes minimum. The half width of the most narrow spectrum obtained for CaF_2 single crystal after the above procedure is 8.5 ppm (scaling factor is 0.5). FID and spectrum are shown in Fig. 4-19.
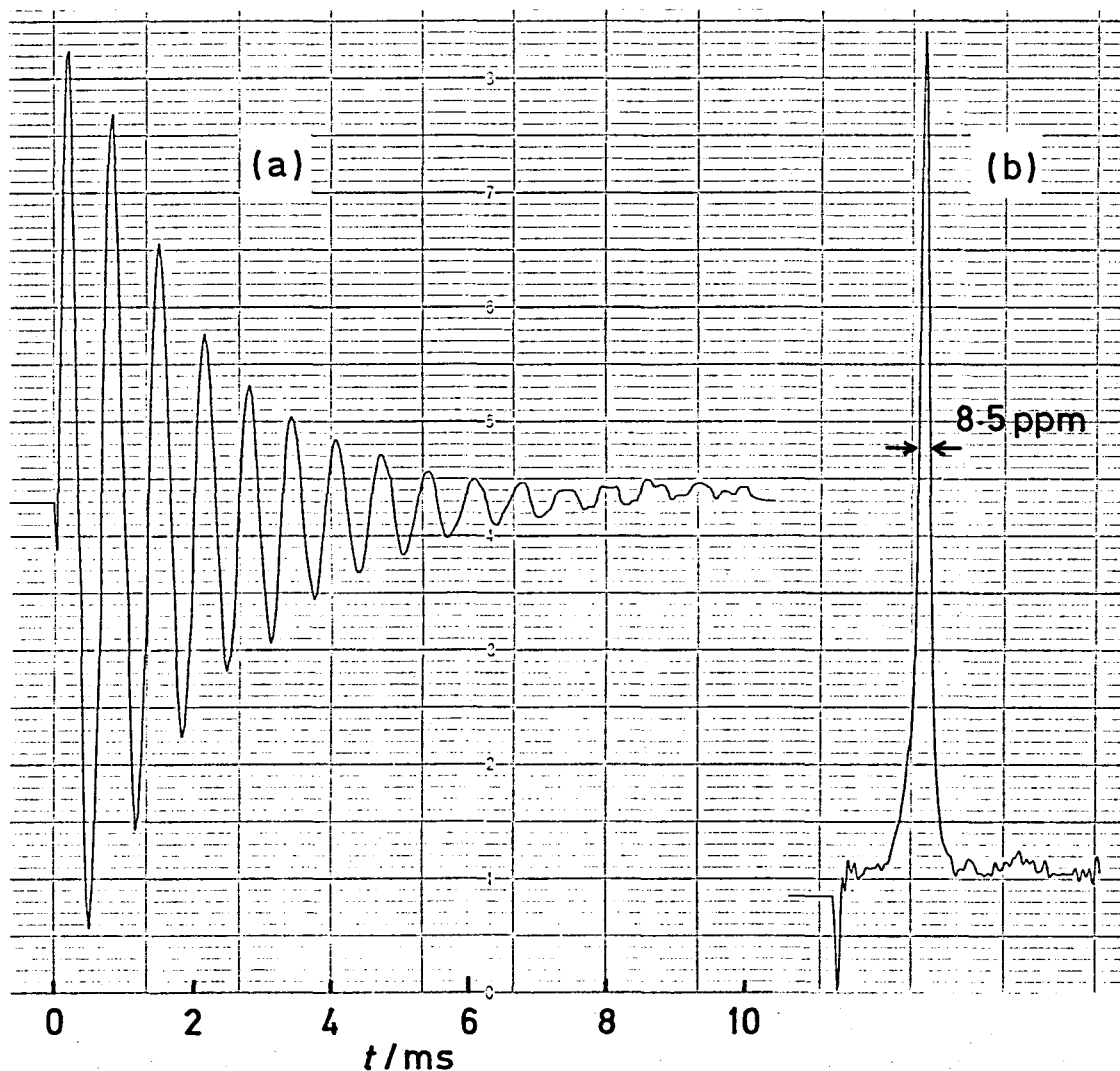
Fig. 4-19. (a) FID of CaF_2 single crystal with MREV-8 pulse sequence. (b) FFT spectrum of FID in (a).

Chemical shift values obtained in multiple pulse measurement is small compared with the true shift obtained in usual high-resolution technique. The reduction factor called scaling factor must therefore be evaluated to discuss the multiple pulse NMR spectra on the same ground as the common high resolution NMR. Two scaling techniques employed are described below.

(1) In Fig. 4-20, the position of the center of ^{19}F NMR spectrum in K_2SiF_6 powder is plotted against the carrier frequency.
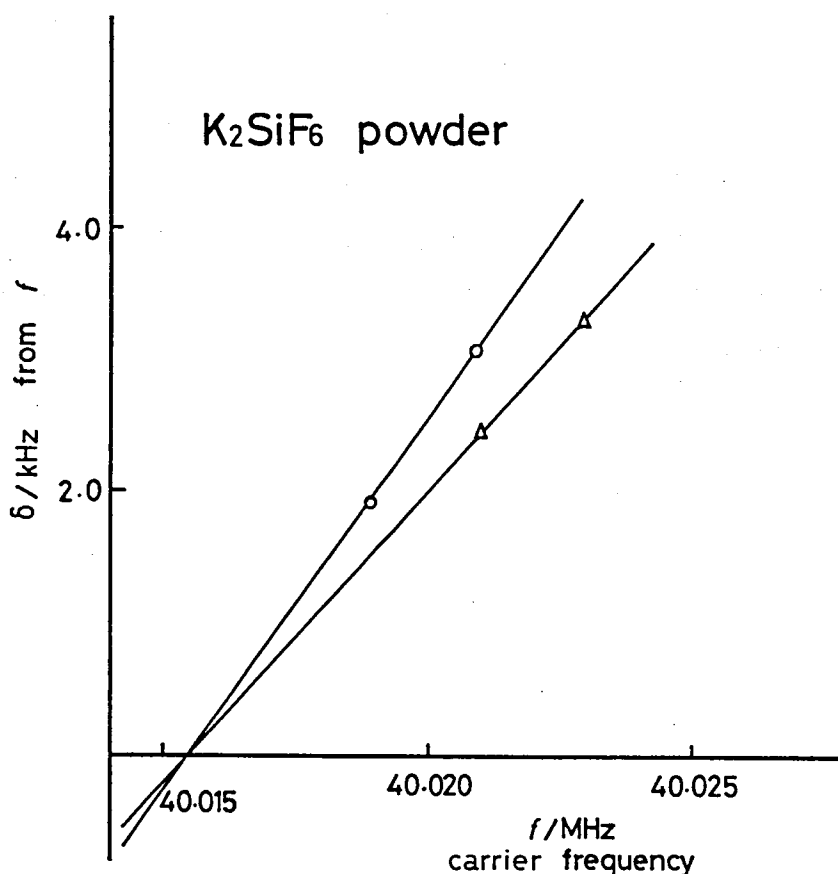
Fig. 4-20. [19]F resonance positions at different carrier frequencies in K_2SiF_6 powder. Circles and triangles have different scaling factors from each other due to a little pulse width difference.

We can estimate the scaling factor by comparing the change of the carrier frequency (real change) with apparent shift of ^{19}F NMR spectrum. The scaling factors for circles and triangles are different due to a small difference in pulse width. The point at which the frequency axis is crossed is the resonance frequency of ^{19}F in K_2SiF_6 at the DC field.

(2) Fig. 4-21(a) shows the ^{19}F NMR spectra in $p-CF_3C_6H_4F$ neat liquid in capillary with MREV-8 pulse sequence. Left hand side peak is due to F in $-CF_3$, and the right hand side due to F in $F-C_6H_4-$. Fig. 4-21(b) was obtained for the sample containing both $p-CF_3C_6H_4F$ neat liquid and powdered K_2SiF_6. A fairly broad spectrum at the right hand side is from ^{19}F in the K_2SiF_6 powder. Since the position of ^{19}F NMR in $p-CF_3C_6H_4F$ are known, Scaling factor can be determined and so chemical shift of ^{19}F in the K_2SiF_6 powder is obtained immediately.

Fig. 4-21. ^{19}F NMR spectra of (a) p-CF$_3$C$_6$H$_4$F neat liquid and (b) p-CF$_3$C$_6$H$_4$F neat liquid and K$_2$SiF$_6$ powder. The scale is apparently 60 ppm, but really 95 ppm.
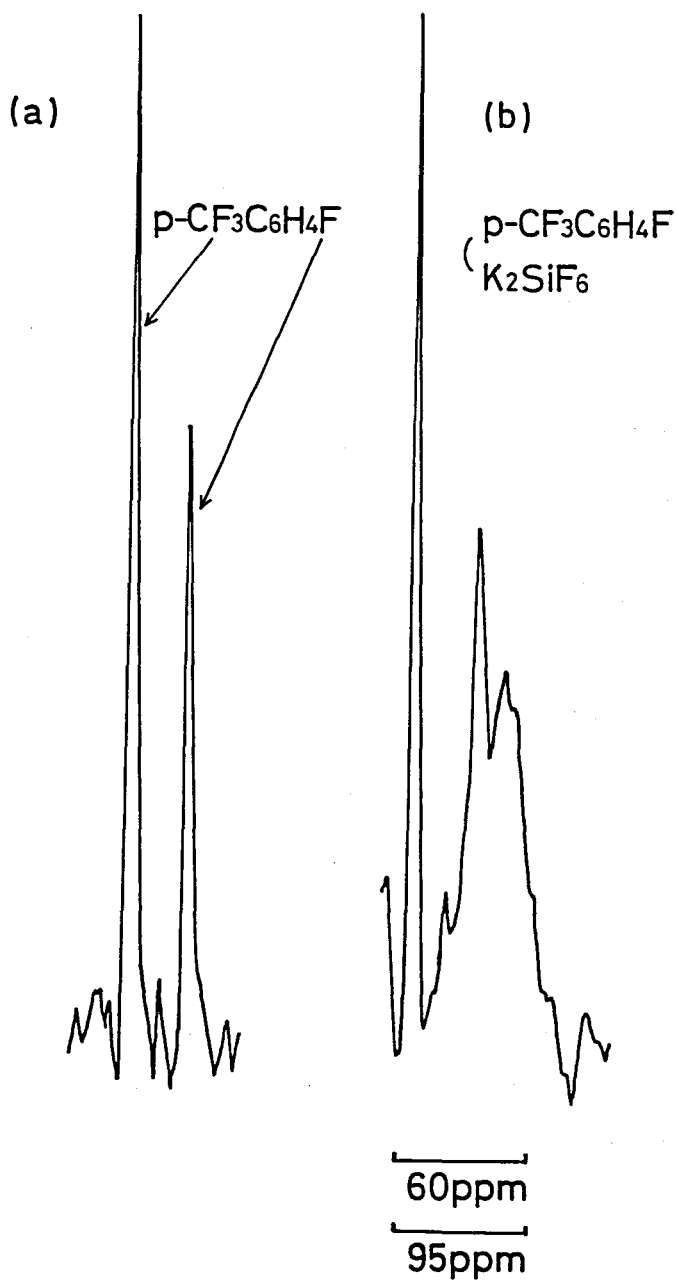
4-4 Discussion

This spectrometer gives a high resolution signal of ^{19}F in CaF$_2$ single crystal with the optimum line width of 8.5 ppm (340 Hz). This resolution is sufficiently high for most studies of ^{19}F resonance, but insufficient for usual ^{1}H resonance which gives the chemical shift of only 10 ppm.

The origin of the degradation of the resolution will be discussed below: In current experiments the RF power is decreased to about 500 W in order to avoid the droop of the RF pulse power in the pulse train. Since the volume of the sample coil is about 0.22 cm^3 in the present work, the 500 W RF pulses produce the RF field of about 70 G. Therefore, the power of the RF pulses is still high enough to obtain the high-resolution spectra of ^{1}H system.

The dead time of this spectrometer is about 5 μs, then the longest pulse interval had to be set longer than 10 μs in order to sample the FID signal effectively. This pulse interval is slightly too long to average the dipolar interaction between ^{1}H nuclei. One of the fatal sources that degradate the resolution of the spectrometer comes from the fact that the pulse interval cannot be shorten due to relatively long dead time of the receiver system.

Among many other sources for the line broadning in the present spectrometer system the error in the phases of the RF pulses, the stabilities in the pulse timing, the RF carrier frequency, and the Zeeman static field, the inhomogeneity of the static field should be checked: The phases of carriers can be adjusted precisely. The error is seemed within 3° which does not produce any artificial broadning of the spectral line.

The timing of the pulses is controled by a clock generator using a qualtz oscillator, therefore the error in the timing is within ten nanoseconds which also doesn't cause any line broadning.

The stability of the RF source is better than $\pm$ 0.2 ppm and that of the Zeeman field is controlled to within $\pm$ 1 ppm for several hours which also does not effect the line width of the order of few ppm.

The optimum line width of liquid sample was found to be 2.3 ppm. This line width may be brought about by some inhomogeneity of the static field. This inhomogeneity effect is another fatal source to degradate the resolution of the spectrometer.

References to Chapter 4

1) K. P. Jeffrey, J. Magn. Reson., $\underline{37}$, 465 (1980).

2) H. T. Stokes, Rev. Sci. Instr., $\underline{49}$, 1011 (1978).

3) W. G. Clark, Rev. Sci. Instr., $\underline{35}$, 316 (1964).

4) M. Fukazawa, CQ ham radio, No. 11, 273 (1980).

5) I. J. Lowe and C. E. Tarr, J. Phys. $\underline{E1}$, 320 (1968).

6) The FFT program was firstly developed by H. Nakayama (M.D. thesis, Osaka University, 1981). The program was modified for multiple pulse high resolution NMR method by the author.

7) U. Haubenreisser and B. Schnabel, J. Magn. Reson., $\underline{35}$, 175 (1979).

5 Chemical Shift Anisotropy of ^{19}F in Some Fluorine-containing Compounds

5-1 Introduction

Three dimensional information about the electronic structure of the molecules can in principle be obtained by high resolution NMR in solid state. The aim of the present work is to obtain ^{19}F high resolution spectra of several fluorine-containing materials in order to discuss the results in relation to the nature of the chemical bond.

As the object of the present work an aromatic conjugated system, 1,3,5-trichloro-2,4,6-trifluorobenzene (sym-$C_6Cl_3F_3$), and a series of inorganic compounds (K_2MF_6; M = Si, Ge, Sn) were selected. The chemical shift tensors in these compounds were determined by the high resolution spectra in their crystalline state and the bond nature, such as π-bonding and ionic character, in the above compounds will be discussed in relation to the chemical shift data.

High resolution spectrum can also provide fruitful information about molecular motions in solids. In the present study the molecular motions in sym-$C_6Cl_3F_3$ and K_2SiF_6 were discussed on the point of view of the high-resolution NMR.

5-2 1,3,5-trichloro-2,4,6-trifluorobenzene (sym-$C_6Cl_3F_3$)

5-2-1 Sample Preparation and Crystal Symmetry

Sym-$C_6Cl_3F_3$ was purchased from Alfa Chemical Co. Ltd. Single crystals were grown at 30 °C or 5 °C by slow evaporation of a heptane solution. The crystal was colorless and transparent with a shape of hexagonal pyramid. Single crystal with the size of about 3 mm x 3 mm x 2 mm was used for the high resolution NMR study. Sym-$C_6Cl_3F_3$ is a molecule having the D_{3d} symmetry. An early NQR study found a single resonance line at 39.312 MHz at 77 K,[1] showing that all chlorines in the crystal are crystallographically equivalent. This shows that all fluorines in the crystal are crystallographically equivalent at the same time.

5-2-2 Measurements of Chemical Shift Anisotropy of ^{19}F
        in Sym-$C_6Cl_3F_3$

The single crystal was placed between two polystyrene plates and set into the sample coil. The MREV-8 pulse method was used to obtain the high resolution spectra at 20 °C. The short pulse interval, τ, was 6.7 μs and the sampling interval was 40.2 μs. FID signal was accumulated 10 or 20 times every 20 min, and FFT was done to obtain the absorption spectra using 1024 data points. In most cases, initial 100 actual data points were used for FFT and the rest was set to be zero. One of the spectra obtained is shown in Fig. 5-1. Rotational patterns were obtained by rotating the probe about an axis perpendicular to the Zeeman field. The
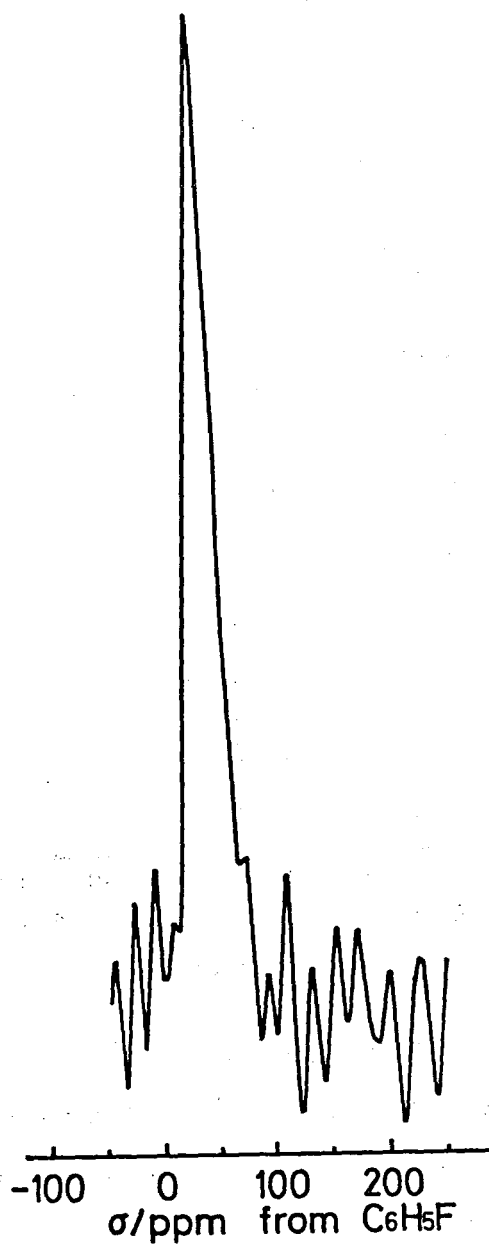
Fig. 5-1. ^{19}F NMR spectrum of sym-$C_6Cl_3F_3$ single crystal. This is the spectrum at a* in Fig. 5-2.

results are shown in Fig. 5-2.

shift from C6H5F
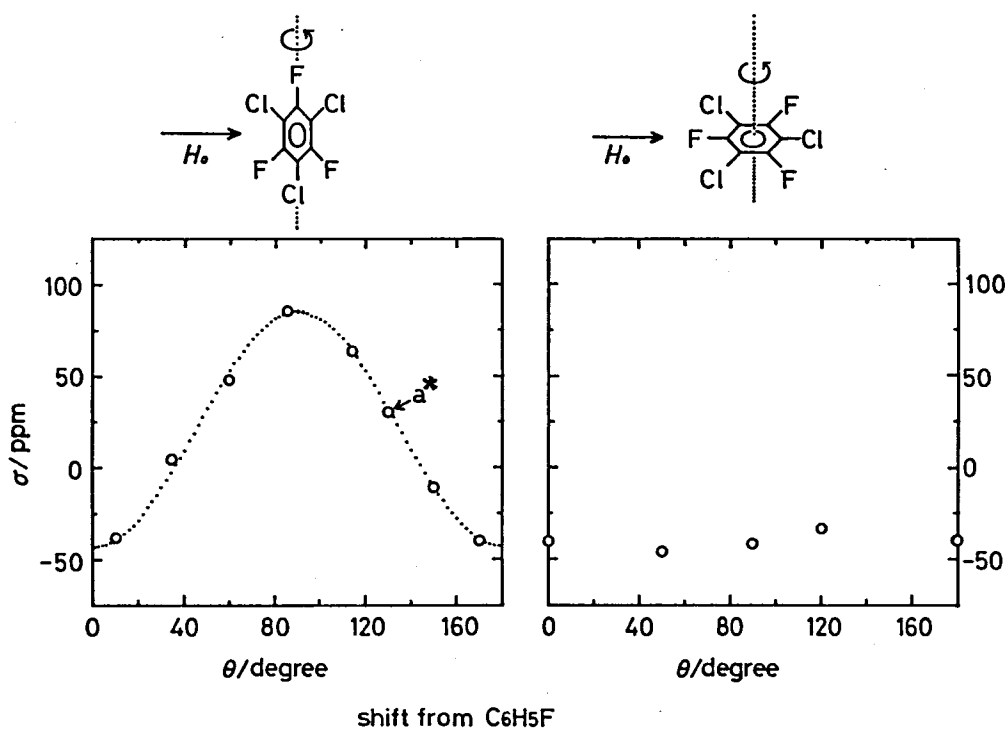
Fig. 5-2. Angular dependence of the ^{19}F chemical shifts in sym-$C_6Cl_3F_3$ single crystal at 20°C. The rotational pattern on the right was obtained when the Zeeman field was perpendicular to the apparent hexagonal C axis of the crystal. The pattern on the left was observed when the Zeeman field was rotated in a plane which contains the C axis. The spectrum in Fig.5-1 corresponds to the point marked a[*].

The rotational pattern on the right was obtained when the Zeeman field was perpendicular to the apparent hexagonal C axis of the crystal. There is the only one absorption line with a line width of about 30 ppm (1.2 kHz) at any rotational angle. The ^{19}F chemical shift does not show the angular dependence and has the value of -43 ppm from liquid C_6H_5F. The left one was obtained when the Zeeman field was rotated in a plane which contains the C axis. Although there is the only one absorption line with a line width of about 30 ppm in spite of the change of the rotational angle, the angular dependence of the ^{19}F chemical shift is observed. The chemical shift takes the maximum value of +83 ppm from liquid C_6H_5F when the Zeeman field is in the direction of the C axis.

5-2-3 Discussion

The ^{19}F high resolution NMR spectrum on single crystal of sym-$C_6Cl_3F_3$ gave only one absorption line with a linewidth of about 30 ppm (1.2 kHz), indicating not only that all the fluorines are crystallographically equivalent but also that all the C-F bond directions are effectively averaged by some molecular motion. When the external field Ho is rotated about the apparent hexagonal C axis of the crystal, the chemical shielding tensor assumes an almost constant value (-43 ppm from liquid C_6H_5F). On the other hand when Ho is rotated in a plane which contains the C axis, the chemical shift takes the maximum value (+85 ppm) when Ho is in the direction of the C axis. Such characteristic rotational patterns indicate that the direction of the molecular C_3 axis coincides with that of the crystalline C axis and that the molecules undergo a reorientation about their C_3 axes at room temperature.

The most shielded direction is perpendicular to the benzene ring as in the other fluorinated benzenes that have been reported.[2] Thus, Raber and Mehring measured the shielding tensor values in analogous compounds.[3] Their values as well as ours are listed in Table 5-1 and shown in Fig. 5-3.

According to Raber et al.[3] the least shielded direction is perpendicular to the C-F bond and lies in the benzene ring plane, and σ_{22}, which assumes a medium value, is almost constant in spite of the changes of the functional groups. $(\sigma_{11} + \sigma_{22})/2$ in Table 5-1 and Fig. 5-3 indicates the motionally averaged value of the two directions in the molecular plane.

	σ_{11}	σ_{22}	σ_{33}	σ_{av}
1,3,5-$C_6H_3F_3$ [3)	-79	2	63	-5
1,3,5-$C_6Cl_3F_3$	$(\sigma_{11} + \sigma_{22})/2 = -43$		85	0
C_6F_6 [3)	-3	-3	155	50

Table 5-1. Chemical shift tensor elements ($\sigma_{11} < \sigma_{22} < \sigma_{33}$) in ppm. Values are quoted from C_6H_5F. The 1-axis is perpendicular to the C-F bond, but in the molecular plane. The 2-axis is parallel to the C-F bond. The 3-axis is perpendicular to the benzene ring.
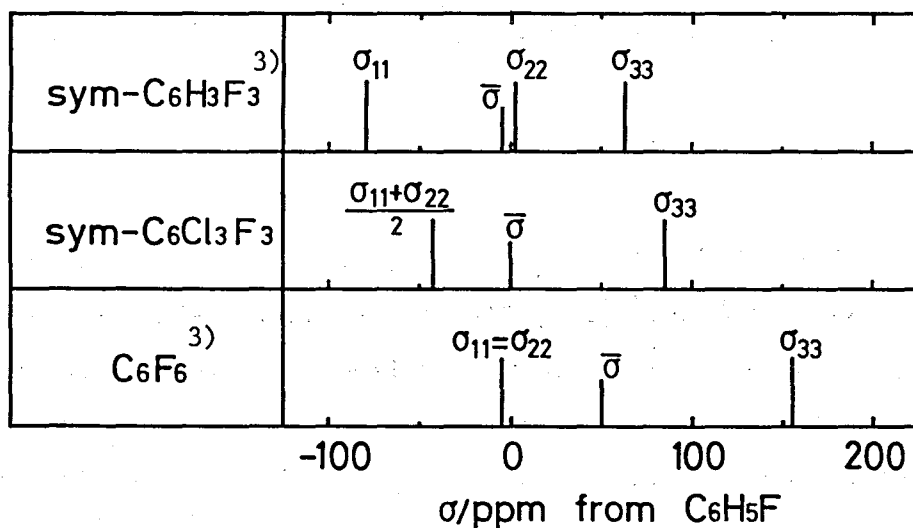

Fig. 5-3. Pictorial representation of the chemical shift tensor elements σ_{11}, σ_{22} and σ_{33} of ^{19}F in fluorobenzenes.

The chemical shift tensor can be separated into two different parts according to Ramsey[4]

$$\underline{\sigma} = \underline{\sigma}^d + \underline{\sigma}^p, \tag{5-1}$$

where $\underline{\sigma}^d$ and $\underline{\sigma}^p$ are obtained by first-order and second-order perturbation theory, respectively. A variational treatment gives similar results.[5] $\underline{\sigma}^d$ is the diamagnetic part of the chemical shift tensor and $\underline{\sigma}^p$ is the paramagnetic part. Gierke and Flygare[6] showed that $\underline{\sigma}^d$ and $\underline{\sigma}^p$ expanded into six terms as follows;

$$\sigma_{\alpha\beta}{}^d = I + II + III + IV, \qquad \alpha,\beta = x,y,z \tag{5-2}$$

where

$$I = \sigma_{atom}, \tag{5-3}$$

$$II = (e^2/2mc^2)\sum_i z_i r_i{}^{-3}(r_i{}^2\delta_{\alpha\beta} - \alpha_i\beta_i), \tag{5-4}$$

$$III = (e^2/2mc^2)\sum_i \{r_i{}^{-3}\left[2\underline{r}_i\cdot<\underline{\rho}>\delta_{\alpha\beta} - (\alpha_i<\beta_i> + \beta_i<\alpha_i>)\right]$$
$$- 3r_i{}^{-5}(r_i{}^2\delta_{\alpha\beta} - \alpha_i\beta_i)\underline{r}_i\cdot<\underline{\rho}>_i\}, \tag{5-5}$$

$$IV = (e^2/2mc^2)\sum_i r_i{}^{-3}<\rho^2/3>_i(3r_i{}^{-2}\alpha_i\beta_i - \delta_{\alpha\beta}), \tag{5-6}$$

and

$$\sigma_{\alpha\beta}{}^p = V + VI, \tag{5-7}$$

where

$$V = (e^2/2mc^2)(C_{\alpha\beta}I_{\alpha\beta}c)/(e\hbar\mu_o g_I), \tag{5-8}$$

$$VI = -(e^2/2mc^2)\sum_i z_i r_i{}^{-3}(r_i{}^2\delta_{\alpha\beta} - \alpha_i\beta_i) = -II. \tag{5-9}$$

Here $\underline{r}_i = (x_i, y_i, z_i)$ is the vector from the shielded nucleus to a neighbouring atom i, with the atom dipole moment $<\underline{\rho}>_i$ and the atom electronic second moment $<\rho^2>_i$, and $\delta_{\alpha\beta}$ is the Kronecker's symbol. z_i is the atomic number of nucleus i and the sum $\sum_i$ runs over all nuclei with the shielded nucleus being omitted. All terms I - IV can be calculated once the molecular structure and the atomic dipole moment and electronic second moment are known. The term

V, however, is related to a different molecular quantity, namely $C_{\alpha\beta}$, which is the spin rotation interaction tensor, where $I_{\alpha\beta}$ is the corresponding moment of inertia, μ_o is the nuclear magneton and g_I is the nuclear g value of the shielded nucleus. All other parameters have their usual meaning. The tensor $\sigma_{\alpha\beta}$ can be diagonalized and the principal axes and the principal elements are readily evaluated, once all the molecular parameters are known.

The terms II - IV are calculated according to Eqs. (5-4) and (5-6) for sym-$C_6Cl_3F_3$ discussed in this work by using the appropriate dipole moments,[6] second moments [6] and the molecular structure deduced from analogous compounds such as C_6F_6 and C_6Cl_6 [7] All angles and bond lengths have been taken to be standard values. The so-called dipolar contribution (term III) amounts to about 1 ppm and may be neglected in an analysis of this kind. Term II and IV cancel each other and reflect the gauge dependence of σ^d and σ^p. The spin-rotation interaction term V can then be estimated by means of the experimental shift tensor and term I, III, and IV as

$$V = \sigma^{p'} = \sigma_{exp} - (I + III + IV) = \sigma_{exp} - (I + IV)$$
$$= \sigma_{exp} - \sigma^{d'}.$$
$$(5-10)$$

The "gauge independent" terms $\sigma^{d'}$ and $\sigma^{p'}$ were calculated according to Eqs. (5-6)-(5-10). In this calculation the σ_{22} component of ^{19}F in sym-$C_6Cl_3F_3$ is assumed to be the same as that in sym-$C_6H_3F_3$ since the σ_{22} components in several fluorinated benzenes have almost the same value. The calculated values are listed in Table 5-2 together with Raber's[3] value for analogous compounds.

	$\sigma_{11}{}^{d'}$	$\sigma_{22}{}^{d'}$	$\sigma_{33}{}^{d'}$	$\sigma_{11}{}^{p'}$	$\sigma_{22}{}^{p'}$	$\sigma_{33}{}^{p'}$
$1,3,5\text{-}C_6H_3F_3$[3]	161	191	157	-240	-189	-94
$1,3,5\text{-}C_6Cl_3F_3$	162	191	157	-250	-189	-72
C_6F_6 [3]	162	192	156	-165	-194	-1

Table 5-2. Calculated values of $\sigma^{d'}$ and $\sigma^{p'}$.

The $\sigma^{d'}$ value is not very sensitive to substitution on the benzene ring, as can been seen in Table 5-2. This is due to the fact, that the quadrupolar term (IV), Eq. 5-6, does not depend very much on substitution "far away" from the nucleus considered, since this interaction falls off as r^{-3}. Then, all the experimentally observed variations in the chemical shift tensor are attributed to $\sigma^{p'}$. The change in $\sigma_{22}{}^{p'}$ is very small and gradual change can be seen in $\sigma_{11}{}^{p'}$ and $\sigma_{33}{}^{p'}$ components. $\sigma^{p'}$ can be related to the spin-rotation coupling constant through Eq. 5-8. The knowledge of the spin-rotation interaction tensor is generally of considerable interest in molecular physics, but in the case of large molecules like fluorobenzenes the extraction of the spin-rotation interaction tensor from the molecular beam experiments is extremely difficult and even in the simplest case, namely mono-fluorobenzene, no reliable data can be obtained. Spin-lattice relaxation of ^{19}F or ^1H via chemical shift anisotropy and spin-rotation interaction[8] has also attracted much attention.

Here, the relation between the reorientational correlation time
is of considerable interest, concerning different models for molecular
motion each other. A better knowledge of the chemical shift tensor and
the spin-rotation interaction tensor will help to elucidate the
feature of the molecular motion.

Substitution from Eq. 5-8 into Eq. 5-10 gives

$$C_{\alpha\beta}/h = (mc\mu_o g_I)/(\pi e I_{\alpha\beta})\sigma_{\alpha\beta}{}^{p'}. \qquad (5\text{-}11)$$

The values used in calculating the spin-rotation interaction
tensor are as follows:

$$m = 9.108 \times 10^{-28} \text{ g}$$

$$c = 2.998 \times 10^{10} \text{ cm/s}$$

$$e = 4.803 \times 10^{-10} \text{ e.s.u.}$$

$$\mu_o = 5.050 \times 10^{-24} \text{erg/gauss}$$

$$g_F = 5.257$$

$$R(C\text{-}F) = 1.327 \times 10^{-8} \text{ cm}$$

$$R(C\text{-}C) = 1.394 \times 10^{-8} \text{ cm}$$

$$R(C\text{-}Cl) = 1.715 \times 10^{-8} \text{ cm}.$$

The calculated values are as follows,

$$C_{11}/h = -910 \text{ Hz}$$

$$C_{22}/h = -687 \text{ Hz}$$

$$C_{33}/h = -131 \text{ Hz}$$

$$\overline{C_{av}}/h = -576 \text{ Hz}$$

$$\sqrt{\overline{c^2}}/h = \left[(C_{11}{}^2 + C_{22}{}^2 + C_{33}{}^2)/3\right]^{\frac{1}{2}}/h = 662 \text{ Hz}.$$

To obtain some insight into the electronic structure of the
molecule, the theory of Karplus and Das[9] will be used. According
to them, one of the paramagnetic components is given by

$$\sigma_{xx}{}^{(p)} = (3/2)\sigma_o(P_{yy} + P_{zz} - P_{yy}P_{zz}). \qquad (5\text{-}12)$$

Here, y and z components are given by cyclic permutation for the indices for the y- and z- components in Eq. 5-12, where the P_{ii} represent populations of the fluorine p orbitals and the cross terms P_{ij} are neglected. σ_o is a semiemperical parameter as defined by Karplus and Das.[9] For a closed shell ion all the P_{ii} should be two, leading to zero paramagnetic shift. Thus a deviation from a closed shell form can lead to a nonvanishing paramagnetic shift.

Since experimentally observed variations in the chemical shifts are loaded onto the paramagnetic contribution as mentioned above in relation to $\sigma^{P'}$, only the paramagnetic part may be considered to investigate the electronic structure.

A deviation from the closed shell ion state will be defined by the following parameters:

$$\begin{aligned} P_{xx} &= 2 - \rho_x, \\ P_{yy} &= 2 - \rho_y, \\ P_{zz} &= 2 - \varepsilon, \end{aligned} \qquad (5\text{-}13)$$

where ρ_x and ρ_y may be taken as the double bond characters and

$$\varepsilon = 1 - (I + S - IS), \qquad (5\text{-}14)$$

where I is the ionic character and S the degree of sp hybridization. Eq. (5-15) is derived from Eqs. (5-13) and (5-14).

$$\sigma_{xx}{}^P = (3/2)\sigma_o\left[\varepsilon + \rho_y(1 - \varepsilon)\right] \qquad (5\text{-}15\text{a})$$

$$\sigma_{yy}{}^P = (3/2)\sigma_o\left[\varepsilon + \rho_x(1 - \varepsilon)\right] \qquad (5\text{-}15\text{b})$$

$$\sigma_{zz}{}^P = (3/2)\sigma_o(\rho_x + \rho_y - \rho_x\rho_y). \qquad (5\text{-}15\text{c})$$

Here, the x axis is perpendicular to the benzene ring, the y axis lies in the plane and is perpendicular to the C-F bond, and the z axis is parallel to the C-F bond. Assuming that the double bond

character of a C-F bond within the plane (ρ_y) is zero, simpler relations are obtained as follows,

$$\sigma_{xx}{}^P = (3/2)\sigma_o \varepsilon, \qquad\qquad (5\text{-}16a)$$

$$\sigma_{yy}{}^P = (3/2)\sigma_o \left[\varepsilon + \rho_x(1 - \varepsilon)\right], \qquad (5\text{-}16b)$$

$$\sigma_{zz}{}^P = (3/2)\sigma_o \rho_x. \qquad\qquad (5\text{-}16c)$$

Since the most shielded direction is in the z axis direction, σ_{xx} is equal to σ_{33}. The bond direction component (σ_{zz}) is σ_{22}, and σ_{yy} is σ_{11}. Comparing the chemical shift tensor components of the three compounds listed in Table 5-1 and Table 5-2 or shown in Fig. 5-3, the z component $\sigma_{zz}(\sigma_{22})$ is almost insensitive to substitution. This indicates little change of ρ_x, that is, π electron density is not affected by the substitution. The component σ_{xx} is gradually increased from sym-$C_6H_3F_3$ to C_6F_6. This indicates a gradual change of ε in Eq. (5-16a). ε becomes small since $\sigma_{xx}{}^P$ is negative. The decrease in ε is attributed to an increase of the ionic character I of Eq. (5-14). This shows that the ionicity in a C-F bond is gradually increased on going from sym-$C_6H_3F_3$, sym-$C_6Cl_3F_3$, to C_6F_6. The gradual change of σ_{xx} and the insensitivity of σ_{zz} by substitution indicate that in these aromatic conjugated system π electron density is changed little and σ electron density varies gradually by substitution. Above conclusion agrees with the ^{13}C NMR measurement by Miyajima.[10] He showed that π electron density on ^{13}C is not affected by substitution, on the other hand σ electron density is affected easily by substitution.

5-2-4 Molecular Motion and Phase Transition

As is mentioned in Section 5-2-3 it was found during the analysis of ^{19}F chemical shift rotational patterns that the molecules undergo reorientation about its C_3 axis at room temperature. In order to obtain more detailed information about the molecular motion in this compound, the spin-lattice relaxation time (T_1) and the spin-spin relaxation time (T_2) of ^{35}Cl NQR were measured by the use of MATEC 5800 pulsed NQR spectrometer system. The results are given in Fig. 5-4. The gross feature concerning T_1 agrees with a previous result[11]. The T_1 can be reproduced by the relation

$$T_1^{-1} = 3.27 \times 10^{-4}T^2 + 3.90 \times 10^{-6}\exp(-18.2 \text{ kJmol}^{-1}/RT).$$

The activation energy of 18.2 ± 0.5 kJmol^{-1} is slightly larger than that by Alymov et al.[11](17.7 kJmol^{-1}). The decrease in T_2 above 200 K is an evidence of marked line broadning above this temperature.

The correlation time, τ_c, for the three-fold reorientation is calculated by using the relation[12]

$$\tau_c = (3/4)T_1$$

and is plotted in Fig. 5-5. This figure shows that τ_c at 300 K is about 5×10^{-4} s, which is just the order of magnitude to average out the parallel components of the ^{19}F shielding tensor being consistent with the conclusion of the ^{19}F high-resolution NMR study mentioned above.

Heat capacity measurements[13] found a higher order phase transition in this substance at T_c = 296.7 K with an enthalpy change of only 18 Jmol^{-1}. ^{35}Cl NQR frequency up to the melting
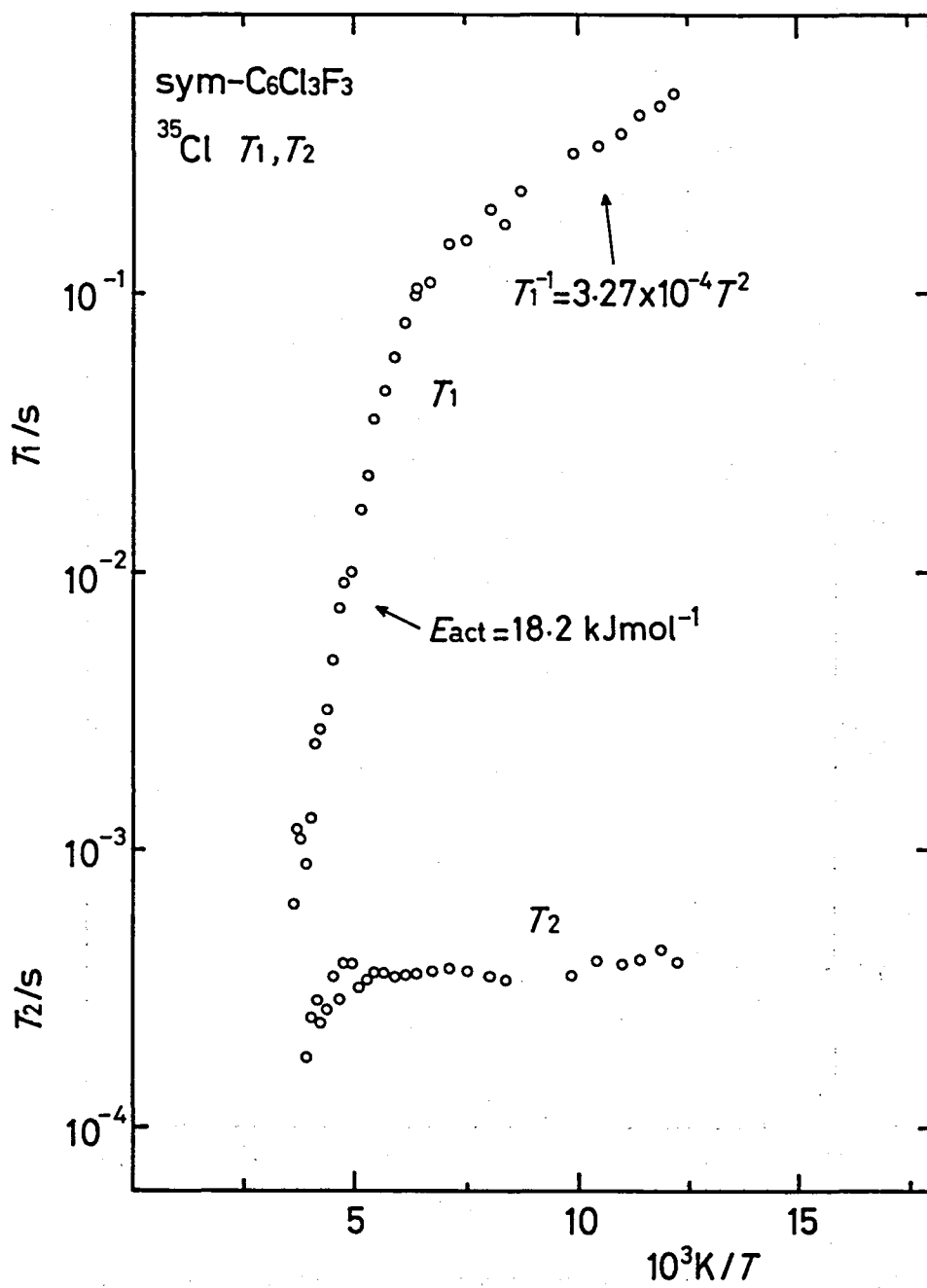
Fig. 5-4. The spin-lattice and spin-spin relaxation times of ^{35}Cl.

The figure shows a plot with:
- Title: sym-C$_6$Cl$_3$F$_3$
- ^{35}Cl T_1, T_2
- Y-axes: T_1/s and T_2/s
- X-axis: 10^3K/T
- $T_1^{-1} = 3.27 \times 10^{-4} T^2$
- $E_{act} = 18.2$ kJmol^{-1}
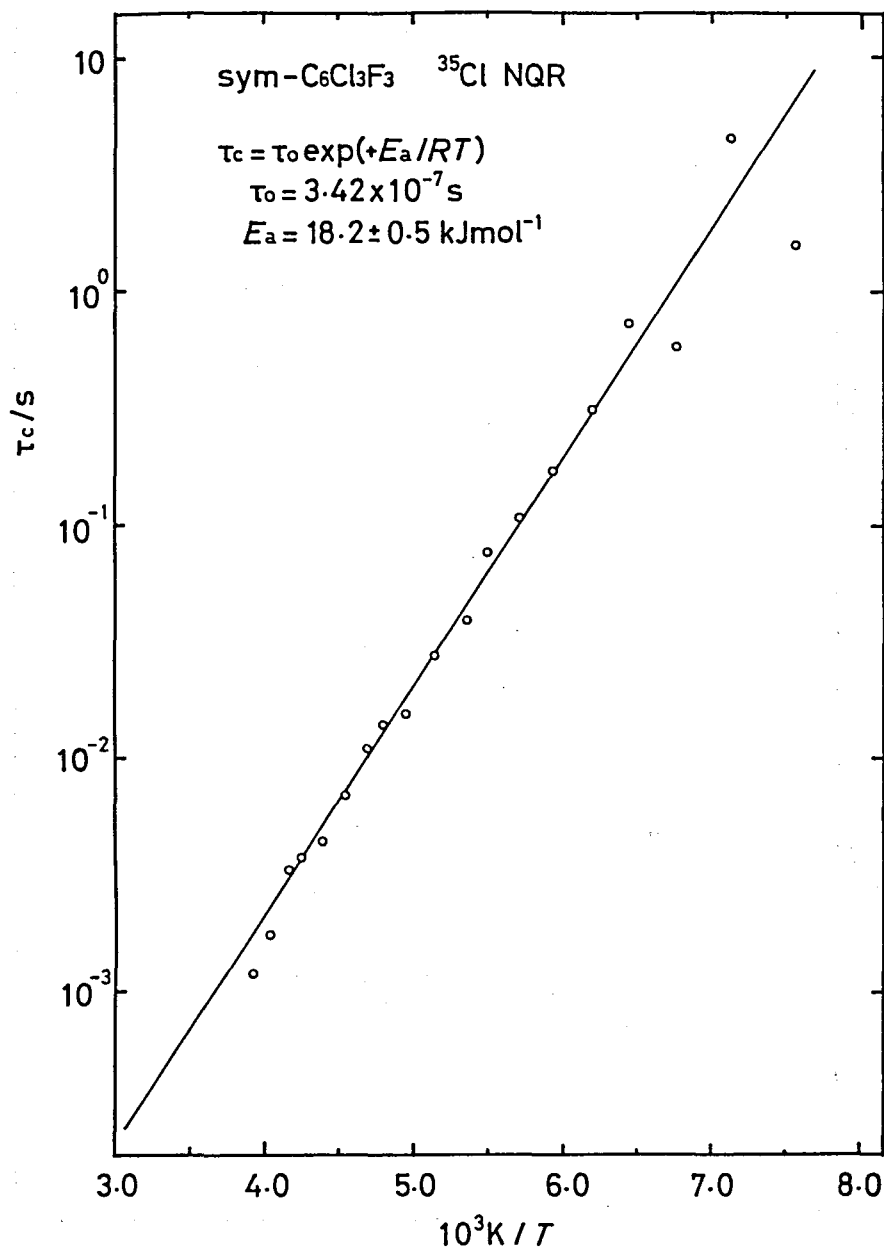- Data curves labeled T_1 and T_2

Fig. 5-5. The correlation time for the three-fold reorientation of molecules.

point (334.9 K)[13] was measured as shown in Fig. 5-6. The NQR
frequency shows only small deflection at T_c, suggesting the
absence of any large structural change at the phase transition.

   ^{19}F high resolution NMR spectra in powdered specimen were
observed from 293 K to 337 K (up to just above the melting point).
The spectra show no discernible change from 293 K up to the
melting point. This indicates that no other kind of molecular
motion than the three-fold molecular reorientation is excited in
the high-temperature phase in the time scale of ^{19}F high
resolution spectra (130 ppm = 5.2 kHz).

   Raman spectra were also collected on a single crystal at 289 K
and 308 K. No detectable change in the spectra was observed in
the frequency range between 0 cm^{-1} and 1000 cm^{-1}.

   Hence the mechanism of the phase transition in this material
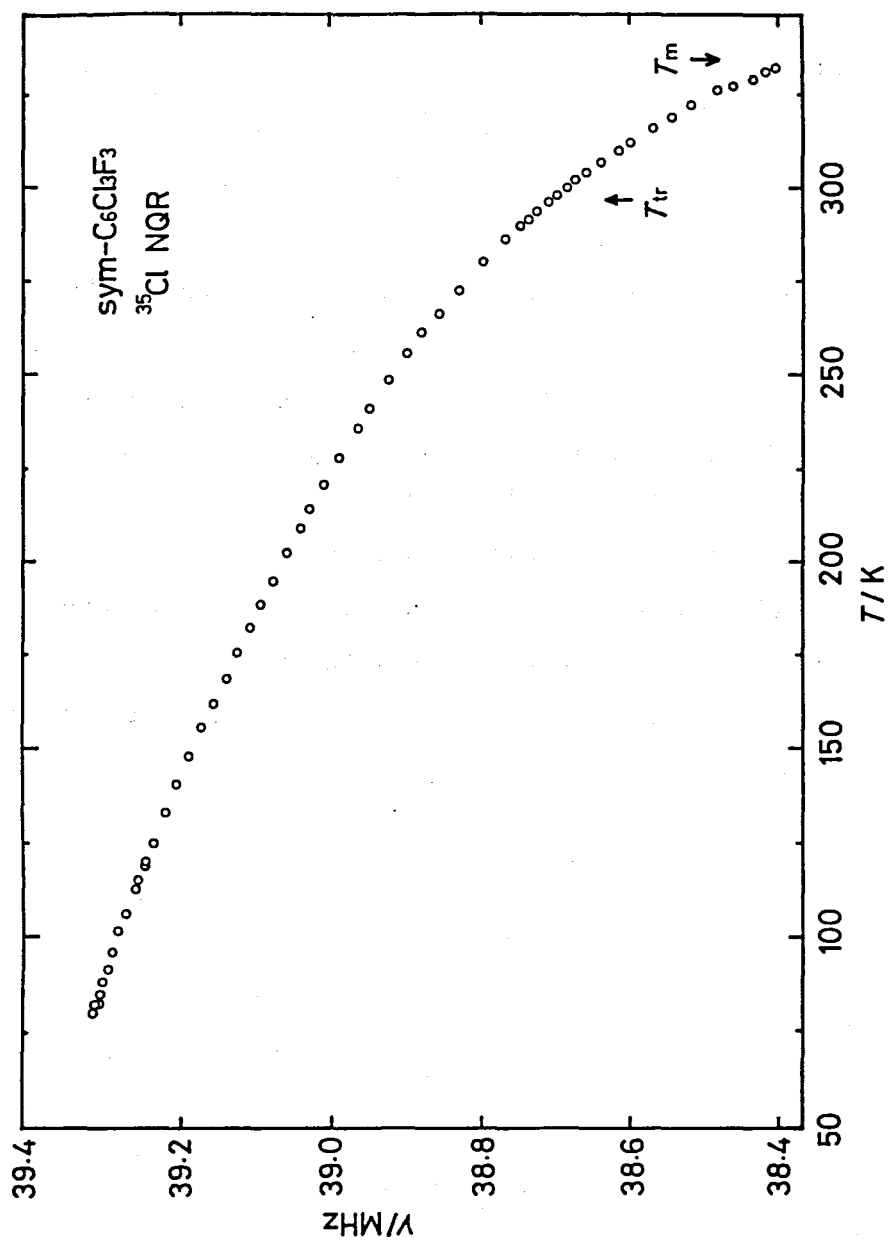will remain unsolved.

Fig. 5-6. Temperature dependence of ^{35}Cl NQR frequency.

5-2-5 Conclusion

High resolution ^{19}F NMR spectrum was observed in a single crystal of sym-$C_6Cl_3F_3$ and chemical shift shielding tensor was obtained. The most shielded direction is perpendicular to the molecular plane and the least shielded direction is perpendicular to the C-F bond but lying in the molecular plane. The most shielded component (σ_{33}) and the least shielded component (σ_{11}) change gradually from sym-$C_6H_3F_3$ to C_6F_6, whereas the C-F bond direction component (σ_{22}) changes little. From the analysis of components of shielding tensors in sym-$C_6H_3F_3$, sym-$C_6Cl_3F_3$, and C_6F_6, it is indicated that π-electron density distribution varies little and σ-electron density is changed when other substituents are introduced.

At 20 $^{\circ}C$, sym-$C_6Cl_3F_3$ molecule rotates about its figure axis and its motion averages out the shielding tensor components within the molecular plane.

5-3 K_2MF_6 type compounds (M = Si, Ge, Sn)

5-3-1 Lattice types and site symmetry of K_2MF_6 type compounds

At room temperature the lattice type of K_2SiF_6 is cubic[14] and others are trigonal[15] as shown in Figs. 5-7 and 5-8. The site symmetry of Si in the former compound is Oh and that of the central atoms in the other compounds is D_{3d}. Although the latter two anions have D_{3d} site symmetry in the solid state, each $(M)^{4+}$ ion is surrounded by six F^- ions which form a slightly distorted regular octahedron. All the anions in the crystal are equivalent. Since MF_6^{2-} ions are of approximately regular octahedron, the electron distributions in the M-F bond may be close to the axial symmetry. Therefore, axially symmetric chemical shift tensors will be expected.
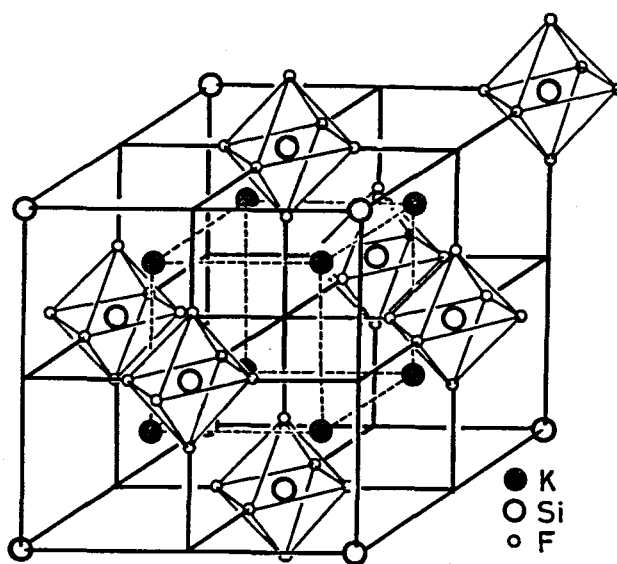
Fig. 5-7. Structure of K_2SiF_6.
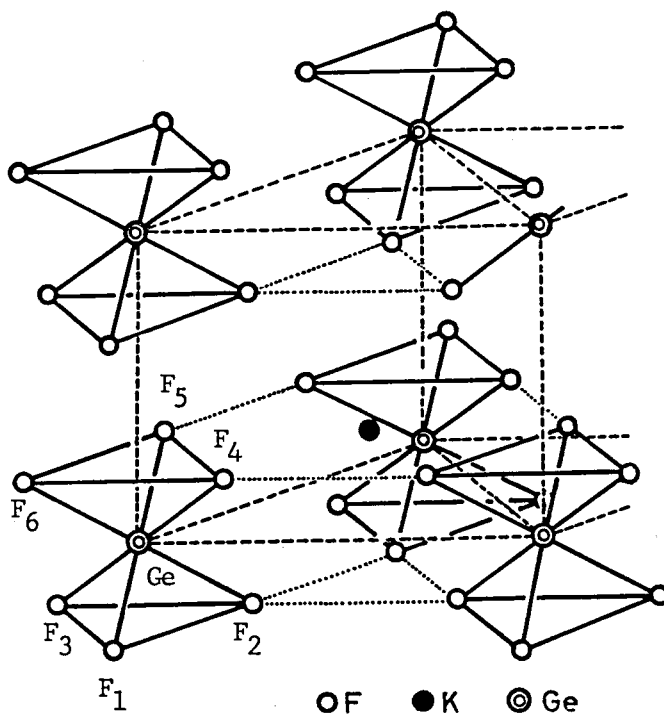
Fig. 5-8. Structure of K_2GeF_6. K_2SnF_6 is isomorphous with it.

5-3-2 Potassium Hexafluorosilicate

(1) Sample preparation and measurements

Powdered K_2SiF_6 was purchased from Nakarai Chemical Co. Ltd. An attempt to grow a single crystal by slow evaporation of 47 % hydrofluoric acid solution was unsuccessful.

Using powdered specimen, multiple pulse NMR measurements were made with MREV-8 pulse method at 300 K and 77 K. The spectra

obtained are shown in Fig. 5-9. The spectrum at 300 K has the half height width of 30 ppm and seems to have no anisotropy. The line width at 77 K is larger than that at 300 K and a small hump appears on the high field side.

(2) Determination of Chemical Shift Tensor

The spin-lattice relaxation time of ^{19}F was measured in the temperature range between 77 K and 973 K by Moskvich et al.[16] According to their data, the reorientational correlation time τ_c is about 10^{-6} s at 300 K and so it is expected that the motion fully contributes to the averaging the shielding anisotropy. The spectrum observed at 300 K in this work shows a single pesk as shown in Fig. 5-9, being explained by the above averaging effect according to Moskvich et al. The value for σ_{iso} (isotropic averaged value) obtained is 16 ppm from liquid C_6H_5F.

The spectra at 77 K does not show the rigid lattice powder pattern (usual powder pattern of rigid lattice is shown in Fig.3-1), as shown in Fig. 5-9. There is a small hump on the high field side. The reorientational motion at this temperature is thought to affect the line shape. Spiess et al.[17] calculated the powder pattern for trigonal bipyramidal, tetrahedral, and octahedral molecules with axially symmetric shielding tensor in the presence of some characteristic molecular motion in each case. They showed that a small hump may appear when the reorientational correlation time of molecule approaches the inverse of the chemical shift anisotropy under the hypothesis of jump model. The powder pattern
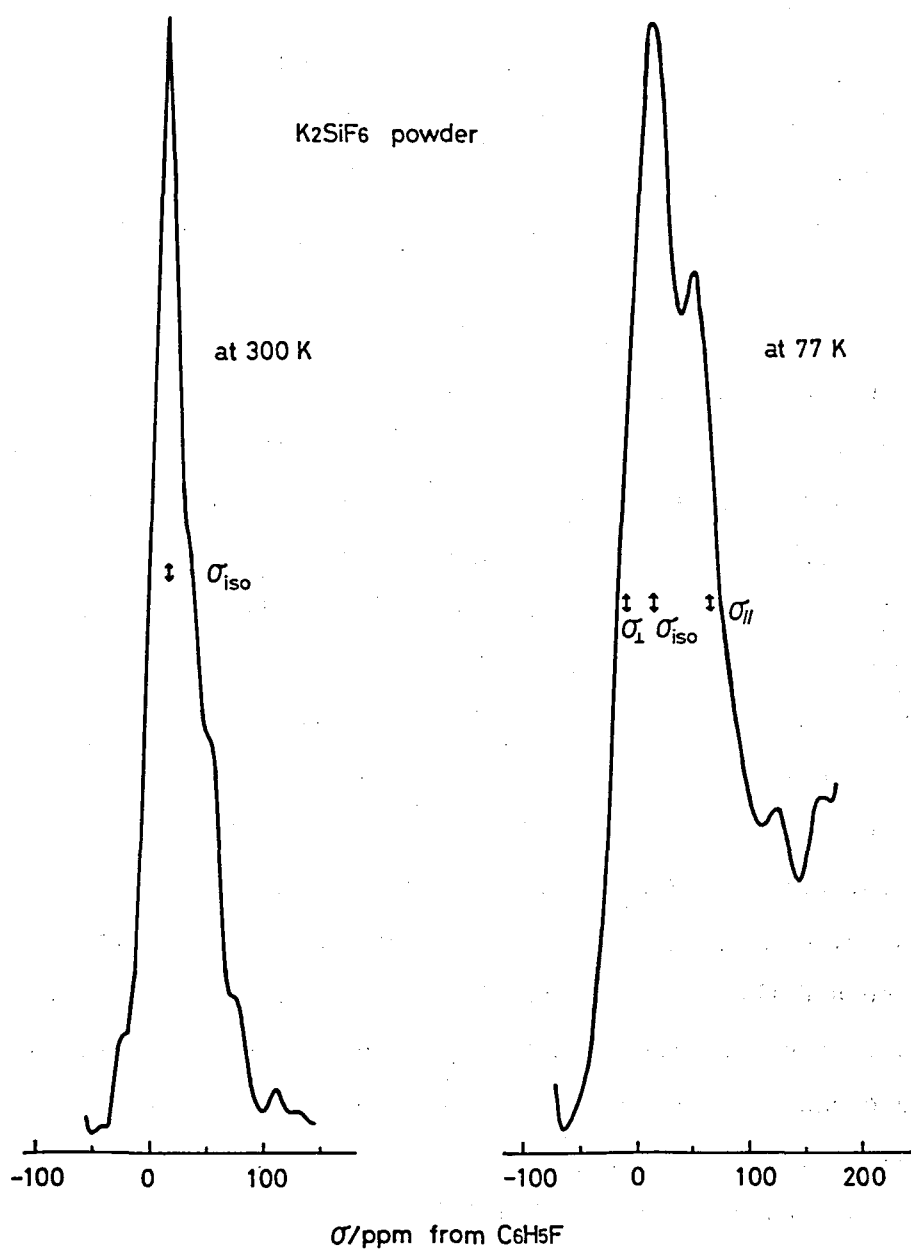
Fig. 5-9. High resolution NMR spectra of ^{19}F in powdered K_2SiF_6 at 300 K and 77 K. The reference material for the chemical shift is liquid C_6H_5F.

of K_2SiF_6 at 77 K can be reasonably explained by this isotropical jump model. From the line shape analysis, the jump frequency is estimated to be about 3 kHz and correlation time is about 3.3×10^{-3} s, and σ_{33} is 66 ppm and $\sigma_{22} = \sigma_{11}$ is -9 ppm from liquid C_6H_5F.

SiF_6^{2-} ion is considered to form regular octahedron in crystal, and so chemical shielding tensor is expected to be axially symmetric. This expectation agrees well with the spectral analysis. The symmetry axis of axially symmetric shielding tensor coinsides with the Si-F bond. Therefore one can consider two types of axially symmetric shielding tensors as shown in Fig. 5-10. In type (a) the maximum shielding direction is along the Si-F bond, and in this case the powder pattern of type (a)' is obtained. In the case of type (b) the least shielded direction is along the Si-F bond, and the powder patter should be of the type (b)'. The analysis of the powder pattern of K_2SiF_6 indicates that the shielding tensor in this compound belongs to type (a). Its most shielded direction is along Si-F bond and the value of the chemical shift is 60 ppm. Its least shielded direction, on the other hand, is perpendicular to the Si-F bond and its chemical shift is -9 ppm.

Chemical shift of SiF_6^{2-} in solution[18] is 12 ppm, a little smaller than that in solid (16 ppm).
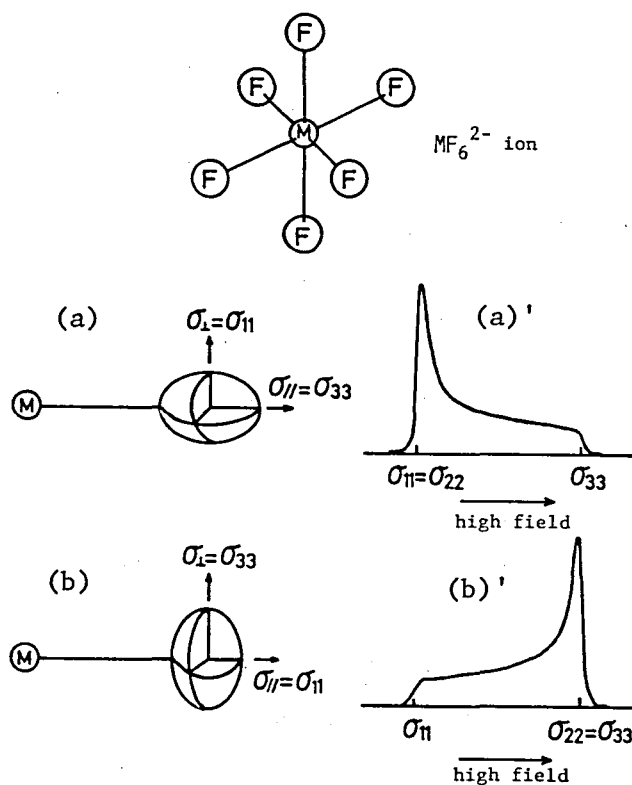
Fig. 5-10. Axially symmetric shielding tensor models and their powder pattern.

5-3-3 Potassium Hexafluorogermanate

(1) Sample Preparation and Measurements

A colorless, transparent single crystal of the shape of hexagonal plate was obtained by slow evaporation at 30 $^{\circ}$C of solution prepared by dissolving stoichiometric GeO_2 and KF in 47 % hydrofluoric acid. This substance is trigonal, D_{3d}^3, with Z=1 and the C_3 axis of GeF_6^{2-} ion is parallel to the crystallographic C_3 axis [15] (see Fig. 5-8).

GeF_6^{2-} ion is of the shape of nearly regular octahedron and so all F^- ions have the same axially symmetric shielding tensors. Therefore a pair of lines will be observed if the Zeeman field is rotated in the plane on which F_5, Ge, and F_1 atoms and the C_3 axis sit (see Fig. 5-8). If the Zeeman field is rotated in the plane, the rotational patterns will consists of two curves and their intensity ratio will be 2:1. One typical example of the FID signals is shown in Fig. 5-11, and its FFT spectrum in Fig. 5-12. FID signals were accumulated 20 times every 1800 s, and then Fourier-transformed. The Zeeman field was rotated in the above mentioned plane of the crystal and the rotational patterns in Fig. 5-13 were obtained. The intensity of the line labelled by A is stronger than that of B. The intensity ratio is approximately 2:1.

(2) Determination of Chemical Shift Tensor

Sergienko et al. [19] observed the second moment of ^{19}F as a function of temperature and concluded that neither the isotropic
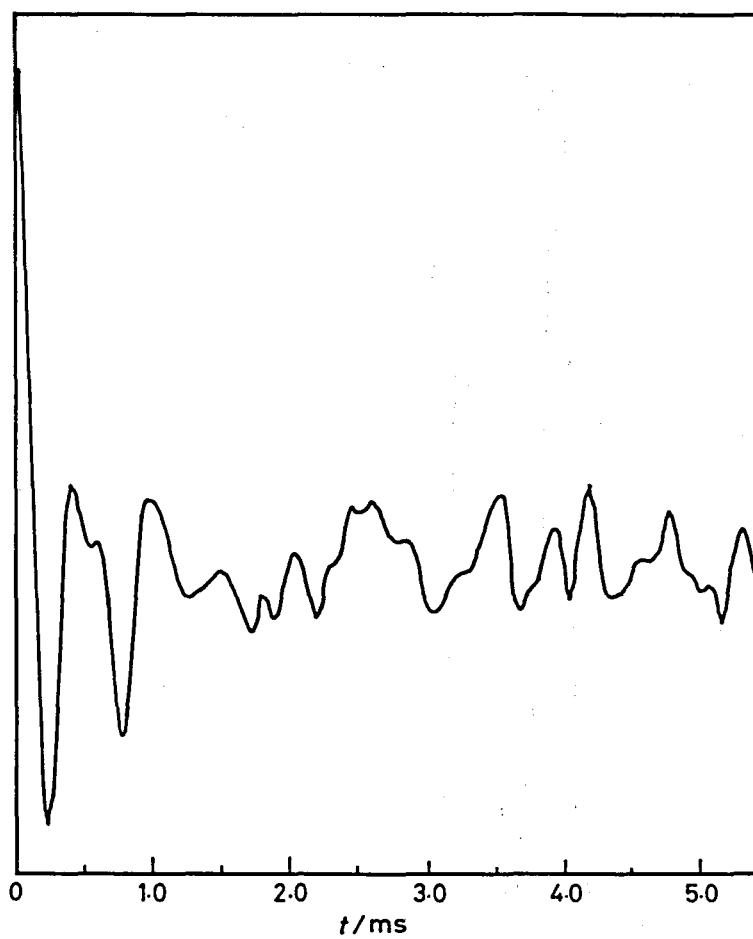
Fig. 5-11. FID signal of ^{19}F in K_2GeF_6 single crystal.
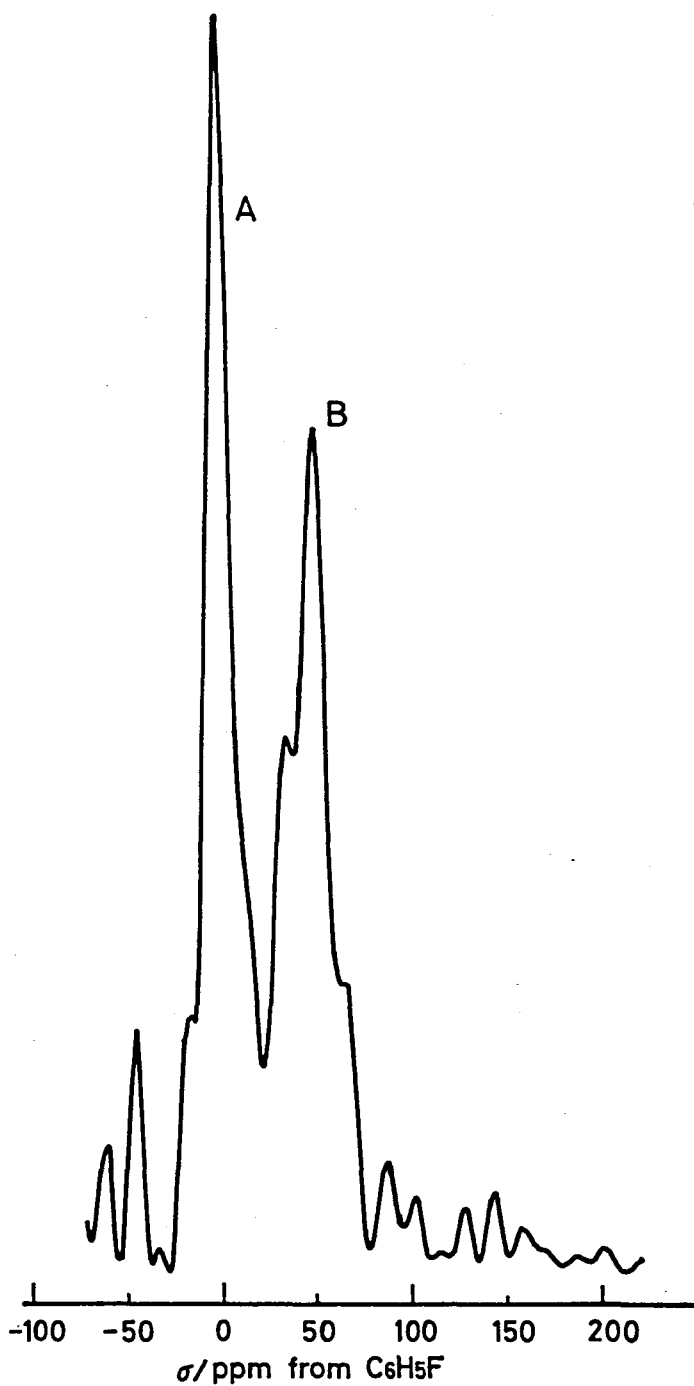
Fig. 5-12. ^{19}F NMR spectrum obtained by FFT of FID in Fig. 5-11. The spectrum corresponds to the orientation, a*, in Fig. 5-13.
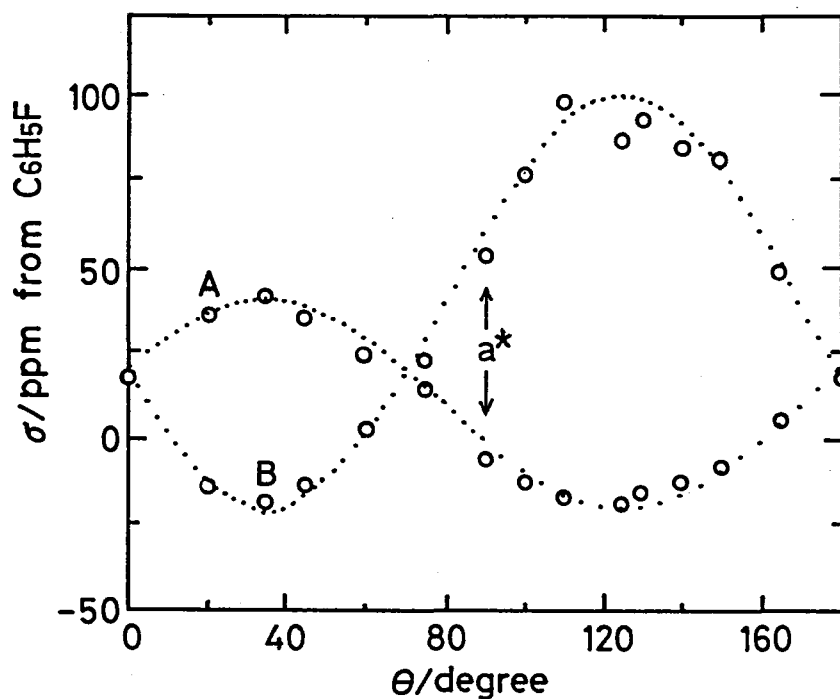
Fig. 5-13. Angular dependence of the ^{19}F chemical shifts of
K_2GeF_6 single crystal. This pattern was obtained when the
Zeeman field was rotated in the plane on which F_5, Ge, and F_1
atoms and the C_3 axis sit (see Fig. 5-8). The C_3 axis and the
Zeeman field become parallel at 0 °.

rotation nor the free rotation of the anion about an axis was "seen" even at 300 K. The above mentioned high resolution spectra also indicated no anion motion. Therefore, the shielding tensor can easily be determined from the rotational pattern of Fig. 5-13. The dotted lines in Fig. 5-13 are the calculated ones on the assumption of axially symmetric shielding tensor. The maximum point of the curve B corresponds to a Ge-F bond direction, that is, at this orientation the F_1-Ge-F_5 bond (see Fig. 5-8) is parallel to the Zeeman field, where the curve A has a minimum value and the Zeeman field is perpendicular to both F_2-Ge-F_6 and F_3-Ge-F_4 bonds. Therefore, similarly to the case of K_2SiF_6, the most shielded direction is along Ge-F bond, and the least shielded direction is perpendicular to the Ge-F bond. Their shift values are 99 ppm and -20 ppm from the resonance of liquid C_6H_5F, respectively. The mean value of the chemical shift is 19 ppm, being fairly larger than that in solution (7 ppm).[18]

5-3-4 Potassium Hexafluorostannate

(1) Sample Preparation and Measurements

A K_2SnF_6 single crystal (about 10 mm x 10 mm x 10 mm) was obtained by slow evaporation at 30 $^\circ$C of its solution prepared by dissolving $K_2Sn(OH)_6$ into 47 % hydrofluoric acid. The crystal belongs to a trigonal system and the site symmetry of Sn is D_{3d}.

Multiplu pulse measurements were made with the same expectation as in the case of K_2GeF_6 single crystal. Although several attempts were made at 300 K, an angular dependence of the chemical shift was not observed. Then the powder patterns at 77 K and 300 K were obtained due to make sure that there is a motional effect to the chemical shift at 300 K. The powder patterns are shown in Fig. 5-14. The spectrum at 300 K shows a single peak, whereas at 77 K, the spectrum gives an asymmetric line shape.

(2) Determination of Chemical Shielding Tensor

The powder pattern at 300 K shows a single peak. It is considered that the correlation time of the reorientational motion of SnF_6^{2-} ion is so short compared with the magnitude of the chemical shift anisotropy that the anisotropic part of the chemical shift may be averaged out. This agrees with the result that the rotational pattern showed no angular dependence. The correlation time at 300 K could be similar to that in K_2SiF_6. From the powder pattern at 77 K, $\sigma_{//}$ = 183 ppm and

$\sigma_{\perp} = 33$ ppm were obtained on the assumption of axially symmetric shielding tensor. Isotropic average value σ_{iso} is 83 ppm. To compare with this value, the value in solution σ_{sol} is 40 ppm. The fact that σ_{iso} is much larger than σ_{sol} suggests that the interaction in solid is stronger than in solution.
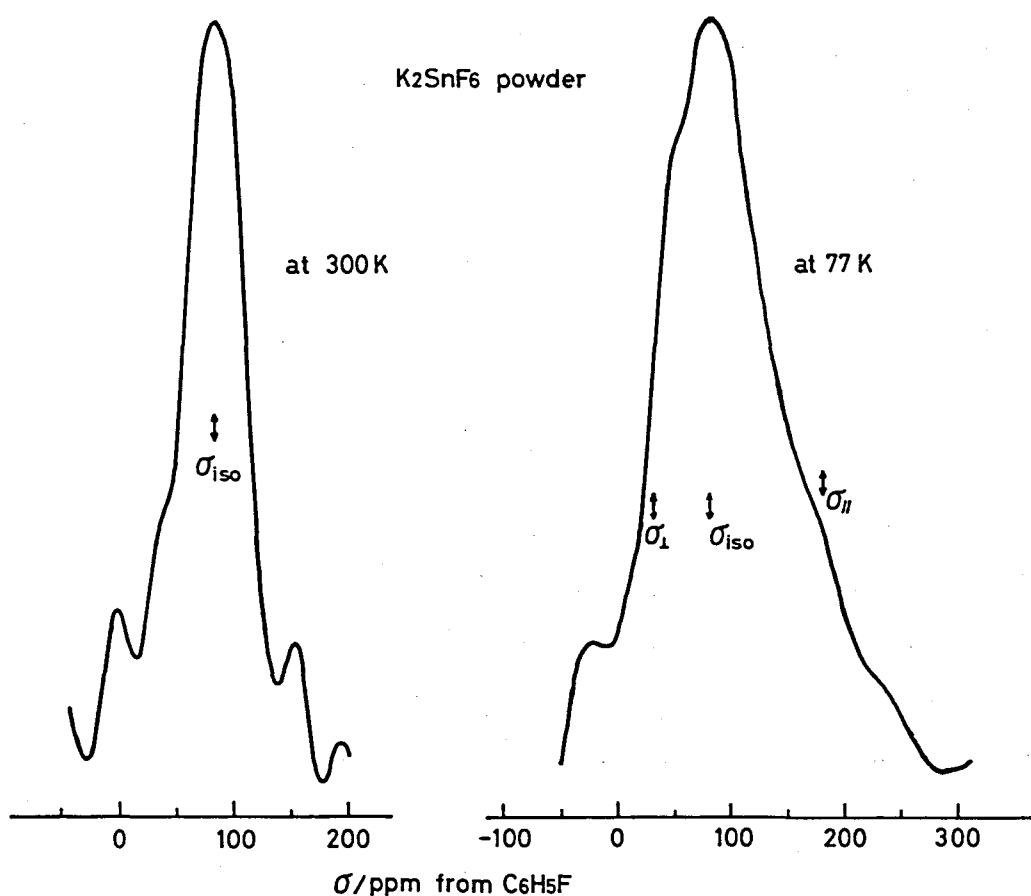

Fig. 5-14. Powder pattern of ^{19}F NMR in K_2SnF_6.

5-3-5 Discussion

Silicon compounds show an outstanding behavior in the several type of measurements on the compounds of IVb sub-group elements (C, Si, Ge, Sn, Pb). Some of the results will be reviewed here briefly.

(i)   nuclear quadrupole resonance of ^{35}Cl, ^{63}Br, ^{127}I in
     MX_4 (M = C, Si, Ge, Sn; X = Cl, Br, I)[20]

The nuclear quadrupole resonance frequencies in a series of MX_4 (M = C, Si, Ge, Sn; X = Cl, Br, I) compounds does not follow the law of corresponding state: anomalous decrease of the nuclear quadrupole resonance frequency in Si-compounds relative to C- and Ge- compounds has been observed so far.

(ii) ^{35}Cl NMR in MCl_4 (M = C, Si, Ge, Sn)[21]

Although ^{35}Cl chemical shifts in MCl_4 (M = C, Si, Ge, Sn) is expected to increase from CCl_4 to $SnCl_4$, the shift in $SiCl_4$ is anomalously high comparative to that in $GeCl_4$

(iii) ^{19}F NMR in MF_4 and NH_4MF_6 in solutions (M = C, Si, Ge, Sn)[18,22]

^{19}F chemical shifts in MF_4 as well as in NH_4MF_6 in solutions (M = C, Si, Ge, Sn) are expected to shift gradually to high field side from C-, Si-, Ge- to Sn-compounds. However, the shifts in SiF_4 and NH_4SiF_6 are anomalously high and nearly equal to that in germanium compounds.

(iv) ^{13}C NMR in (CH_3)$_4$M solution (M = C, Si, Sn, Pb)[23]

  As a whole, ^{13}C chemical shifts in (CH_3)$_4$M in solution (M = C, Si, Ge, Pb) gradually increase from (CH_3)$_4$C to (CH_3)$_4$Pb except (CH_3)$_4$Si which gives anomalously high ^{13}C chemical shift.

(v) ^{59}Co NMR in $X_3MCo(CO)_4$ single crystal (M = Si, Ge, Sn, Pb; X = C_6H_5, Cl, Br, I)[24].

- 103 -

The chemical shift of the ^{59}Co were observed in $X_3MCo(CO)_4$ single crystal (M = Si, Ge, Sn, Pb; X = C_6H_5, Cl, Br, I). The chemical shift components along the Co-M bond ($\sigma_{//}$) vary little in above compounds. On the other hand, the components perpendicular to the Co-M bond ($\sigma_{\perp}$) vary with M and X. $\sigma_{\perp}$ in silicon and tin compounds lie at high field side than that in germanium compounds. From the results of $\sigma_{\perp}$, Spiess et al.[24] concluded that the π-backbondings in M-Co bonds in silicon and tin compounds are stronger than that in germanium compounds.

Three dimensional information about the electronic structure can be obtained by high resolution NMR in solid state and so this technique is thought to be useful in investigating the anomalous behavior of these compounds, in which the law of corresponding state is destroyed. Si, Ge, and Sn have sp^3d^2 hybridization in MX_6 type compounds or ions (M = Si, Ge, Sn), and vacant d-orbitals of M and p-orbitals of X constitute the π-backbonding as shown in Fig. 5-15. Through this back bonding, some electrons are transferred from X to M.
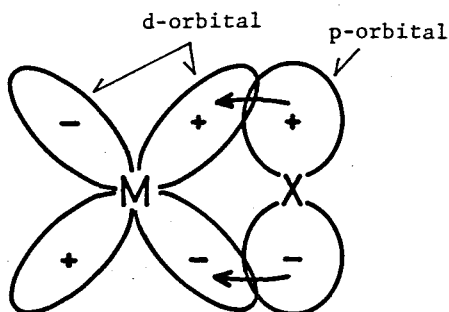
Fig. 5-15. The system of π-backbonding in MX_6 (M = Si, Ge, Sn) compounds.

The origin of the anomaluos behavior in Si compounds have been attributed to such a π-backbonding [20]. The data to be obtained by high resolution NMR in solid is thought to help elucidate the nature of bonding in these compounds. The paramagnetic part, which is responsible for the variation of ^{19}F chemical shift, has already been given in eq. 5-15, and can be rewritten as follows under the assumption of axial symmetry of $\underline{\sigma}$;

(i) bond direction component ($\sigma_{//}^{P}$)

$$\sigma_{//}^{P} = (3/2)\sigma_{o}(2\rho_{\perp} - \rho_{\perp}^{2}) \qquad (5\text{-}17a)$$

(ii) component perpendicular to the M-F (M = Si, Ge, Sn) bond ($\sigma_{\perp}^{P}$)

$$\sigma_{\perp}^{P} = (3/2)\sigma_{o}\left[\varepsilon + \rho_{\perp}(1 - \varepsilon)\right] \qquad (5\text{-}17b)$$

The $\sigma_{//}$ component increases gradually from K_2SiF_6 to K_2SnF_6 as shown in Fig. 5-16.

Fig. 5-16. Pictorial representation of the chemical shift tensor elements in K_2MF_6 (M = Si, Ge, Sn) compounds.

The $\sigma_\perp$ component of K_2SiF_6 is abnormally large. The anomaly in K_2SiF_6 is attributed to the anomalous character in the Si-F bond. The gradual change in $\sigma_{//}$ component indicates that there is a corresponding change in $\sigma_{//}{}^P$. Since $\sigma_{//}$ increases on going from K_2SiF_6 to K_2SnF_6, $|\sigma_{//}{}^P|$ must decrease in this order. According to eq. 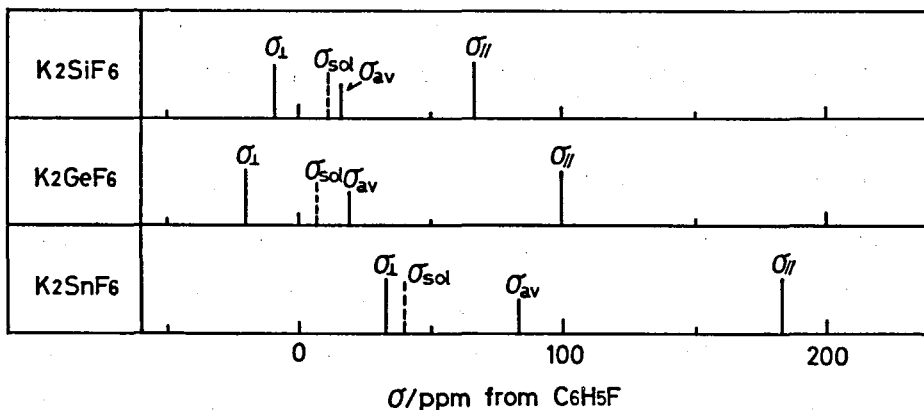5-17a, it is concluded that the double bond character, $\rho_\perp$, decreases gradually from K_2SiF_6 to K_2SnF_6. This shows that π-backbonding is the strongest in K_2SiF_6. Since $\sigma_\perp{}^P$ is given by eq. 5-17b, $\sigma_\perp{}^P$ must decrease from K_2SnF_6 to K_2SiF_6 if ε does not change. In order to explain the anomalous behavior in $\sigma_\perp$, a decrease in ε must be large enough to counter-balance the increase in $\rho_\perp$. The smallness of ε shows a high ionicity of Si-F bond. This means that the electronegativity of Si must be smaller than that of Ge. In fact, recently, the periodicity of the electronegativity is reported to be destroyed in the third row of the periodic table.[25] Sanderson [25] shows that the electronegativity decreases in the order, C > Ge > Sn > Pb > Si. Such anomalous behavior in Si compounds is therefore attributed to the extraordinarily small electronegativity of Si.

σ_{av} is the averaged value of components of the chemical shift tensor in the solid state. σ_{sol} is the corresponding averaged value in solution. The value ($\sigma_{av} - \sigma_{sol}$) is the largest in K_2SnF_6. It is interesting to note that the solubility of K_2MF_6 compounds in water increases from K_2SiF_6 to K_2SnF_6. The large value of ($\sigma_{av} - \sigma_{sol}$) may be attributed to the large difference of environment of MF_6^{2-} ion between solid and liquid state. It is considered that SnF_6^{2-} is surrounded by H_2O molecules more

strongly since the solubility of K_2SnF_6 is the largest, and that this interaction causes a large change of electron distribution.

5-3-6 Conclusion

High resolution ^{19}F NMR spectra were observed in K_2SiF_6, K_2GeF_6, and K_2SnF_6 and chemical shift shielding tensors were obtained. Shielding tensors are all axially symmetric and the most shielded direction is parallel to the MF (M = Si, Ge, Sn) bond. Gradual change of shielding tensor elements ($\sigma_{//}$ and $\sigma_{\perp}$) were observed on going from K_2SiF_6 to K_2SnF_6 except for the $\sigma_{\perp}$ component of K_2SiF_6. From the analysis of shielding tensor components, it is indicated that π-backbonding is the strongest in the Si-F system and anomalous behavior of Si compounds is attributed to the extraordinarily low electronegativity of Si.

At room temperature, reorientational motion of MF_6 (M = Si and Sn) ions are rapid enough to average out the shielding tensor components. On the other hand, ionic reorientation does not affect the chemical shift tensor in K_2GeF_6 at room temperature. At 77 K, the correlation time of reorientation of SiF_6^{2-} ion is evaluated as 3.3×10^{-3} s from the powder pattern analysis. In K_2SnF_6, reorientational motion of SnF_6^{2-} does not affect the powder pattern at 77 K.

The magnitude of the difference of chemical shifts in solid and in solution is considered to serve as a measure of the magnitude of interaction between MF_6^{2-} ion and surrounding ions or H_2O molecules.

References to Chapter 5

1) G. K. Semin, L. S. Kobrina, and G. G. Yakobson, Izv. Sib. Otdel.
   AN SSSR, Ser. Chem. Sci., $\underline{9}$, 84 (1968).

2) R. G. Griffin, H. N. Yeung, M. D. LaPrade, and J. S. Waugh,
   J. Chem. Phys., $\underline{59}$, 777 (1973).

3) H. Raber and M. Mehring, Chem. Phys., $\underline{26}$, 123 (1977).

4) N. F. Ramsey, Phys. Rev., $\underline{77}$, 567 (1950).

   N. F. Ramsey, Phys. Rev., $\underline{78}$, 699 (1950).

   N. F. Ramsey, Phys. Rev., $\underline{86}$, 243 (1952).

5) a) J. G. Powls, Rep. Progr. Phys., $\underline{22}$, 433 (1959).

   b) J. A. Pople, W. G. Schneider, and H. J. Bernstein, "High
      Resolution Nuclear Magnetic Resonance", Chap. 12.
      McGrow-Hill, New York, 1959.

   c) D. W. Davies, "The Theory of the Electronic and Magnetic
      Properties of Molecules", p.179. Wiley, London and New York,
      1967.

6) T. D. Gierke and W. H. Flygare, J. Am. Chem. Soc., $\underline{94}$, 7277
   (1972).

7) J. H. S. Green and D. J. Harrison, J. Chem. Thermodin., $\underline{8}$,
   529 (1976).

8) a) W. E. Hull and B. D. Sykes, J. Mol. Biol., $\underline{98}$, 121 (1975).

   b) T. E. Bull, J. Chem. Phys., $\underline{59}$, 6173 (1973).

   c) J. H. Chaffin and P. S. Hubbard, J. Chem. Phys., $\underline{46}$,
      1511 (1967).

9) M. Karplus and T. P. Das, J. Chem. Phys., $\underline{34}$, 1683 (1961).

10) G. Miyajima, Doctoral Dissertation, Osaka University, 1972.

11) I. M. Alymov, V. M. Burberlo, V. A. Egorov, and R. S. Lotfullin, First Specialized "Colloque Ampere", 186 (1973).

12) S. Alexander and A. Tzalmona, Pyhs. Rev., A138, 845 (1965).

13) a) I. E. Paukov and L. K. Glukhikh, Russ. J. Phys. Chem., 43, 120 (1969).

    b) R. J. L. Andon and J. F. Martin, J. C. S. Faraday Trans., 169, 871 (1973).

14) J. A. A. Ketelaar, Z. Kristallogr. 92, 155 (1935).

15) a) J. L. Hoard and W. B. Vincent, J. Am. Chem. Soc., 61, 2849 (1939).

    b) A. Lari-Lavassani, G. Jourdan, C. Avinens, and L. Cot, C. R. Hebd. Seances Acad. Sci., Ser. C, 279, 193 (1974).

16) Yu. N. Moskvich and B. I. Cherkasov, Yader Magnit. Rezonans v Kristallakh, Krasnoyarsk, 96 (1978).

17) H. W. Spiess, Chem. Phys., 6, 217 (1974).

18) P. A. W. Dean and D. F. Evans, J. Chem. Soc. (A), 698 (1967).

19) V. I. Sergienko, L. N. Ignatieva, P. S. Gordienko, M. F. Eiberman, and S. F. Bogdan, Spectrosc. Lett., 11, 877 (1978).

20) a) R. Livingston, J. Phys. Chem., 57, 496 (1953).

    b) A. Schlawlow, J. Chem. Phys., 22, 1211 (1954).

    c) H. Robinson, H. G. Dehmelt, and W. Gordy, J. Chem. Phys., 22, 511 (1954).

21) K. J. Johnson, J. P. Hunt, and H. W. Dodgen, J. Chem. Phys., 51, 4493 (1969).

22) H. S. Gutowsky and C. J. Hoffman, J. Chem. Phys., 19, 1259 (1951).

23) P. C. Lauterbur, Ann. N. Y. Acad. Sci., 70, 841 (1958).

24) H. W. Spiess and R. K. Sheline, J. Chem. Phys., $\underline{53}$, 3036 (1970).

25) R. T. Sanderson, J. Am. Chem. Soc., $\underline{105}$, 2259 (1983).

Appendix

The BASIC Program for Data Processing

```
0010 PRINT "FT PROGRAM"
0020 PRINT
0030 PRINT
0040 DIM A$[3]
0050 DIM X[3,255],U[3,255]
0060 DIM Y[3,255],V[3,255]
0070 PRINT "TYPE-IN G OF N=2↑G,WHERE N IS NUMBER OF DATA,";
0080 PRINT "YOU NEED"
0090 INPUT G
0100 LET N=2↑G
0110 PRINT "TYPE-IN FREQUENCY/MHZ,SAMPLING INTERVAL/MICRO SEC."
0120 INPUT F,S
0130 PRINT
0140 REM DATA INPUT ROUTINE
0170 FOR J=0 TO 3
0180    FOR K=0 TO 255
0190       LET X[J,K]=0
0200       LET U[J,K]=0
0210       LET Y[J,K]=0
0220       LET V[J,K]=0
0230    NEXT K
0240 NEXT J
0250 LET C=0
0260 LET N5=INT((N-1)/1024)
0270 LET N6=INT((N-1-1024*N5)/256)
0287 LET A=0
0288 PRINT "TYPE IN NUMBER OF ACCUMULATION "
0289 INPUT W
0290 FOR H=1 TO W
0300    CALL 2,C
0310    FOR I=0 TO N5
0320       FOR J=0 TO N6
0330          FOR K=0 TO 255
0340             CALL 3,A
0350             IF I=1 THEN GOTO 0380
0360             LET X[J,K]=X[J,K]+A/W
0370             GOTO 0390
0380             LET U[J,K]=U[J,K]+A/W
0390          NEXT K
0400       NEXT J
0410    NEXT I
0420    CALL 1
0430 NEXT H
0440 PRINT "DO YOU NEED DATA OUTPUT,YES OR NO ?"
0450 INPUT A$
```

```
0460  IF A$[1,1]="N" THEN GO TO 0690
0470  GOSUB 1800
0690  PRINT " DO YOU NEED PRINT-OUT DATA ,YES OR NO ?"
0700  INPUT A$
0710  IF A$[1,1]="N" THEN GO TO 0820
0720  PRINT "TYPE-IN THE INITIAL AND FINAL NUMBER OF PRINT-OUT";
0730  PRINT " DATA,YOU NEED"
0740  INPUT Q1,Q2
0750  PRINT "FREQUENCY=";F;"MHZ    NUMBER OF ACCUMULATION=";W;
0760  PRINT " N=";N;"SAMPLING INTERVAL=";S;"MICRO  SEC."
0770  PRINT
0780  PRINT "TIME/S"; TAB(8);"REAL X"; TAB(21);"IMAGINARY Y"
0790  GOSUB 3000
0800  PRINT "DO YOU NEED MORE DATA,YES OR NO ?"
0810  INPUT A$
0815  IF A$[1,1]="Y" THEN GO TO 0720
0820  PRINT "DO YOU NEED NEW ACCUMULATION,YES OR NO?"
0823  INPUT A$
0827  IF A$[1,1]="Y" THEN GO TO 0145
0830  PRINT "TYPE-IN THE FIRST NUMBER OF DATA,YOU NEED"
0840  INPUT Q
0850  FOR T=0 TO 1023
0860     LET T1=INT(T/256)
0870     LET T2=T-256*T1
0880     LET T3=INT((T+Q)/1024)
0890     LET T4=INT((T+Q-1024*T3)/256)
0900     LET T5=T+Q-1024*T3-256*T4
0910     IF T=>1024-Q THEN GO TO 0940
0920     LET X[T1,T2]=X[T4,T5]
0930      GO TO 0950
0940     LET X[T1,T2]=U[T4,T5]
0950  NEXT T
0960  FOR T=1024 TO 2047
0970     LET T1=INT((T-1024)/256)
0980     LET T2=T-1024-256*T1
0990     LET T3=INT((T+Q-1024)/256)
1000     LET T4=T+Q-1024-256*T3
1010     IF T=>2048-Q THEN GO TO 1040
1020     LET U[T1,T2]=U[T3,T4]
1030      GO TO 1042
1040     LET U[T1,T2]=0
1042  NEXT T
1053  PRINT "DO YOU NEED BASE LINE COMPENSATION ,YES OR NO?"
1055  INPUT A$
1057  IF A$[1,1]="Y" THEN GO SUB 7000
1060  PRINT
1070  REM FFT ROUTINE
1080  PRINT "DO YOU NEED FFT,YES OR NO ?"
1090  INPUT A$
1100  IF A$[1,1]="N" THEN GO TO 1710
1110  GOSUB 4000
1120  PRINT
1130  REM RESULTS OUTPUT ROUTINE
```

```
1140  PRINT "DO YOU NEED RESULTS OUTPUT,YES OR NO ?"
1150  INPUT A$
1160  IF A$[1,1]="N" THEN GOTO 1480
1410  GOSUB 1800
1480  PRINT "DO YOU NEED PRINT-OUT RESULTS,YES OR NO ?"
1490  INPUT A$
1500  IF A$[1,1]="N" THEN GOTO 1610
1510  PRINT "TYPE-IN THE INITIAL AND FINAL NUMBER OF PRINT-OUT";
1520  PRINT " RESULTS,YOU NEED"
1530  INPUT Q1,Q2
1540  PRINT "FREQUENCY=";F;"MHZ    NUMBER OF ACCUMULATION=";W;
1550  PRINT " N=";N
1560  PRINT "SAMPLING INTERVAL=";S;"MICRO SEC.";
1570  PRINT "  RESOLUTION=";10↑3/(S*N);"KHZ"
1580  PRINT
1590  PRINT "SHIFT/R"; TAB(8);"ABSORPTION"; TAB(21);"DISPERSION"
1600  GOSUB 3000
1610  PRINT "DO YOU NEED AMPLITUDE SPECTRUM,YES OR NO ?"
1620  INPUT A$
1630  IF A$[1,1]="N" THEN GOTO 1710
1640  FOR J=0 TO 3
1650     FOR K=0 TO 255
1660        LET X[J,K]=X[J,K]↑2+Y[J,K]↑2
1670        LET U[J,K]=U[J,K]↑2+V[J,K]↑2
1680     NEXT K
1690  NEXT J
1700  GOTO 1140
1710  PRINT "WANT YOU COMPENSATE SAME FID DATA AGAIN,YES OR NO?"
1711  INPUT A$
1712  IF A$[1,1]="Y" THEN GOSUB 7900
1713  END
1800  REM
1810  REM SUBROUTINE OUTPUT
1820  LET O=0
1822  LET P=0
1824  FOR L=0 TO 1
1826     FOR J=0 TO 3
1828        FOR K=0 TO 255
1830           IF L=1 THEN GOTO 1842
1832           IF O=<X[J,K] THEN GOTO 1836
1834           LET O=X[J,K]
1836           IF P=>X[J,K] THEN GOTO 1840
1838           LET P=X[J,K]
1840           GOTO 1850
1842           IF O=<U[J,K] THEN GOTO 1846
1844           LET O=U[J,K]
1846           IF P=>U[J,K] THEN GOTO 1850
1848           LET P=U[J,K]
1850        NEXT K
1852     NEXT J
1854  NEXT L
1856  FOR J=0 TO 3
1858     FOR K=0 TO 255
```

```
1860        LET X[J,K]=(X[J,K]-0)*2000/(P-0)
1862        LET U[J,K]=(U[J,K]-0)*2000/(P-0)
1864     NEXT K
1866 NEXT J
2000 REM
2010 REM  SUBROUTINE OUTPUT
2020 FOR I=0 TO 1
2030    FOR J=0 TO 3
2040       FOR K=0 TO 255
2050          IF I=1 THEN GOTO 2090
2060          LET B=X[J,K]
2070          CALL 4,B
2080          GOTO 2110
2090          LET B=U[J,K]
2100          CALL 4,B
2110       NEXT K
2120    NEXT J
2130 NEXT I
2140 CALL 1
2150 PRINT "DO YOU NEED CRO DISPLAY,YES OR NO ?"
2160 INPUT A$
2170 IF A$[1,1]="N" THEN GOTO 2310
2230 PRINT "TYPE-IN NUMBER OF DISPLAYS"
2240 INPUT D
2250 CALL 5,D
2260 LET C=1
2270 CALL 2,C
2280 PRINT "DO YOU NEED ONE MORE DISPLAY,YES OR NO ?"
2290 INPUT A$
2300 IF A$[1,1]="Y" THEN GOTO 2230
2310 PRINT "DO YOU NEED RECORDER OUT,YES OR NO ?"
2320 INPUT A$
2330 IF A$[1,1]="N" THEN GOTO 2441
2370 PRINT "TYPE IN X TO RECORDE!"
2390 INPUT Z
2400 LET C=2
2410 CALL 2,C
2420 PRINT "DO YOU NEED ONE MORE RECORDING,YES OR NO ?"
2430 INPUT A$
2440 IF A$[1,1]="Y" THEN GOTO 2370
2441 FOR J=0 TO 3
2442    FOR K=0 TO 255
2443       LET X[J,K]=X[J,K]*(P-0)/2000+0
2444       LET U[J,K]=U[J,K]*(P-0)/2000+0
2445    NEXT K
2446 NEXT J
2450 RETURN
3000 REM
3010 REM  SUBROUTINE PRINT-OUT
3020 FOR Q=Q1 TO Q2
3030    LET Q3=INT(Q/1024)
3040    LET Q4=INT((Q-1024*Q3)/256)
3050    LET Q5=Q-1024*Q3-256*Q4
```

```
3060    IF Q3=1 THEN GOTO 3090
3070    PRINT Q; TAB(8);X[Q4,Q5]; TAB(21);Y[Q4,Q5]
3080    GOTO 3100
3090    PRINT Q; TAB(8);U[Q4,Q5]; TAB(21);V[Q4,Q5]
3100 NEXT Q
3110 RETURN
4000 REM
4010 REM FFT SUBROUTINE 1
4020 LET P=8*ATN(1)/N
4030 FOR L=0 TO G-1
4040    LET G1=2↑(G-L-1)
4050    LET M=0
4060    FOR I=1 TO 2↑L
4070       LET K1=INT(M/G1)
4080       GOSUB 4710
4090       LET Y1=COS(P*K2)
4100       LET Y2=-SIN(P*K2)
4110       FOR J=1 TO G1
4120          LET M1=INT((M+G1)/1024)
4130          LET M2=INT((M+G1-1024*M1)/256)
4140          LET M3=M+G1-1024*M1-256*M2
4150          LET M4=INT(M/1024)
4160          LET M5=INT((M-1024*M4)/256)
4170          LET M6=M-1024*M4-256*M5
4180          LET E1=(1-M1)*Y[M2,M3]+M1*V[M2,M3]
4190          LET D1=(1-M1)*X[M2,M3]+M1*U[M2,M3]
4200          LET D2=(1-M4)*X[M5,M6]+M4*U[M5,M6]
4210          LET E2=(1-M4)*Y[M5,M6]+M4*V[M5,M6]
4220          LET Y3=D1*Y1-E1*Y2
4230          LET Y4=D1*Y2+E1*Y1
4240          IF M1=1 THEN GOTO 4300
4250          LET X[M2,M3]=D2-Y3
4260          LET Y[M2,M3]=E2-Y4
4270          LET X[M5,M6]=D2+Y3
4280          LET Y[M5,M6]=E2+Y4
4290          GOTO 4380
4300          LET U[M2,M3]=D2-Y3
4310          LET V[M2,M3]=E2-Y4
4320          IF M4=1 THEN GOTO 4360
4330          LET X[M5,M6]=D2+Y3
4340          LET Y[M5,M6]=E2+Y4
4350          GOTO 4380
4360          LET U[M5,M6]=D2+Y3
4370          LET V[M5,M6]=E2+Y4
4380          LET M=M+1
4390       NEXT J
4400       LET M=M+G1
4410    NEXT I
4420 NEXT L
4430 FOR I=0 TO N-1
4440    LET K1=I
4450    GOSUB 4710
4460    IF K2=>I THEN GOTO 4690
```

```
4470    LET I1=INT(I/1024)
4480    LET I2=INT((I-1024*I1)/256)
4490    LET I3=I-1024*I1-256*I2
4500    LET I4=INT(K2/1024)
4510    LET I5=INT((K2-1024*I4)/256)
4520    LET I6=K2-1024*I4-256*I5
4530    LET K3=(1-I1)*X[I2,I3]+I1*U[I2,I3]
4540    LET K4=(1-I1)*Y[I2,I3]+I1*V[I2,I3]
4550    IF I1=1 THEN GOTO 4610
4560    LET X[I2,I3]=X[I5,I6]
4570    LET Y[I2,I3]=Y[I5,I6]
4580    LET X[I5,I6]=K3
4590    LET Y[I5,I6]=K4
4600    GOTO 4690
4610    LET U[I2,I3]=(1-I4)*X[I5,I6]+I4*U[I5,I6]
4620    LET V[I2,I3]=(1-I4)*Y[I5,I6]+I4*V[I5,I6]
4630    IF I4=1 THEN GOTO 4670
4640    LET X[I5,I6]=K3
4650    LET Y[I5,I6]=K4
4660    GOTO 4690
4670    LET U[I5,I6]=K3
4680    LET V[I5,I6]=K4
4690 NEXT I
4700 RETURN
4710 REM FFT SUBROUTINE 2
4720 LET K2=0
4730 FOR K=1 TO G
4740    LET K3=K1-2*INT(K1/2)
4750    LET K1=INT(K1/2)
4760    IF K3=0 THEN GOTO 4780
4770    LET K2=K2+2↑(G-K)
4780 NEXT K
4790 RETURN
6000 FOR J=250 TO 255
6100    PRINT X[0,J]
6200 NEXT J
7000 REM
7010 REM SUBROUTINE BASE LINE COMPENSATION
7012 DIM R[255]
7014 FOR K=0 TO 255
7016    LET R[K]=0
7018 NEXT K
7020 FOR K=0 TO 255
7022    LET R[K]=X[0,K]
7024 NEXT K
7040 LET X1=0
7041 LET X2=0
7042 LET X3=0
7043 LET X4=0
7044 LET X5=0
7045 LET X6=0
7050 LET X7=0
7053 LET X8=0
```

```
7054 LET X9=0
7055 LET Z1=0
7056 LET Z2=0
7057 PRINT "TYPE-IN TIME CONSTANT AND CUT OFF NUMBER!"
7058 INPUT Z1,Z2
7060 FOR K=Z2 TO 255
7061    LET X[0,K]=0
7064 NEXT K
7069 FOR K=0 TO Z2-1
7070    LET X1=EXP(-K/Z1)
7080    LET X2=X2+X[0,K]
7090    LET X3=X3+X1
7100    LET X4=X4+X1*X[0,K]
7110    LET X5=X5+X1*X1
7120    LET X6=X6*X[0,K]↑2
7130 NEXT K
7140 LET X7=(Z2*X4-X2*X3)/(Z2*X5-X3↑2)
7150 LET X8=(X2-X7*X3)/Z2
7160 FOR K=0 TO Z2-1
7170    LET X9=X8+X7*EXP(-K/Z1)
7180    LET X[0,K]=X[0,K]-X9
7190 NEXT K
7192 PRINT "BASE LINE FUNCTION"
7194 PRINT "         Y =";X8;"+";X7;"* EXP ( - K /";Z1;")"
7200 PRINT "DO YOU WANT DATA OUTPUT,YES OR NO?"
7210 INPUT A$
7220 IF A$[1,1]="Y" THEN GOSUB 1800
7500 PRINT "DO YOU WANT PRINT-OUT DATA,YES OR NO?"
7510 INPUT A$
7520 IF A$[1,1]="N" THEN GOTO 7700
7530 PRINT "TYPE-IN INITIAL AND FINAL NUMBER OF DATA YOU WANT"
7540 INPUT Q1,Q2
7550 PRINT "FREQUENCY=";F;"MHZ    NUMBER OF ACCUMULATION=";W;
7560 PRINT " N=";N;"SAMPRING INTERVAL=";S;"MICRO SEC."
7570 PRINT
7580 PRINT "TIME/S"; TAB(8);"REAL X"; TAB(21);"IMAGINARY Y"
7590 GOSUB 3000
7600 PRINT "DO YOU WANT MORE DATA,YES OR NO?"
7610 INPUT A$
7620 IF A$[1,1]="Y" THEN GOTO 7530
7700 PRINT "DO YOU NEED NEW BASE LINE COMPENSATION,YES OR NO?"
7710 INPUT A$
7720 IF A$[1,1]="N" THEN GOTO 1080
7730 REM ONCE MORE DATA READ
7740 FOR K=0 TO 255
7750    LET X[0,K]=0
7760 NEXT K
7770 FOR K=0 TO 255
7780    LET X[0,K]=R[K]
7790 NEXT K
7800 GOTO 7040
7900 REM SUBROUTINE SECOND COMPENSATION AFTER FFT
7902 FOR J=0 TO 3
```

```
7904    FOR K=Ø TO 255
7906      LET X[J,K]=Ø
7908      LET U[J,K]=Ø
7910      LET Y[J,K]=Ø
7912      LET V[J,K]=Ø
7914    NEXT K
7916 NEXT J
7918 GOTO 7770
8000 REM BASE SHIFT FOR ONE PULSE
8010 LET R1=Ø
8020 FOR K=Ø TO 255
8030    LET R1=R1+U[3,K]/256
8040 NEXT K
8045 PRINT R1
8050 PRINT "PRINT Z IF YOU NEED BASE SHIFT!"
8060 INPUT Z
8080 FOR J=Ø TO 3
8090    FOR K=Ø TO 255
8100      LET X[J,K]=X[J,K]-R1
8110      LET U[J,K]=U[J,K]-R1
8120    NEXT K
8130 NEXT J
8140 END
9000 REM COMPENSATION FOR MREV-8
9010 FOR K=Ø TO Z2/2-1
9020    LET X[Ø,2*K+1]=(X[Ø,2*K]+X[Ø,2*K+2])/2
9030 NEXT K
9040 GOTO 7200
9100 LET S3=Ø
9102 LET S4=Ø
9110 FOR K=Z2/2-31 TO Z2/2-1
9120    LET S3=S3+X[Ø,2*K]/31
9130    LET S4=S4+X[Ø,2*K+1]/31
9140 NEXT K
9150 FOR K=Ø TO Z2/2-1
9160    LET X[Ø,2*K]=X[Ø,2*K]-S3
9170    LET X[Ø,2*K+1]=X[Ø,2*K+1]-S4
9180 NEXT K
9190 PRINT "EVEN SHIFT";S3;"ODD SHIFT";S4
9200 GOTO 7200
9400 LET S5=Ø
9405 FOR K=150 TO 250
9410    LET S5=S5+X[Ø,K]/101
9415 NEXT K
9416 PRINT S5
9420 FOR K=Ø TO 255
9425    LET X[Ø,K]=X[Ø,K]-S5
9430 NEXT K
9435 END
9500 FOR J=1 TO 3
9510    FOR K=Ø TO 255
9520      LET X[J,K]=Ø
9530      LET U[J,K]=Ø
```

```
9540    NEXT K
9550 NEXT J
9560 FOR K=0 TO 255
9570    LET U[0,K]=0
9580 NEXT K
9590 END
9600 FOR J=2 TO 3
9610    FOR K=0 TO 255
9620       LET X[J,K]=0
9630    NEXT K
9640 NEXT J
9650 FOR J=0 TO 3
9660    FOR K=0 TO 255
9670       LET U[J,K]=0
9680    NEXT K
9690 NEXT J
9695 END
9700 FOR J=0 TO 3
9710    FOR K=0 TO 126
9720       LET X[J,2*K+1]=(X[J,2*K]+X[J,2*K+2])/2
9730    NEXT K
9740 NEXT J
9760 FOR J=0 TO 2
9770    LET X[J,255]=(X[J,244]+X[J+1,0])/2
9780 NEXT J
9790 END
9800 LET S6=0
9810 FOR K=0 TO 255
9820    LET S6=S6+X[1,K]/256
9830 NEXT K
9840 PRINT S6
9850 FOR J=0 TO 1
9860    FOR K=0 TO 255
9870       LET X[J,K]=X[J,K]-S6
9880    NEXT K
9890 NEXT J
9895 END
```